

The expansion of the universe observed with supernovae

Pierre Astier

LPNHE, CNRS/IN2P3, Université Pierre et Marie Curie Paris 6,
Université Paris Diderot Paris 7, 4 place Jussieu, 75005 Paris, France

Over the last 20 years, supernovae have become a key tool to constrain the expansion history of the Universe through the construction of Hubble diagrams, using luminosity distances to supernovae belonging to the “Ia” subtype. This technique was key for the discovery that the expansion of the Universe is now accelerating. We review the principle and difficulties of the measurements, the classification and diversity of supernovae, and the physics of the explosion. We discuss the systematic uncertainties affecting the cosmological conclusions with some emphasis on photometric calibration. We describe the major supernova cosmology surveys, the presented analyses and their conclusions, together with the present status of the field. We conclude on the expectations for the near future.

CONTENTS

1. Introduction	2	8. Light curve fitters, distance estimation	16
2. Cosmological framework	4	8.1. K-corrections	16
2.1. The cosmological principle and Friedman equation(s)	4	8.2. Brighter-bluer relation and extinction	17
2.2. Cosmological distances and dark energy	4	8.3. Supernova empirical light curve models	17
2.3. Standard candles and Hubble diagram	5	8.3.1. The MLCS model	17
2.4. What can we probe with distance data?	5	8.3.2. SALT and SALT2 models	18
2.5. A few possibilities for dark energy	5	8.3.3. The SiFTO model	18
2.5.1. The cosmological constant	5	8.3.4. Tripp distance estimators	19
2.5.2. Quintessence	6	8.3.5. Comparing light curve fitters	19
2.5.3. Alterations to gravity	6	8.4. Other distance estimators	20
2.5.4. Back-reaction	7	9. Photometric calibration	20
3. Astronomical observation techniques	7	9.1. The traditional way	20
4. Pioneering works on supernovae and the path to current classification	8	9.2. Instrumental calibration from calibrated laboratory sources	21
5. Observational characteristics and diversity of SNe Ia	8	9.3. Ground-based observations and atmospheric extinction.	21
5.1. Light curves and colours	8	9.4. Linearity issues	21
5.2. Spectra	9	9.5. Prospects for improvements	21
5.3. Variability	9	10. Astrophysical systematic uncertainties affecting SN distances	21
5.4. Correlations with host galaxy properties	9	10.1. Evolution of supernovae	21
6. The paradigm of SNe Ia explosions	10	10.1.1. Light curve rise time	22
6.1. Progenitors and initial state at ignition	10	10.1.2. Spectroscopic evolution tests	22
6.2. Explosion models	11	10.1.3. Segregation according to host galaxy types	22
6.3. Radiative transfer	12	10.2. Gravitational lensing of supernovae	22
6.4. Models at late times	12	11. SN surveys and their cosmological findings	23
6.5. Explosion models and cosmological use of supernovae	12	11.1. Nearby samples	23
7. Observing and reduction techniques for SN surveys	13	11.2. The SCP and HZT pioneers: the twin papers	24
7.1. Finding supernovae	13	11.3. First Hubble Space Telescope samples	25
7.2. Rolling searches	13	11.4. HST searches	26
7.3. Spectroscopy of candidates	14	11.5. Ground-based rolling searches: ESSENCE, SNLS, and SDSS-II	26
7.3.1. Host galaxy subtraction	14	11.6. Supernova compilations	27
7.3.2. Type and redshift	14	12. Prospects for supernova cosmology	28
7.4. Measuring light curves and photometry techniques	15	12.1. Space missions concepts	29
		12.2. Ground-based SN projects	29
		13. Summary and conclusions	30

Acknowledgments	30
References	30

1. INTRODUCTION

Kinematics of test masses probe the sources of gravitational field, both in a Newtonian framework and in general relativity (GR). In a Universe following the cosmological principle, namely homogeneous and isotropic, the motion of test masses (e.g. galaxies) constrains the mean density of the Universe and its evolution with time.

In 1927, Lemaître derived from Einstein's general relativity equations that the velocity of recession is proportional to distance to the first order, and also extracted from the measurements of distances to galaxies (deduced from their apparent brightness) and their recession velocity (from their spectral shift) that this property might be realized in nature [1]¹. In 1929, Hubble presented distances to a sample of galaxies extending further out and also proposed a linear relation between distance and recession velocity [3]. This was the discovery of the expansion of the Universe and the Hubble law states that distance is proportional to recession velocity, at least at a small velocity, and ignoring “peculiar motions” due to spatial density variations. The proportionality coefficient is now called the “Hubble constant” H_0 . Although its value has been revised by almost an order of magnitude since Hubble's initial determination, the discovery of the proportionality itself remains one of the major early steps of observational cosmology. In modern parlance, the fractional spectral shift towards the red, the “redshift” z has replaced the recession velocity: $z = \lambda_{\text{reception}}/\lambda_{\text{emission}} - 1$. Because it is a direct observable, redshift is used by cosmologists to index cosmic time. In the current standard model of cosmology, $z = 0.1$ corresponds to $\sim 10\%$ of the current age of the Universe (about 13.7 Gy), $z = 0.5$ to 40%, $z = 1$ to 55%. The first stars were probably formed around $z = 10$ (0.5 Gy after the Big Bang).

The Hubble constant H_0 has the dimension of the inverse of a time, usually expressed in units of km/s/Mpc. It defines the expansion rate today, and sets the time and distance scales of the expansion. Without diminishing the importance of the Hubble constant determination, one should note that its value does not convey sufficient information to define the current average energy content of our Universe: GR relates the expansion rate at a given epoch with energy density *and* spatial curvature at the same epoch. The Hubble constant defines the average density of the Universe only if the latter is flat (i.e. has zero curvature). The density for which the curvature changes sign is called the critical density and depends only on the Hubble constant and Newton's constant.

In order to constrain gravitation sources driving the expansion, one has to measure the expansion beyond first order in

recession velocity (or redshift). Namely, as one studies the velocity *variations* with time of free falling bodies to measure the gravitational field of the Earth, one should probe how the expansion rate evolves with time in order to characterize the mean Universe content. In the GR framework, the expansion rate *evolution* provides a handle on the fractions of various Universe components, including curvature. Practically, probing the distance-velocity relation beyond first order makes it possible to constrain the evolution of the energy density in the Universe, which in turn constrains the proportions of various components in the admixture, after assuming how each of the involved components dilutes with expansion. We will discuss in §2.3 why determining the proportions of the various components does not require measuring the Hubble constant H_0 .

How practical is it to measure the distance-redshift relation? Measuring a redshift might be considered as relatively easy, at least if the target is bright enough to allow one to acquire a spectrum: redshifts of galaxies are routinely measured to three decimal places from spectroscopy in the visible. But measuring cosmological distances is not as straightforward. Hubble derived distances to galaxies from assumptions about intrinsic luminosities of stars. The overall intrinsic luminosity scale turned out to be wrong and yielded a Hubble constant about 7 times larger when compared with modern determinations. But the real weakness of galaxies as distance indicators is in fact more serious (e.g. [4]): these are evolving too rapidly with time to provide reliable distances, even if one concentrates on relative distances. Supernovae were then introduced and used as a more reliable distance indicator [5, 6], and eventually proposed to constrain the evolution of expansion [7].

Walter Baade and Fritz Zwicky introduced, in 1934, the term “supernova” to describe extremely bright explosions of stars that appear and fade on timescales of months to years. Supernovae are classified today into a handful of types and subtypes. The subtype of type Ia supernovae (SNe Ia) displays reproducible luminosities: at low redshift, the apparent brightness scales as the inverse square of the redshift (e.g. [5, 8]). By extension, plots of apparent brightness of similar objects versus redshift are often called Hubble diagrams.

Precision supernova photometry started in the 1990s with the advent of CCD imagers mounted on telescopes. The Calan-Tololo survey delivered, in 1996, precise and homogeneous CCD-based photometry in several bands for 29 SNe Ia events [9], and derived distances to those [8]. Although the Calan-Tololo survey should be regarded as the keystone of supernova cosmology, redshifts were limited to $z \lesssim 0.1$, too low to constrain the distance-redshift relation to second order. At about the same time, two teams targeted the detection of SNe Ia at significantly higher redshifts, also using CCD imagers. After a slow initial period, both teams eventually succeeded in finding and measuring redshifts and distances to about 50 SNe Ia events in total, at $\langle z \rangle \sim 0.5$. Both teams compared their own distant sample to the Calan-Tololo nearby events (§11.2 & [10, 11]) and reached, in 1998, the same striking conclusion: the distant events appear too faint compared with nearby ones, in any matter-dominated Universe. In terms of kinematics, this means that the expansion is accel-

¹ Note that the English translation [2], probably carried out by Lemaître himself in 1931, misses the key paragraphs that propose the observational evidence for expansion.

erating at late time, which is impossible under matter domination (where matter is defined as “tracing the expansion”). Cosmologists named the conjectured fluid that sources the acceleration “dark energy”, and it represents about 3/4 of the total energy density now, so that our Universe is no longer matter-dominated. The discovery of accelerated expansion (or dark energy) constitutes one of the major recent discoveries in physics: it causes persistent perplexity (for reasons summarized in §2.5), and still sources an enormous flow of scientific literature. The discoverers of accelerated expansion were awarded the 2011 Nobel Price in Physics. Dark energy studies constitute the main scientific driver for large astronomical projects such as LSST and Euclid (§12).

There had been earlier hints that our Universe might not follow the flat matter-dominated scenario. Different indications of a low matter density (i.e. well below the theoretically favoured critical density) were presented in the early 1990s, mostly based on galaxy clustering (e.g. [12]) or primordial nucleosynthesis and galaxy clusters (e.g. [13]). The arguments in favour of a low matter density turned out to be correct, but this does not directly imply an accelerated expansion. In the 1990s, settling between a (observationally favoured) low-density Universe and a (theoretically favoured) critical Universe constituted a key question, and the kinematics of expansion seemed an obvious decisive observational test, if possible. The enterprises aiming at producing Hubble diagrams of SNe Ia were conceived within this framework.

Within the cosmological principle and GR, acceleration of the expansion happens when a fluid that does not expand (or expands slowly) starts to dominate the energy density budget. The simplest cosmological model that describes the observations consists in a flat Universe consisting, today, of about 1/4 of matter (diluting with expansion and time) and 3/4 of “dark energy”, insensitive to expansion and of constant density. Their densities were equal at $z \sim 0.45$, and matter dominated earlier, while the initial domination of radiation energy over matter lasted until $z \simeq 3300$. A possible incarnation of dark energy of static density is the cosmological constant Λ introduced by Einstein in the GR field equations. It plays, in the cosmological framework, exactly the same role as a uniform fluid with static density. The “ Λ CDM” cosmological model consists (at late time) in this admixture of a fluid of static density Λ and matter which has to be dark and cold, hence coined cold dark matter or CDM.

Cosmologists have considered a broader range of dark energy models and describe them in terms of the “equation of state” of dark energy, namely how the dark energy density varies with time and redshift (§2.1). Describing dark energy using the equation of state concept should not be taken too literally: this constitutes a phenomenological description which does not require the assumption that acceleration is indeed due to some fluid. This description of the phenomenon applies to actual fluids, to the cosmological constant, and it can even be rephrased in terms of alterations to GR if one ignores density perturbations.

The discoverers of the accelerated expansion from supernovae readily considered alternatives to the cosmological constant paradigm, and found their observations to be compatible

with it (§11.2). Since then, the result has been consolidated mainly on two fronts: firstly, second-generation supernova surveys have been conducted and have confirmed the early results with more events and better measured distances extending to higher redshifts. Secondly, we now have strong evidence for dark energy from other cosmological probes although with less sensitivity (e.g. §4.1 in [14]). To date, large-scale cosmological observations have been described well by the Λ CDM model (e.g. [15]), sometimes called the concordance model.

Constraining cosmology from distances to supernovae relies on a strong hypothesis: SNe Ia are good “standard candles”. The tight scatter of the Hubble diagram of SNe Ia indicates that the events are reproducible over a small redshift interval, but this does not prove that distant and nearby events are identical. They could, indeed, be of different nature because distant events happen earlier in star formation history than nearby ones. This whole issue is referred to as “evolution” and can be addressed observationally: the standard candle hypothesis can be falsified, and is reinforced by every failed attempt to do so. We will, however, see that the picture we have of the SN Ia explosion mechanism makes it a fundamental “self-calibrated” process, weakly sensitive to environmental influences.

Photometric calibration has recently become a serious issue for supernova cosmology. Although the core of the method consists in comparing fluxes, these fluxes have to be measured in different observer bands because of redshift: nearby supernovae are usually measured in blue and green bands, and the same restframe region lies around $1 \mu\text{m}$ for supernovae at $z \sim 1$. To take full advantage of current supernova statistics, these flux ratios should be calibrated to better than 1%, which hits fundamental limitations of current astronomical photometric calibration techniques. Today, supernova cosmology is probably the most demanding field of astronomy in terms of photometric calibration across the visible and near infrared range.

The plan of this review goes as follows: §2 covers the minimal necessary cosmological background, how distances constrain cosmological parameters, and a summary of the leading hypotheses for dark energy; §3 introduces the minimal background in astronomy techniques required for this review, for readers unfamiliar with the field; §4 covers the observational aspects of supernova taxonomy; §5 concentrates on the “Ia” subclass delivering almost all cosmological constraints, and §6 covers the pre-explosion and explosion issues. We then enter the observational and reduction techniques (§7), and devote the next section (§8) to light curve fitting, almost always involved in distance estimation. §9 covers photometric calibration, the basement of supernova cosmology, and studies of other astrophysical systematic uncertainties are reviewed in §10, including gravitational lensing (§10.2). §11 covers supernova surveys and their cosmological conclusions; §12 briefly discusses the prospects of the field. We summarize and conclude in §13.

For interested readers, we provide here an incomplete set of reviews with similar or highly related scopes: [16] parallels this one; [17] concentrates on explosion models; [18] focuses

on the physics of SNe Ia in relation to their cosmological use; [19] discusses the determination of the Hubble constant which we will not discuss here; [20] presents theoretical and observational aspects of dark energy and the accelerating Universe, while [21] studies dark energy probes in great detail.

2. COSMOLOGICAL FRAMEWORK

2.1. The cosmological principle and Friedman equation(s)

The cosmological principle states that the Universe is isotropic and homogeneous. Although we have ample evidence that this is wrong on small distance scales, the quasi-isotropy of the cosmic microwave background (CMB) [22], and the homogeneity of the distribution of galaxies [23] support this framework for large scales. Within General Relativity, this principle is encoded into symmetries of the metric:

$$ds^2 = dt^2 - R^2(t) \left(\frac{dr^2}{1 - kr^2} + r^2(d\theta^2 + \sin^2 \theta d\phi^2) \right)$$

usually called the Friedman-Lemaître-Robertson-Walker (FLRW) metric. $R(t)$ is called the scale factor, and $k = -1, 0$ or 1 , is the sign of spatial curvature. We set “ $c = 1$ ” in what follows. Objects with constant coordinates (r, θ, ϕ) are called comoving. Cosmologists attach comoving coordinates to the matter fluid, so that $R(t)$ scales with the separation of matter tracers (typically galaxies). In the FLRW framework, it is easy to show that photons (following paths with $ds^2 = 0$), emitted by comoving sources and detected by comoving observers, see their wavelength scale with $R(t)$:

$$\frac{\lambda_{\text{reception}}}{\lambda_{\text{emission}}} = \frac{R(t_{\text{reception}})}{R(t_{\text{emission}})} \equiv 1 + z$$

where z is called the redshift of the emitting source. GR postulates relations between the metric and the gravitation sources. For the FLRW metric, these are two differential equations for $R(t)$, the Friedman equations [24]:

$$H^2(z) \equiv \left(\frac{\dot{R}}{R} \right)^2 = \frac{8\pi G}{3} \rho - \frac{k}{R^2(t)} + \frac{\Lambda}{3} \quad (1)$$

$$\frac{\ddot{R}}{R} = -\frac{4\pi G}{3}(\rho + 3p) + \frac{\Lambda}{3} \quad (2)$$

where Λ is the cosmological constant, ρ stands for the proper energy density and p for the pressure. $H(z)$ is the expansion rate and $H_0 \equiv H(z=0)$. The energy conservation equation:

$$\frac{d}{dt}(\rho R^3) = -3pR^2\dot{R} \quad (3)$$

relates pressure to density evolution and also applies separately to the various fluids in the Universe. For non-relativistic matter, $\rho_M R^3$ is constant and hence $p_M = 0$. A fluid with static density ($\dot{\rho} = 0$) has $p = -\rho$. The cosmological constant Λ plays exactly the same role as a fluid with static density $\rho_\Lambda = -p_\Lambda = \Lambda/8\pi G$, and can be summed into the ρ and p

quantities in the Friedman equations. Relation (3) can be obtained by eliminating \ddot{R} between equations 1 and 2.

Fluids can be characterized by a relation between p and ρ . The equation of state of each fluid w_X is defined by $p_X = w_X \rho_X$, and equation 3 implies $\rho_X(t) \propto R(t)^{-3(1+w_X)}$. Given the densities at one epoch (e.g. now) and the equations of state of the fluids of the Universe, one can solve the first Friedman equation (equation 1) for $R(t)$. The critical density is defined as the energy density for which $k = 0$:

$$\rho_c = \frac{3H_0^2}{8\pi G}$$

where $H_0 = (\dot{R}/R)_{\text{now}}$ is the Hubble constant. Densities are usually parametrized through their value “today”, in units of the current critical density:

$$\Omega_M \equiv \frac{\rho_M}{\rho_c} = \frac{8\pi G \rho_M}{3H_0^2}, \quad \Omega_\Lambda \equiv \frac{\Lambda}{3H_0^2}, \quad \Omega_k \equiv -\frac{k}{R_0^2 H_0^2}$$

and the first Friedman equation implies $1 = \Omega_M + \Omega_\Lambda + \Omega_k$. This assumes that our Universe is composed only of matter and Λ . One might consider other fluids such as an implementation of dark energy different from the cosmological constant (see §2.5) and radiation density.

2.2. Cosmological distances and dark energy

Cosmological distances should be defined from observables. For example, one defines the luminosity distance through the energy flux f of a source of proper energy luminosity \mathcal{L} through $d_L^2 = \mathcal{L}/4\pi f$. For a source observed at a redshift z , it reads [25]:

$$d_L(z) = \frac{(1+z)}{H_0 \sqrt{|\Omega_k|}} \text{Si}n \left\{ |\Omega_k|^{1/2} \int_0^z \frac{dz'}{H(z')/H_0} \right\} \quad (4)$$

$$\frac{H^2(z)}{H_0^2} = \left[\Omega_M(1+z)^3 + \Omega_\Lambda + \Omega_k(1+z)^2 + \Omega_R(1+z)^4 \right] \quad (5)$$

where $\text{Si}n(x) = \text{sin}(x)/x$, $x, \text{sinh}(x)$ for $k = 1, 0, -1$; note that the expression is continuous in $\Omega_k = 0$. In $z = 0$, the integrand is 1 and the Taylor expansion reads $d_L(z) = z/H_0 + O(z^2)$, so that densities are not constrained by distances at a small redshift. Distances to higher redshifts become sensitive to densities, although in a somehow degenerate way. For sake of completeness, the expression for $H^2(z)$ (5) contains a radiation term Ω_R , which now represents less than 10^{-4} of the energy budget and is usually neglected. It represents about 10% of the total at $z \sim 1000$.

One can generalize equation 4 to alternatives to Λ by replacing the Ω_Λ term by the (reduced) density of the considered fluid. For a constant equation of state, $\Omega_\Lambda \rightarrow \Omega_X(1+z)^{3(1+w)}$, and for a varying equation of state $w(z)$, $\Omega_\Lambda \rightarrow \Omega_X \exp[3 \int_0^z \frac{1+w(z')}{1+z'} dz']$.

The discovery of accelerated expansion relied on supernovae at $z \simeq 0.5$ being observed to be fainter (i.e. at a larger distance) than expected from their low redshift counterparts

in a matter-dominated Universe. Inspecting equation 4, one notes that for a flat Universe ($\Omega_k = 0$, $\Omega_\Lambda = 1 - \Omega_M$), a positive Ω_Λ indeed increases distances (at given z) with respect to $\Omega_\Lambda = 0$. The argument also holds for non-flat universes.

The angular distance d_A is defined via the apparent angular size θ of an object of comoving physical size D : $d_A \equiv D/\theta$. Because photons follow null-geodesics of the metric [26], we have $d_L = (1+z)^2 d_A$ and hence d_L and d_A convey the same cosmological information. d_L measurements rely on “standard candles” while d_A measurements rely on “standard rulers”.

2.3. Standard candles and Hubble diagram

Standard candles are defined as objects of reproducible luminosity and enable one to measure distances through their observed energy flux: $f = \mathcal{L}/4\pi d_L^2(z)$, where \mathcal{L} stands for the proper intrinsic luminosity (energy per unit source proper time). Practically, we have to measure fluxes within bounded spectral bands, and in order to compare objects at different redshifts we will do our best to compare the same *restframe* bands which implies measuring high-redshift objects through redder (observer) bands than nearby objects. In supernova parlance, a Hubble diagram reports the apparent flux (or magnitude) of standard candles as a function of redshift.

If one measures a Hubble diagram, we note that all fluxes scale with the factor $\mathcal{L}H_0^2$, which conveys no information about cosmological densities. In the cosmological analysis, this overall factor will be estimated together with the other cosmological parameters: it enters as a nuisance parameter in the analysis. Since $H_0 d_L(z)$ does not depend on H_0 , the Hubble constant enters the problem only through this global flux scale. If the luminosity of the standard candle \mathcal{L} can be estimated without using the flux-redshift relation, measuring $\mathcal{L}H_0^2$ from the latter constrains H_0 . We hence note that objects with an unknown luminosity do not help determining H_0 from a redshift-flux relation, and the initial determinations of the Hubble constant were off because a wrong luminosity was assumed. We also note that determining H_0 entirely decouples from measuring the reduced densities from a Hubble diagram, and we refer to [19, 27] (and references therein) for a detailed description of the role of SNe Ia to measure H_0 . We just mention here that, using the standard candle property, SNe Ia are used to extrapolate distances from local events to distant ones, and constitute the last step of the “cosmic distance ladder” used to establish the value of H_0 and hence the cosmic distance scale.

2.4. What can we probe with distance data?

A set of distances as a function of redshift probes a weighted sum of densities (equation 4), with weights evolving with redshift. Since distance measurements deliver a single number at every redshift, a redshift span is mandatory to break degeneracies of cosmological parameters [28]. As discussed in the above section, supernovae impose (at least) one extra nuisance parameter, which illustrates why measuring a

single cosmological parameter like Ω_M in a matter-dominated Universe requires a finite redshift interval.

Although distances over a finite redshift interval formally break the degeneracy of the sum, supernova surveys still deliver elongated constraints in the $(\Omega_M, \Omega_\Lambda)$ or (Ω_M, w) planes (see e.g. [10, 11]), even for surveys with the largest redshift span (e.g. figures 8 and 9 in [29]).

Accelerated expansion is indeed supported by supernovae alone, since the first measurements (discussed in §11.2) and even more today (see figure 8), but with some caveats, (e.g. [30]). However, distances to supernovae are most usually merged with other cosmological probes in order to produce the tightest cosmological constraints and to decouple parameters. Standard examples include anisotropies of the cosmic microwave background (see e.g. [15, 31]), and baryon acoustic oscillations (BAOs, see e.g. [32, 33]) measured in the correlation function of galaxies. BAO mostly deliver an (angular) distance constraint, with the same degeneracies as luminosity distances, but the size of the measured “standard rod” also depends on cosmological parameters (mainly Ω_M in the concordance model, see e.g. [34]), and the constraints hence exhibit different degeneracies than mere distances. As shown in [33], BAO now deliver distance-redshift relations similar to the ones obtained from SNe, but not yet as precise. CMB anisotropies probe the same geometrical feature as BAO, but at a much higher redshift ($z \simeq 1089$) which makes CMB constraints even more complementary to distances to supernovae typically at $z \lesssim 1$ to 2.

Even if supernovae on their own constrain only combinations of cosmological parameters, they are currently key to constrain dark energy: ignoring supernova distances degrades dark energy constraints by factors of ~ 2 or more (see e.g. table 4 and fig 12 of [15]).

2.5. A few possibilities for dark energy

Right after the discovery of the accelerated expansion, modellers produced an enormous corpus of literature devoted to implementations of dark energy. Those can be classified into three categories: the mere cosmological constant, vacuum energy, and alterations to GR. All these implementations involve new physics. A fourth class of proposals for dark energy, free of new physics, consists in noting that the effective Friedman equation in a non-homogeneous matter-dominated Universe plausibly contains a term somehow mimicking dark energy, increasing with density fluctuations. We now briefly describe these possibilities and refer to [35] for more details. From an observational point of view, the current tightest constraints (§11, 11.5) are compatible with a static dark energy density, which can be incarnated by the cosmological constant.

2.5.1. The cosmological constant

In the original papers that introduce GR, the cosmological constant was absent. It was later introduced by Einstein

himself in order to allow for a static Universe (see [36], and [37] for the historical aspects). Although the addition became useless after the discovery of expansion, it is very natural to allow for such a term in the Einstein equations. One even expects such a term because it is algebraically indistinguishable from the contributions as gravitational sources of all “zero point energies” (also called vacuum energy) expected in theories of particle physics. “The cosmological constant problem” (see [37] and references therein), is that the expected energy density from zero point energies of particle physics theories is “about” 120 orders of magnitude larger than what astronomical observations indicate². Several classes of solutions together with their weaknesses are discussed in [37]. For example, super-symmetry would solve the problem because fermions and bosons then contribute equally but with opposite signs to vacuum energy, but exact super-symmetry also cancels the anomalous magnetic moment of the electron, which is now measured to be non-zero to nine decimal places [38].

So in practice, one is forced to assume that the contribution of vacuum energy to gravitation sources is zero or extremely small, for some yet unknown reason. This does not forbid the introduction of a fundamental cosmological constant directly in the theory, and the observational consequence is that the associated (dark) energy density does not vary with time: it has an equation of state $w = -1$. In addition to postulating one more fundamental constant, this incarnation of dark energy raises the “coincidence problem” (e.g. [35]): how come that the matter density varying as $(1+z)^3$ and dark energy of constant density now take similar values?

2.5.2. Quintessence

The word “quintessence” was introduced in [39] to name a (fifth) component (after baryons, dark matter, neutrinos and radiation) in the Universe, proposed there as a scalar field, with a self-interaction parametrized with its potential energy. In most implementations, it interacts with other fluids only through gravitation. The dynamics of these models depend on the initial conditions and the shape of the potential, for which we have little theoretical guidance. In order to be less arbitrary than the cosmological constant paradigm, these models try to avoid the “coincidence problem” by proposing a potential in which the scalar field density tracks the matter density, being subdominant at early times and becoming slightly dominant at late times, and where the dynamics exhibit an attractor, making the system insensitive to initial conditions. Power-law and exponential potentials (e.g. [39–43]) deliver dynamics roughly compatible with the observations. Such potentials not only emerge in effective field theories (e.g. from extra dimensions or standard model extensions like SUGRA),

but also provide the small numerical factors required to generate the very low observed density [44]. The equation of state of a scalar field is confined to $[-1,1]$: at $w = -1$ the potential energy dominates, while the kinetic energy dominates at $w = +1$. In order to reproduce the observational constraints (i.e. $w \simeq -1$), quintessence dark energy models should be essentially static at late times. “Natural” quintessence models commonly exhibit late equations of state around $w > \sim -0.8$ (e.g. [44]) which falls about 3σ away from the latest measurements. Without fine tuning, the effective mass of the quintessence field is of the order of H_0 [45] (i.e. 10^{-33} eV), and hence its spatial inhomogeneities only develop on scales comparable to the horizon today. Well-motivated quintessence models should “protect” such a small mass from quantum corrections by some symmetry (as proposed in e.g. [43]).

As measurements increasingly favour a static dark energy density, the quintessence scenario loses its appeal. In contrast, if we detected an evolution of the dark energy density, quintessence would likely become a very serious candidate.

2.5.3. Alterations to gravity

Since dark energy is required when assuming that GR holds on large scales, one may question the theory itself. In the GR framework, the evolution of structure formation is sensitive to the expansion history and hence constitutes an alternative probe of the Universe content. Precision measurements of the growth of structure in the past constitute a key test of the dark energy paradigm in the GR framework and a strong justification of dark energy space missions (see e.g. [46, 47]). Correlations of the cosmic shear (e.g. [48]) are a dark energy probe sensitive to both structure formation and expansion history.

Before altering GR, one should note that it successfully passed demanding tests in the solar system (e.g. [49]) and that alterations to GR should only affect cosmological scales³. Embedding our 4D space-time into a 5D Minkowski space provides some room for alterations to standard GR ([53], and [54] for a simplified introduction). Although one could originally fit the data without dark energy in this framework [54], improved data sets now rule out some specific 5D models [55, 56].

The standard 4D GR action integrates \mathcal{R} (the scalar curvature, not the scale factor) and alterations to this action are called “ $f(\mathcal{R})$ ” theories and have been considered as alternatives to dark energy. Quoting [57], “All $f(\mathcal{R})$ modified gravity theories are conformally identical to models of quintessence in which matter is coupled to dark energy with a strong coupling”, while in the simplest effective dark energy models (such as Λ), matter and dark energy are coupled only gravitationally. One should hence expect a significantly different phenomenology: comparing predictions to data, several

² This 10^{120} ratio of energy densities comes from summing the modes of quantum oscillators up to the Planck scale. This is arguable, but setting the cutoff to the electroweak scale “only” reduces the discrepancy to $\sim 10^{60}$. In order to reconcile the zero point energies with cosmological densities, the cutoff should lie in the meV regime [37].

³ The “Pioneer anomaly” [50, 51] is the only evidence a GR “failure” on small scales. Improved models of radiative transfers on the spacecraft have recently been presented which may account for the whole effect [52].

works [57–59] exclude a wide class of $f(\mathcal{R})$ models and disfavour those as an alternative to dark energy.

2.5.4. Back-reaction

The standard derivation of Friedman equations assumes a homogeneous Universe which is obviously a simplification. In [60], it is shown that in an inhomogeneous Universe, a spatially averaged Friedman equation may convey a term causing acceleration, only due to matter inhomogeneities. This “back-reaction” mechanism relies on the non-linear structure of GR, and at variance with all other dark energy incarnations does not involve new physics. In this scheme, dark energy is a “mirage” from structure formation and the “coincidence problem” vanishes.

Since one should question whether alterations of the average Friedman equation indeed alter the average distance-redshift relation in the same way as for homogeneous models, explicit toy models have been built. By “punching” low-density spherical voids in a homogeneous matter background, with a continuous density, one obtains a Swiss-cheese Universe, for which analytic solutions have been derived (see e.g. [61] and references therein). In a periodic lattice of spherical voids, distances differ significantly from a homogeneous dark energy free Universe, but do not mimic the concordance model distance-redshift relation (figure 5 of [61]), even with voids as large as 350 Mpc. Randomizing void locations makes the disagreement even worse [62].

Another stream of back-reaction attempts develops second-order perturbation theory in order to evaluate the contribution of perturbations to source terms of Einstein’s equations (see e.g. [63, 64]). Although one finds contributions that would contribute as some effective dark energy in the Friedman equations, their physical meaning and gauge invariance have been questioned [65]. It has also been argued that corrections to large-scale distances from density contrasts are very small (e.g. [66]).

Because back-reaction is technically very involved, whether it constitutes an alternative to dark energy is debated: compare, e.g., [67] and [65]. One should, however, remark that (perhaps for excellent reasons, [67]) the back-reaction mechanism does not deliver yet the Λ CDM phenomenology without dark energy.

3. ASTRONOMICAL OBSERVATION TECHNIQUES

This short section, for readers unfamiliar with astronomy, introduces the minimal concepts and parlance of astronomical observation at optical wavelengths, and we refer to [68] for a textbook devoted to observation techniques.

Astronomical observations at optical wavelengths consist mostly in imaging and spectroscopy. Imaging is almost always carried out through filters, in particular for measuring distances to SNe Ia. There are two sets of common filters in the visible, the UBVRI “Standard filters” [69] and the ugriz SDSS filters [70], displayed in figure 1. Practical implementations

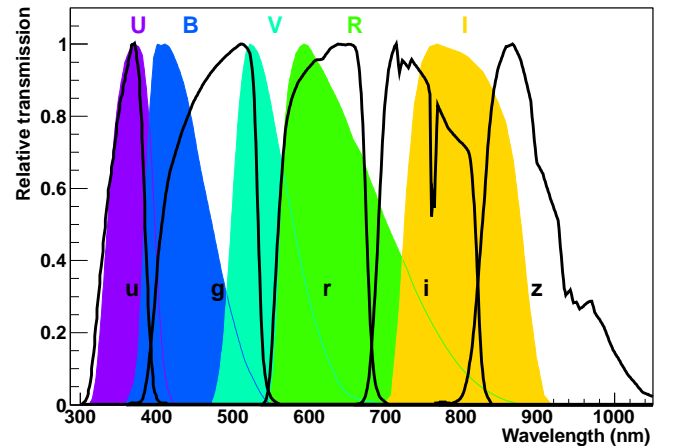


FIG. 1. Shape of commonly used photometric bands in the visible, arbitrarily normalised. U, B, V, R, I refer to standard bands from [69], and u, g, r, i, z to the SDSS bands from [70]. The latter integrate representative atmospheric absorptions experienced from the ground.

of filters are always slightly different from the archetypes. In the visible range, light sensors are now essentially always silicon CCDs, which have a red cutoff at around $1.1 \mu\text{m}$ and deliver pixelized images that can now reach millions of pixels per device. Before the 1990s, images were mostly acquired with photographic plates (in particular wide-field images), and precision photometry used vacuum tubes, typically photo-multipliers. CCDs became common during the 1990s and wide-field imaging is now carried out using mosaics of CCDs, with tens to thousands of individual devices. Typical imaging observations consist in several minutes of integration (where the integration time is defined by a mechanical shutter) followed by about 1 min of read out. Typical read-out cadences are $O(100\,000)$ pixels per second, in order to limit the contribution of electronic noise to ~ 5 electrons per pixel. The dominant noise affecting ground-based CCD images is most usually the shot noise of the sky glow, except for the brightest sources where the shot noise of the object itself contributes. Image quality (IQ), which directly determines the photometric accuracy for point-like objects such as stars (and supernovae), is usually described through the size of these point-like sources, and the best ground-based sites routinely reach IQ below $1''$ FWHM in the visible. This figure is almost one order of magnitude better in space. Astronomers usually report flux measurements as magnitudes defined as $m = -2.5 \log_{10}(\text{flux}) + C$, where C is defined to attribute a certain magnitude to some reference object, either real (such as Vega) or some spectrum such as AB magnitudes (see [71]). How these magnitude systems are related to physical fluxes is described in §9. “Colour” refers to magnitude combinations insensitive to overall brightness, such as $B-V$. For quasi-static stars, colours are a rough proxy for temperature.

For spectroscopy, one relies on a dispersing element, commonly a grating. To select the light from the object of interest,

the most common technique consists in positioning a narrow slit in the image plane and then dispersing the light in the direction perpendicular to the slit. The slit can be replaced by fibre optics [72] or systems of lenslets [73]. Multi-object spectroscopy (MOS) consists in simultaneously acquiring spectra, either using fiber optics positioned on the targets in the telescope focal plane, or machined multi-slit masks. Currently, high-multiplex MOS instruments typically acquire O(1000) spectra at a time. In space, one can perform slit-less spectroscopy by placing a disperser in front of an imager, and still separate the object light from the sky light, thanks to the low sky brightness. The spectral resolution $\delta\lambda$ is commonly expressed through $R \equiv \lambda/\delta\lambda$. As imaging, spectroscopy in the visible also uses CCDs. Synthetic photometry from slit spectra is generally inaccurate, because the fraction of light missing the slit is both unknown and wavelength dependent. Some spectrograph designs explicitly tackle this limitation (e.g. [73, 74]).

Observations in the near infrared (NIR) now rely on low band-gap pixelized semiconductor devices (e.g. [75]), coupled to integrated readout electronics. Observing around and above $1 \mu\text{m}$ from the ground is difficult, because the atmosphere glow rises very rapidly with wavelength, and also features numerous absorption lines. Both atmospheric glow and absorption are variable on timescales of minutes to hours.

Observations from space benefit from a much improved IQ. Compared to ground, the sky background is reduced, with a dramatic improvement in the NIR [76]. On the other hand, ionizing radiation hitting the sensors affects the acquired data via local charge deposition, and also degrades the performance with integrated dose.

4. PIONEERING WORKS ON SUPERNOVAE AND THE PATH TO CURRENT CLASSIFICATION

Already in the late 20's, Baade and Zwicky were searching transients by visually comparing photographic plate pairs exposed for about 30 min, about one month apart, on the Palomar 18 inch telescope, in order to identify transient events. In 1934, they proposed the name "supernovae" [77] to denote a new class of extragalactic "novae" typically 10^4 times brighter than regular novae. They declared these two event classes as totally different phenomena and proposed a supernova rate of about one event per galaxy and per several centuries. They identified that nuclear explosions are necessary to generate the enormous amount of energy they observed. They were able to acquire spectra of their events, which exhibit the broad features characteristic of fast moving ejecta, and which do not show evidence of hydrogen lines. In 1941, a second class of supernovae was proposed [78]: these "type II supernovae" exhibit hydrogen lines and are typically fainter than the original "type I" supernovae. The classification of type I supernovae was refined in 1985 [79], when a subclass of peculiar type I were isolated: those are typically fainter than regular type I and miss the Si II broad absorption at $\sim 610 \text{ nm}$. Type Ia supernovae were then defined as events that display Silicon and no hydrogen whereas type Ib and Ic do not display silicon

nor hydrogen. Type Ib display a strong helium line, and type Ic do not display it.

The current taxonomy of supernovae was sketched in 1993 [80], and its current status and history are detailed in [81]. From a physical point of view, type Ia supernovae are thermonuclear explosions, while all the other types are core-collapse explosions. We refer to [82, 83] for introductory and more advanced material on theory of supernova explosions.

Core-collapse progenitors are massive stars (typically above $8 M_\odot$ [84]) which run "out of fuel" when the chain of successive fusions stops on Fe nuclei: further fusions are endothermic. The gravitational pressure can then no longer be balanced by heat radiation, and the core collapses (e.g. [85] and references therein). Iron nuclei are photodisintegrated and protons are turned to neutrons by electron capture and neutrino emission, producing a neutron star, on which the outer shells fall and bounce. The spectral characteristics depend mainly on the composition of the outer shells, where Ib and Ic have been stripped of H and/or He, and type II have retained their hydrogen. Since the progenitors are massive, they experience a rapid evolution (lifetimes of $10^6 - 10^7$ years), so that the core-collapse SN rate traces the star formation rate. Core-collapse supernovae arise from a variety of progenitors and exhibit a broad distribution of luminosity, even within each subclass [86, 87]. As already noted, these events are on average fainter than SNe Ia [87], and the population of the faint tail is still poorly known.

5. OBSERVATIONAL CHARACTERISTICS AND DIVERSITY OF SNE IA

5.1. Light curves and colours

SNe Ia emit most of their energy in the visible, and the remaining part is essentially confined to near UV and near IR. During the bright phases, the spectrum peaks around 400 nm (see Fig 3). Very rapidly, observers noted that SNe Ia (which were still called SNe I) exhibit reproducible light curves (e.g. [88]).

In the *B*-band (blue light, see figure 1), the light curve rises in about 19 (restframe) days on average (e.g. [89]). About 35 days past maximum the light curve follows a quasi-exponential decay (see figure 2). If one sums the emitted energy, thus building the bolometric light curve, the observed decay rate beyond ~ 50 days after maximum is related to the ^{56}Co half-life: the β and γ decay chain $^{56}\text{Ni} \rightarrow ^{56}\text{Co} \rightarrow ^{56}\text{Fe}$ powers the light curve (e.g. [90–93], and §6).

In the *R*-band ($\sim 650 \text{ nm}$), the light curves exhibit a shoulder 20 to 30 days after maximum, which transforms into a second maximum towards redder bands (up to $\sim 2\mu\text{m}$), taking place 20–30 days after the first one (see Fig 2); the feature is more prominent for bright events, faint events might miss it.

The $B - V$ colour (blue versus green, where V stands for "visible", see also figure 1) reddens during the first 50 days, indicating that the emitting material is cooling. At about 40 days after maximum (i.e. ~ 60 days after explosion) the $B - V$ colour changes slope and then becomes bluer and bluer (e.g.

figure 4 of ([94], figure 1 in [95]). Other colours have different behaviour.

5.2. Spectra

SNe Ia spectra captured early or around maximum are characterized by broad absorption lines of “intermediate-mass” elements, mainly Si and Ca, shifted to the blue with respect to the SN host galaxy redshift, because the absorption takes place in layers ejected at high velocity towards the observer. The velocity of the absorbing region is measured from the blue-shift of absorption features in the spectrum and decreases with time (e.g. [96, 97], and figure 3). The light-emitting region (called photosphere) is characterized by a material density below which photons can escape. As the supernova expands, its density decreases and the light-emitting region proceeds towards the core of the star that just exploded (its nature will be discussed at §6). The supernova eventually enters a nebular phase where emission features dominate.

5.3. Variability

SNe Ia exhibit a variability of the width of their light curve, even after accounting for time dilation in order to compare restframe widths. This variability was initially noticed through a correlation between the decay slope of the B (~ 450 nm) light curve and its peak brightness ([100, 101]). This correlation was refined in 1993 from a small sample of well-measured events [102]. The “brighter-slower”, or Phillips relation quantifies that slower decliners are also intrinsically brighter, which is of paramount importance when measuring distances: all supernova cosmology analyses implement it in some way. Still in the B -band, it has been proposed to describe this variability of light curves by stretching the time axis of a single light curve template [103, 104], and the rise and fall timescales seem to vary together for [104] and [89], while [105] finds them essentially independent.

The distribution of decline rate (or stretch factor) has an rms variation of $\sim 10\%$ [106], exhibits a long tail of hard-to-catch rapidly declining and faint events [107], as well as some bright and slow events. Cosmological analyses have to exclude these extreme events, because the empirical light curve shape parametrizations behave poorly for those [106, 108, 109], and also because the brighter-slower relation changes [107, 110]. Fast decliners are on average redder than slow decliners [110–112].

We will discuss parametrizations of this light curve shape variability when we come to light curve models in §8.3 but all turn out to be essentially equivalent, and all extract the relation of their parameter to luminosity from data.

SNe Ia also exhibit variability of their colours (measured, e.g., at maximum) even at a fixed decline rate. For example, the distribution of the restframe $B-V$ colour has an rms of about 0.1 mag. (see e.g. [106]) and a tail of highly reddened events (e.g. figure 5 in [113]). Different colours of the same event seem to be well correlated: $B-V$ and $U-B$ are related

by a linear relation (see e.g. figure 7 in [106]), as expected if colour variability is attributed to varying amount of absorption along the line of sight. More precisely, colour relations of SNe (such as $U-B$ versus $B-V$) slightly depend on the decline rate, which is easily accounted for (e.g. [109]). As one considers bands bluer than B , the relation between different colours becomes poorer and poorer (e.g. figure 7 in [114], [115, 116]), a tendency confirmed by space-based UV photometry down to 180 nm [117]. As for extinction, one observes that bluer supernovae are brighter, and that different colours do not vary independently: one colour seems enough to parametrize this colour variability. The source of colour variability unrelated to the decline rate is still debated: it could be intrinsic to supernovae (e.g. [118]), it could be due to extinction by dust in the host galaxy, or more likely a mixture of both. There is evidence of narrow Na absorption lines, indicative of dust, particularly for highly reddened events (e.g. [113] and references therein), which are usually excluded from cosmological analyses. One might, however, note that the quantitative agreement of SNe colour variations with known dust properties is poor (see e.g. [108, 109, 112, 119]), with one notable exception [120]. We will discuss relevant parametrizations in §8.2 & 8.3.

The brighter-slower relation becomes shallower when going to redder wavelengths [121], and eventually vanishes at NIR wavelengths [122, 123]. The brighter-bluer relation also becomes shallower, and ignoring both of them delivers accurate distances in NIR bands in particular in the H-band ($[1.5, 1.8]\mu\text{m}$) [123] (but see also [124] and references therein). These findings are so far limited to nearby events, because these NIR restframe bands become increasingly difficult to observe as redshift increases.

SNe Ia variability is often described as a one-parameter family, with extinction by dust in the host galaxy causing some extra colour variation. In practice, and whatever the source of colour variations, cosmological works mostly consider these events as a two-parameter family, where one parameter indexes light curve shape and the other some colour, or colour excess.

5.4. Correlations with host galaxy properties

The physics in galaxies is broadly indexed by the mean age of their stellar population. Early-type galaxies mainly contain evolved stars and form little or no new stars, while late-type galaxies have varying amounts of star formation going on. One might broadly rank galaxies from big, red, passive and elliptical to small, blue, star-forming and spiral or irregular. SNe Ia are observed in all galaxy types, while core-collapse supernovae are observed only in star-forming hosts (see, however, [125]) because their massive progenitors have a very short lifetime.

The SNe Ia rate can be split across the galaxy types (see [126, 127] and references therein), and one finds that star-forming galaxies produce more than 10 times more SNe Ia (per unit stellar mass) than passive galaxies. Fast decliners happen preferably in old stellar environments, or early-type

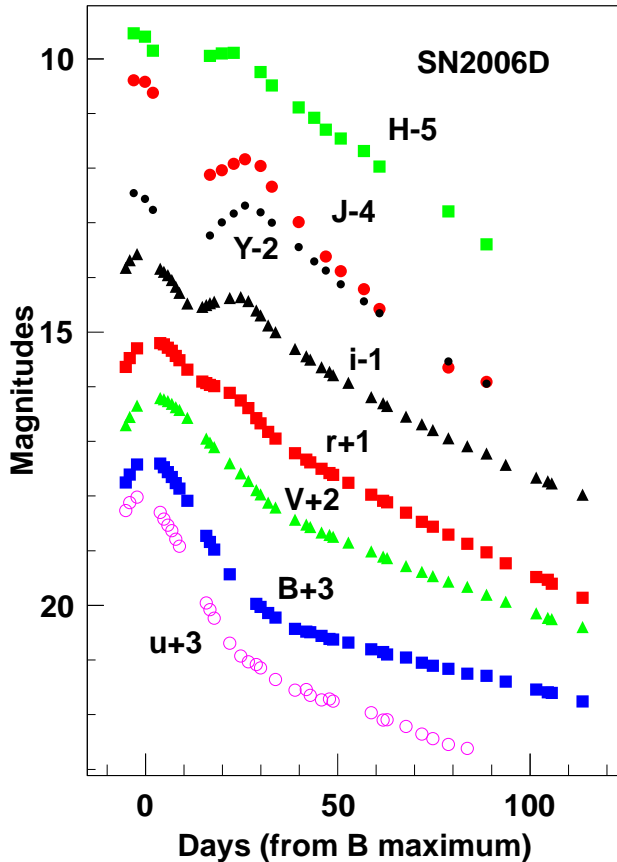


FIG. 2. Light curves of SN2006D ([98]) in bands ranging from the near UV (bottom) to the NIR (top). Bands labelled by upper case letters refer to Vega magnitudes, lower case letters to AB magnitudes.

hosts (figure 4. of [9], e.g. [127–129]), and the cause remains unclear. This probably explains the early finding that SNe Ia are brighter in late-type galaxies [130], and the observation that the average decline rate decreases with redshift [131]. Colours have been compared across environments and found to be compatible [128, 132], which is somehow surprising because if extinction by dust contributes significantly to colour variations, one expects less extinction in passive galaxies because they have less dust than active ones (e.g. [133, 134]). Even more surprisingly, the largest homogeneous SNe Ia sample to date recently indicated [135] that supernovae in passive hosts are slightly but significantly redder than those in star-forming hosts. A similar trend was reported earlier in §4.2.2 of [136]. Some other aspects related to host galaxies are discussed in §10.1.3.

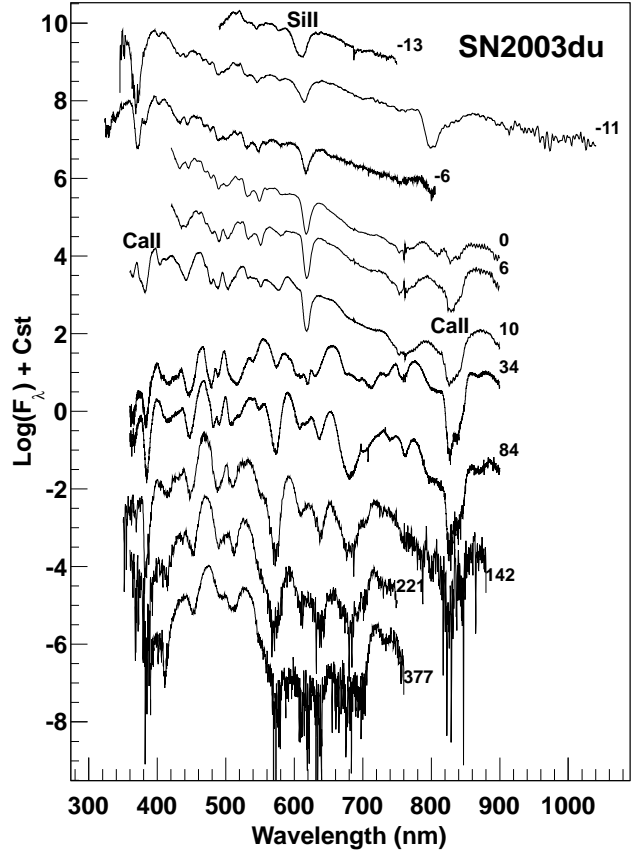


FIG. 3. Spectral sequence of SN2003du ([99]). Spectra are labelled by their phase w.r.t B maximum. Absorption features are attributed to Si and Ca elements. Note that the absorption features of the first spectra shift to the red with time.

6. THE PARADIGM OF SNE IA EXPLOSIONS

6.1. Progenitors and initial state at ignition

The current model for type Ia supernovae explosions assumes that a carbon-oxygen (C-O) white dwarf (WD) accretes mass from a companion until it reaches the Chandrasekhar mass ($M_{\text{Ch}} \equiv 1.38M_{\odot}$), at which the pressure from the degenerate electron gas no longer balances the gravitational pressure [137]. The temperature can then increase enough to trigger carbon fusions [138], and the nuclear flame can “burn” the whole star material within a few seconds. A large consensus has built up around this paradigm [139], because it is supported by several observational facts.

- Fusions of C and O nuclei produce Si, S and Ca, which are observed in the spectra (see figure 3).
- ^{56}Ni is the expected end of a fusion chain starting with C and O since further fusions would not release energy. The $^{56}\text{Ni}(T_{1/2} = 6.1\text{d}) \rightarrow ^{56}\text{Co}(T_{1/2} = 77\text{d}) \rightarrow ^{56}\text{Fe}$ seems to power the light curve, both because of its decay time (e.g. [90–93]), and because of the evolution of

line strength in the late spectra [140].

- The reproducibility of luminosity (e.g. [121]) is a logical consequence of the explosion occurring at a threshold depending only on fundamental constants.
- The lack of H and He in the spectrum is just due to their absence in the initial state.
- The fact that SNe Ia are the only type of SNe observed in old stellar environments such as elliptical galaxies suggests a low-mass (hence long-lived) evolved progenitor. White dwarfs form at the end of the evolution of stars of less than $8 M_{\odot}$, which eject most of their outer layers, leaving a $\sim 1 M_{\odot}$ C-O compact star, too cool to host nuclear reactions, and slowly radiating its energy, possibly for billions of years.

This scenario is strongly supported by a quantitative study of the outcome of nuclear reactions [17, 141]. It, however, faces a major issue: the path to the initial state is still ambiguous ([18, 139] for detailed discussions of the various issues). Since the Chandrasekhar mass has to be reached from below, a mechanism for the WD to gain mass should be proposed. Binary systems (i.e. bound systems of two stars) provide two different paths, the so-called single-degenerate (one WD and some other star) and double-degenerate (two WDs) scenarios. A recent survey of WDs in Sun’s neighbourhood [142] reports that 25% of those are in binary systems, and 6% in double-degenerate systems. Among known low-mass WD binaries, more than 10 systems will merge in less than a Hubble time [143].

The single-degenerate scenario consists in a low-mass WD accreting material from a higher mass companion star until it reaches the Chandrasekhar mass (see e.g. [144]). This requires that the mass donor is a low-surface-gravity and non-degenerate star, and late main-sequence stars or red giants are the most likely candidates. H and He are the more likely elements to be accreted. However, plausible accretion rates face serious issues (see p 206 of [17] and reference therein): slow accretion rates do not compensate for the mass loss due to novae eruptions, or helium flashes; in contrast, at high accretion rates, the steady burning of H and/or He should make these progenitors so bright that they should be easily detectable. The low observed X-ray flux from elliptical galaxies might forbid [145], or not [146], the single-degenerate scenario, at least in elliptical galaxies. However, the arguments relying on the luminosity induced by material accretion may not apply if the progenitor binary systems are enshrouded during their accretion phase. We should stress here that the binary system (and its environment) is complicated enough to take the outcome of models with caution. For example, the role of H and/or He flashes is also controversial [147, 148]. The single-degenerate scenario is more and more challenged by the donor star escaping observations: none was found in pre-explosion archival images [149, 150], nor within SN Ia remnants (e.g. [151] and references therein); the expected UV and X-rays emission from the explosion material colliding with it was not seen [152, 153]. We cannot entirely rule out the single-degenerate scenario, but its viability will be questioned if the

donor star remains elusive. Note that WD are generally far too faint to be detected in pre-explosion archival images.

The double-degenerate scenario assumes an initial binary system of two WDs [154, 155], losing orbital angular momentum by means of gravitational radiation. Stellar population synthesis calculations predict the required statistics for mergers [139]. While this scenario naturally explains the absence of hydrogen in the spectrum, there is no built-in mechanism that leads to a reproducible state at ignition, a simple explanation for the empirical reproducibility of SNe Ia. On the other hand, this initial state naturally provides a mechanism to explain extremely luminous events such as SNLS-03D3bb, which seems to require a super-Chandrasekhar initial state to produce enough ^{56}Ni to explain its apparent luminosity [156]. However, the single-degenerate initial state might also generate supra-Chandrasekhar amounts of ^{56}Ni [157]. A threat to this double-degenerate initial state is that WD mergers lead to off-centre ignition causing gravitational collapse rather than the expected thermonuclear disruption (e.g. [83, 158, 159]), but a recent simulation actually obtains an under-luminous SNe Ia from two $0.9 M_{\odot}$ WDs [160], but requires a narrow mass difference of the involved stars.

6.2. Explosion models

Assuming the initial state can indeed be obtained, modelling the outcome of the explosion is at least a two-step process: one first has to go through the nuclear fusion reactions, and second to evaluate the radiation transfers in the expanding ejecta. Both aspects are physically and computationally extremely challenging [17].

The production of elements through successive fusions during the thermonuclear runaway depends on the reaction conditions, mainly density and temperature: the reaction rates vary extremely rapidly with temperature, and the production of iron-peak elements⁴ favoured under high density. There are roughly two regimes for the propagation of the flame: deflagration (subsonic) and detonation (supersonic), where deflagration allows the unburnt material to expand before reacting. Detonation models (see e.g. [161]) very efficiently convert the input material into ^{56}Ni , and then under-produce intermediate-mass elements (Si, Ca, S,...) which constitute the prominent features of the spectrum around maximum light. The famous W7 explosion model [162] produces intermediate-mass elements via deflagration, and is a fair match to the observed light curve and spectrum at maximum. So, a deflagration phase is required in order to reduce the density of the stellar material prior to nuclear reactions in a M_{Chan} WD [17, 163], in order to avoid the nearly exclusive production of ^{56}Ni [83, 162, 164].

However, pure deflagration models face some discrepancies with observations [162, 163]: overproduction of ^{54}Fe w.r.t to solar abundances (sometimes referred to as over-production

⁴ “Iron peak” refers to a local maximum, around Fe, in the abundance of elements as a function of atomic number. The expression refers here to Fe, Co and Ni.

of neutron-rich elements), some indication of a brighter-faster relation (while we observe a brighter-slower relation), and too narrow an interval of expansion velocities of intermediate-mass elements. To cure these issues, [163] proposes that after an initial episode of deflagration, the flame transitions to detonation (deflagration-detonation transition (DDT)), as observed in laboratory chemical combustion experiments (e.g. [165]). Through the alliance of both combustion modes, intermediate-mass elements are produced over a large range of ejection velocities. DDT simulations hence improve the match to observed light curves and spectra [166], and provide some hints that the density at transition might source the explosion strength variability [166, 167].

6.3. Radiative transfer

The explosion determines the chemical composition of the ejecta and velocities of the various layers, mostly driven by the energy released in the nuclear fusions. From this intermediate state, radiative transfer calculations generate synthetic light curves and spectra, which are mostly powered by the ^{56}Ni β and γ decay chain (e.g. [90–93]) as already discussed. Broadly speaking, the supernova emits less energy than it produces until the maximum, when both quantities are equal [161]. Arnett’s rule ([168]), derived from analytic radiative transfer analysis assuming a grey opacity, states that the maximum light luminosity is proportional to ^{56}Ni mass and has been used to constrain the latter (e.g. [169]): it varies by about one order of magnitude from very fast to very slow decliners, and by about a factor of 2 for the range of decline rates commonly included in cosmological analyses.

Radiation transfer codes simulate, in an expanding and inhomogeneous medium, the conversion of nuclear radiation into the eventually observed light; their sophistication has followed the increase in available computing power. The complexity arises from two causes: first, opacities depend on the ionization states of the atoms, which themselves depend on the radiation flux and temperature, which in turn depend on opacities. One thus has to find a consistent solution, and the convergence speed is a major concern (see [170] and references therein). Second, the opacities are driven by interactions with atomic lines (scattering and fluorescence), which are extremely numerous. In particular, the iron group elements exhibit a wealth of lines in the near UV that mostly shift light to the red, but also produce most of the UV flux around 300 nm ([171, 172]). Both the details of “atomic data” (i.e. the choice of lines involved in the calculation) and the treatment of ionization are shown to have a large influence on the predicted light curves and spectra (e.g. figure 7 of [173]).

The current state of the art mostly consists in 3D solutions. Monte Carlo techniques [174] are efficiently parallelized and the microscopic physics can be incrementally refined. The various implementations (e.g. [173, 175] and references therein) mostly differ in the details of the micro-physics approximations. Hydrodynamic solutions now also accommodate 3D (e.g. [176] and references therein). Going to three dimensions allows one to account for possible anisotropies,

which have been proposed as a potential source of diversity through the random viewing angle [173, 177].

6.4. Models at late times

At about 100 days after maximum light, emission lines start to dominate the spectrum, indicating that the luminous material is scintillating because of the energy deposition of positrons and γ rays. This feature has been used to constrain both the amount of ionizing radiation and the nature of material around it, using models much simpler than in the early phases. At $t > \sim 200$ days, the quasi-exponential slope of light curves is different from band to band [178, 179], possibly due to the increasing amount of (stable) ^{56}Fe which scintillates significantly in the B -band [178], and also because more and more γ -rays and positrons escape [91, 180]. The positron escape fraction constitutes a handle on the magnetic field [92]. Simulations of late SNe Ia [180] and γ -ray observations [181] indicate that “late” positrons from SNe Ia might constitute a dominant contribution to the 511 keV emission in the Galaxy. From the difference of the bolometric late light curve slope with the ^{56}Co decay rate, one can model the escape rate of γ rays and obtain constraints on the ejected mass (e.g. [91, 93]) and on the amount of synthesized ^{56}Ni ([169] and references therein).

6.5. Explosion models and cosmological use of supernovae

The value of H_0 has been inferred from a Hubble diagram of nearby supernovae and numerical simulations to derive the intrinsic luminosity of events [166, 182, 183], and values fully compatible with conventional determinations (mostly relying on the cosmic distance ladder [19]). This approach is probably the sole quantitative contribution to date of SN explosion models for determining cosmological parameters. Because of the complexity of the explosion and the consequent light production, models nowadays only broadly reproduce light curves and spectra and cannot be used as templates for fitting data. If the brighter-slower relation is qualitatively understood and physically attributed to synthesized ^{56}Ni mass variations (e.g. [184] and references therein), there is no consensus on what causes the diversity of the latter (e.g. [185]). Models hence do not yet provide strong guidance to implement the brighter-slower relation. The brighter-bluer relation is a worse case because there is no consensus on whether variability of supernovae (independently of the decline rate) contributes significantly to it (see §8.2).

Cosmologists, however, hope to get some insight from further improving the physical understanding of the initial state, its environment and the explosion mechanism(s). Ideally, we would improve light curve modelling, reduce the distance scatter, and gain insights into redshift-dependent systematic biases of distances. Such goals might look excessively ambitious, but we should remark that qualitative indications might be sufficient. For example, if models point out some measurable indicator of the WD metallicity, the relation of metallicity

to intrinsic luminosity can be inferred from data.

7. OBSERVING AND REDUCTION TECHNIQUES FOR SN SURVEYS

Up to now, most SNe Ia events that were used to measure distances went through three different observing phases: finding the event, identifying it from a spectrum (spectroscopic follow-up), and measuring its light curve (photometric follow-up), possibly in several bands. We will now discuss how the required observations are conducted and handled, with some historical perspective.

7.1. Finding supernovae

Essentially all supernovae are nowadays found using an apparently simple technique: image subtraction. The concept consists in subtracting a search image from a previously acquired image often called reference. The subtraction is done pixel to pixel and point-like positive excesses on the resulting image constitute supernova candidates. If the time gap between the two epochs is chosen to be around 2 weeks (in the restframe), found supernovae are likely to be still rising and a prompt follow-up campaign allows one to capture the maximum light (which allows one to safely estimate peak brightness, and eases spectroscopic identification). Prior to the subtraction itself, both images have to be brought on the same pixel grid, on the same flux scale and their point spread function (PSF, in practice the shape of stars, which varies with atmospheric conditions) should be homogenized. The process aims at making non-variable objects disappear in the subtraction process. Since the concept of image subtraction was initially proposed [186] and demonstrated on the sky [187], the major improvement brought to the technique consists in fitting the convolution kernel for PSF homogenization [188], by explicitly minimizing the subtraction image. Subtractions are vulnerable to small defects of geometrical alignment or PSF matching, or more generally, significantly different observing conditions, and reaching the shot noise limit requires some care. Image subtractions are then essentially always performed using image pairs from the same instrument. One has to promptly find candidates in order to rapidly obtain spectroscopic confirmations and start the photometric follow-up as soon as possible. The computing load involved in finding supernovae has not decreased significantly in the two two decades since the area of silicon sensors (nowadays often assembled into mosaics) used to image the sky, and the computing power of silicon processors used to find supernovae have followed similar slopes. An example of two images tiles and their subtraction is displayed in figure 4.

Searching supernovae requires an imager with as large a field of view as possible. The first sizable SNe Ia sample (at $z < 0.1$) with CCD-measured light curves [9] was found using photographic plates in the early 1990s. Discovering supernovae in a somehow systematical way using CCDs started around 1995: for example, the IAU telegram 6270 announced

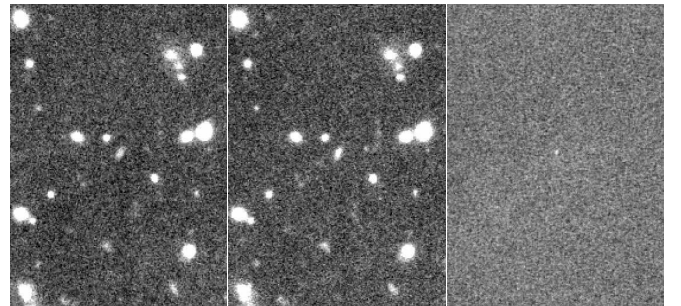


FIG. 4. Small portions of images of the same field. The leftmost was acquired on 8 September 1999 and gathers 3.6 h of integration on CFHT, using the CFH12k imager in I band. The central tile was taken 26 days later with the same instrument. The rightmost tile displays the image subtraction, where a positive excess is visible at the centre, at a brightness $I_{Vega} \simeq 24.7$ and about 6σ . This excess was spectroscopically identified as a type Ia event (SN1999fd) at $z=0.87$.

11 supernovae at $0.35 < z < 0.65$, found using a $16' \times 16'$ single-CCD imager on the CTIO-4m, and spectroscopically confirmed at the Keck (10 m). We note here that a sizable fraction of the distant events reported in the accelerated expansion papers [10, 11] (§11.2) was discovered using this CTIO-4m/Keck combination.

The SN finding techniques and instruments then improved rapidly: in 1999, the IAU telegram 7312 reports 20 spectroscopically confirmed high-redshift supernovae (among which 3 events at $z > 1$), discovered using a $30' \times 40'$ imager at the Canada-France-Hawaii Telescope (CFHT, 3.6 m), and confirmed at Keck. Unfortunately, the photometric follow-up of this wonderful harvest could not be fully conducted, illustrating that actually measuring light curves of distant supernovae was becoming the heaviest part of the observing programme.

7.2. Rolling searches

In this 1999 discovery telegram (IAU 7312), one can easily check from the event coordinates that several supernovae were found on average in the same telescope pointing. This suggests the “rolling search” approach, which consists in repeatedly imaging the same sky patches, and using the image sequence both to find supernovae and to measure their light curve. The spectroscopic identification phase remains unchanged with respect to the “traditional” two-epoch search.

The technique becomes increasingly efficient as more supernovae are measured in the same telescope exposure on average. In order to benefit from this multiplex advantage, three ground-based surveys implemented this technique (see §11.5): ESSENCE on the CTIO-4m with the $36' \times 36'$ Mosaic camera (2002-2008), SNLS on CFHT (3.6 m) using the 1 deg^2 Megacam imager (2003-2008) and the SDSS SN search (2005-2007) on the SDSS 2.5 m with its 1.5 deg^2 fast scanning imager. These three projects were successful in finding and measuring events, essentially at the expected rate.

Rolling searches using the Hubble Space Telescope (HST) imagers have also been implemented (§11.4), however, with a lower multiplex advantage than the ground-based wide-field imagers.

The rolling search technique not only efficiently addresses the observing time shortage that rules astronomic observation, but also improves the data quality over the classical two-epoch search scheme followed by photometry. First, SN light curves are sampled independently of their phase, since observations are not conducted for a specific event; in particular, SN light curves contain very early points, taken even before the event was actually detected. Second, the search is indeed easier than in the early times because photometry for distance estimation requires deeper images than for mere search. One also usually has more than a single image and epoch to turn a light excess into a candidate. Finally, these repeated images can be stacked to reach considerable depths, especially if the survey lasts several years. The wide-field stacks usually deliver the photometric characterization of the supernova galaxy hosts (e.g. [127, 128]). They can also be used for science topics unrelated to supernovae, which can even be the main drivers for the survey, as happened, in particular, for some heavy SN programmes on the HST (§11.4).

7.3. Spectroscopy of candidates

Candidates from supernovae searches have to be confirmed, most of the time using spectroscopy. From reported discoveries, one can draw the crude rule that the telescope used for spectroscopy is twice as large in diameter as the one used for the search via imaging. SNe Ia supernovae at $z \lesssim 1$ are now found using 4 m class telescopes, and the spectroscopic follow-up is conducted on 8 m class facilities, where a target at $0.8 < z < 1$ requires integrating for 1-2 h (see e.g. table 1 in [189]). For nearby supernovae at $z \lesssim 0.1$, searches are typically conducted with 1 m telescopes, and spectroscopy is done in 10-20 mn exposures on 2 m telescopes. In order to use the observing time as efficiently as possible, spectroscopic observations aiming at classification are usually conducted around maximum light, if possible. For distances to SNe Ia, besides positive identification of the event against other SN types, spectroscopy is expected to provide the redshift value, in order to place the event on the Hubble diagram.

The needed spectral resolution is modest: supernovae have no narrow lines, and a resolution ($\lambda/\delta\lambda$) of about 100 is enough to sample properly the peaks and troughs of SNe Ia spectra. One, however, usually uses spectral resolutions around 1000, in order to reduce the impact of telluric absorptions and sky line emissions, and in order to properly measure narrow lines of the host galaxy spectrum, which constitute the best redshift indicator.

At variance with imaging, there is currently no practical way to efficiently multiplex spectroscopic observations of supernovae because the field of view of most spectroscopic instruments is too small. The events are then observed one at a time. When using a multi-object spectrograph, one can still observe other targets (typically galaxies) in parallel with the

SN candidate.

7.3.1. Host galaxy subtraction

Supernovae are point sources while their host galaxy is not. The size of the supernova does not depend on redshift while galaxies get smaller as redshift increases. Hence, the fraction of host galaxy light mixed with the supernova increases with redshift. For photometry, this is addressed by subtraction (or some equivalent technique, see §7.4), but for slit spectroscopy, subtracting a supernova-free observed galaxy spectrum is not practical. Moreover, most surveys do not allocate observing time to collect such spectra.

Increasingly sophisticated approaches to address the host galactic contamination of supernova spectra have been developed, mostly for high-redshift surveys. One can simply ignore the problem, thus selecting against SNe on bright hosts. One can attempt to synthesize the observed spectrum from template libraries of both supernova and galaxies [189]. In [190], both continuum and narrow lines are filtered out (in wavelength space) from the acquired spectrum, thus efficiently removing most of the contaminating host galaxy features, however at the cost of altering the SN spectrum. In long-slit spectroscopy, one can attempt to separate the point-like component (the SN) from a more extended background (the host galaxy), either with some spatial filtering [191], or by relying on the distribution of galactic light along the slit estimated from multi-band imaging [192]. In [115], galaxy models are fitted to supernova-free multi-band imaging measurements of the host galaxy for subsequent subtraction from the observed spectrum.

7.3.2. Type and redshift

At high S/N, the identification of a supernova from its spectrum does not usually require any sophisticated method; problematic cases occur for events departing significantly from the archetypes. At higher redshift (and smaller S/N), the SN identification is carried out by comparing its spectrum to high-S/N archetypal templates, for various phases and SN types, where the quality of the match is often quantified via least squares (e.g. [189, 190]), possibly matching both light curve and spectrum [116]. When present, narrow emission or absorption lines of the host galaxy provide the redshift or at least redshift hypotheses, but one may also add the redshift to the searched parameter space. Redshifts are typically measured to a precision of 0.001 from galactic features and to 0.01 from SNe features (e.g. [189], figure 1 in [193], figure 7 of [194]). The quality of the measured spectrum obviously plays a key role in the identification confidence level. Regarding SNe Ia, a positive identification consists in the observation of Si and/or Ca spectral features (see e.g. [189] for a practical definition of identification confidence levels). figure 5 illustrates the separation of galaxy and SN spectra and the obtention of redshift and type of a high-redshift SN candidate.

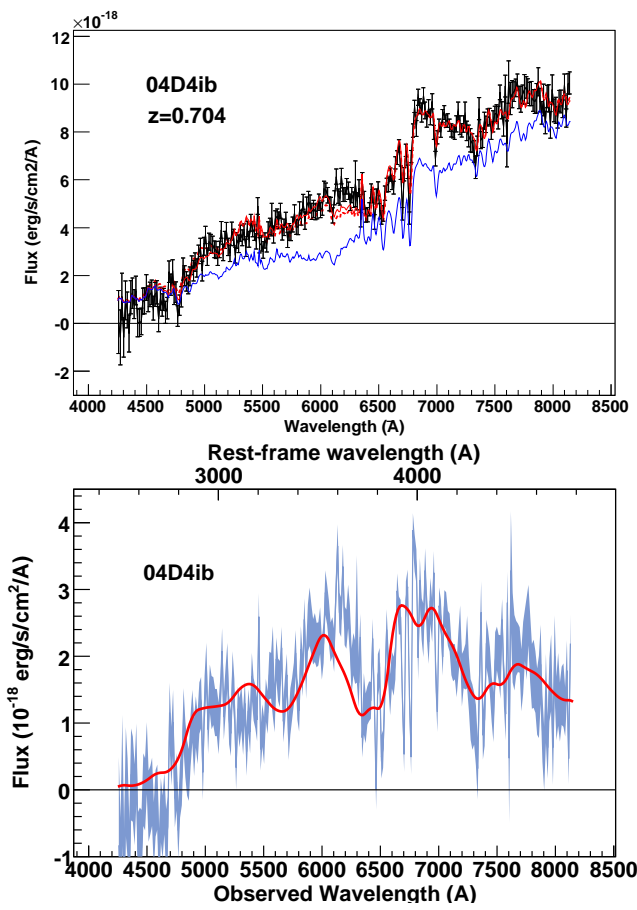


FIG. 5. On the left, measured spectrum (in black) of the SNLS-04D4ib supernova candidate on a relatively bright host, acquired with FORS1 on the VLT, at maximum light. The redshift $z = 0.704$ is unambiguously obtained from the 6800 Å (observer frame) jump due to the galaxy spectrum, confirmed by two H narrow absorption lines at 7000 Å (H- δ) and 7400 Å (H- γ). A simultaneous fit to the measured spectrum and the light curves of the event is carried out using the SALT2 model (§8.3.2), where the spectrum is modelled as the sum (red line) of a galaxy (blue line) and SN Ia templates. On the right, the SN spectrum obtained by subtracting the best fit galaxy template (S0, blue curve on the left) from the measured spectrum, compared to the fitted SN Ia model spectrum (red line). This spectrum displays a broad absorption (characteristic of SNe) around 3800 Å restframe, attributed to CaII, and was identified as a SN Ia because the general shape of the spectrum leaves no ambiguity at this phase (known from photometry). Figure reproduced with permission from [192].

7.4. Measuring light curves and photometry techniques

The collection of photometry points along the SN light curve can be carried out with a small field instrument provided there are enough stars in the images to serve as photometric and geometric anchors. As indicated above, surveys targeting high redshifts now use the repeated imaging approach and hence do not need dedicated and pointed imaging observations.

Supernova photometry consists in measuring the flux of the supernova in the survey images. Since one cannot spatially separate the light of the supernova from that of its host galaxy, images of the field before the supernova explosion or at least one year after are usually required for this task. Explicit or implicit subtraction of these supernova-free images from supernova-on images is generally necessary. Rolling searches obtain these supernova-free images within their core programme if they monitor the same field for at least two years.

Astronomical photometry involves two measurements: one has to measure the source of interest and some standard stars with the same instrument. So, astronomical photometry indeed delivers flux ratios, and we will discuss the calibration of the standards themselves in §9.1. For ground-based observations, the transparency of the atmosphere has to remain sufficiently constant between both sets of observations for the calibration process to deliver anything useful, and astronomers label a night as “photometric” if the ensemble of standard stars observed throughout the night indicates comparable atmospheric extinctions. In order to salvage non-photometric (or uncalibrated) observations of supernovae, one can rely on the assumption that stars in the same images as the supernova are on average non-variable. The task of SN photometry hence consists in delivering the flux ratio of the supernova to neighbouring stars, and the calibration process will have to deliver, once and for all, the flux ratios of these neighbouring stars to some standards. Space-based photometry can rely on the usually excellent long-term stability of the instruments and may follow a simpler calibration path (see e.g. §2.1 in [195]).

For faint sources, photon shot noise constitutes, in practice, the main source of measurement uncertainty, and one will seek a statistically optimal flux estimator, in order to maximize the number of measured events within a fixed observing time allocation. In fact, observing times are usually tailored to deliver some predefined signal-to-noise ratio, assuming an optimal flux estimator. Since both the supernova and surrounding stars are point sources, they have the same spatial shape, namely the Point Spread Function (PSF), which can be modelled on each image using bright stars. One can model the SN observations as a time-variable point source at a fixed position on the sky, possibly on top of a non-varying galaxy. Fitting such a model to the image series delivers statistically optimal estimators of the flux at all epochs, together with their covariance matrix. Practically validated implementations of a simultaneous fit to an image series are described in at least two instances [196, 197], where the latter avoids image resampling. Other approaches to SN photometry are bound to be statistically less or as efficient, as stated by the Cramèr-Rao inequality.

Statistical efficiency is usually not a serious concern for nearby supernovae and the subtraction of supernova-free images from follow-up images with subsequent photometry proves to be sufficient for statistical uncertainties to be subdominant (see e.g. [98]).

Measuring point sources using their shape is referred to as PSF photometry, and is obviously adversely affected by im-

perfections of the PSF model. However, flux ratios are not affected by imperfections of the PSF model, as long as the latter enters in the same way into both terms of the ratio. This is not the case for standard PSF photometry, optimized to fight shot noise (e.g. [198]), which makes the ratio of faint to bright stars depend on the fidelity of the PSF modelling. In contrast [106, 196], one might use for all brightnesses the flux estimator optimal for faint stars. Faint sources are still optimally measured, flux ratios become independent of the PSF fidelity, and fluxes are linear functions of the data. One might indeed regard the latter as a requirement when measuring fluxes for luminosity distances.

One important concern for PSF flux measurement of faint sources is that fitting simultaneously flux and position involves a flux bias at low signal to noise (see e.g. appendix B in [106]), which might have a non-negligible impact when supernovae become faint. The obvious remedy consists in fitting a single common position to all images and even to all bands. In order to limit systematic biases of flux ratios, one should then enforce the same constraint for measuring fluxes of the surrounding stars. For surveys spanning several years, one may have to account for proper motions of stars [197].

One might have noted that SN measurements involve explicit or implicit subtractions, while star measurements do not. This difference might systematically bias flux ratios. For this reason and for mere method validation, supernova photometry is commonly verified by inserting artificial supernovae (either synthetic, or copies of real stars) into real images, in order to bound the bias of recovered flux ratios below dominant systematic uncertainties [196, 197, 199]. Rolling searches allow one to measure pre-explosion SN fluxes, and checking that those average to zero indicates that galaxy fluxes are properly subtracted [106, 197].

Although astronomers usually report magnitudes, it is mandatory that light curves points are reported in flux space, because some low-S/N measurements unavoidably happen to be negative, and retaining those is mandatory for flux estimates to remain unbiased. For the same reason, light curve fitters should operate in flux space [109, 114, 200], but might report their results in magnitudes (as commonly done).

8. LIGHT CURVE FITTERS, DISTANCE ESTIMATION

8.1. K-corrections

In order to compare supernovae, their fluxes have to be expressed in the same way, and in particular using the same restframe bands. Different supernovae are generally not measured using the same photometric setup: first, since the quality of cosmological constraints improves with redshift lever arm, nearby and distant supernovae are measured with different telescopes and hence different spectral bands. Second, even if all supernovae were measured using the same telescope, the filters used for the measurement map differently in the supernova restframe when the redshift varies. We hence need to somehow transform the photometric measurements carried out with an arbitrary setup into what some well-defined instru-

ment, not necessarily real, would have measured.

In the astronomical literature, transforming photometric data obtained with some filter into what would have been measured with some other filter is called K-correction. It is usually presented as a magnitude correction and was originally designed to place galaxies on a Hubble diagram [201]; these galaxies were measured in similar filters but at different (and moderate) redshifts. The principle is simple (e.g. equation (B7) in [201]): correct the flux measurement $f(T_2)$ by a multiplicative factor computed using an assumed spectrum and the involved band passes:

$$f(T_1) = f(T_2) \frac{\int S(\lambda) T_1(\lambda) d\lambda}{\int S(\lambda * (1+z)) T_2(\lambda) d\lambda} \quad (6)$$

where T_2 is the transmission function of the filter that was used for the measurement, T_1 is the transmission function of the filter that would have been used ideally, and S is the assumed restframe spectrum of the object (at redshift z). Originally, the concept was developed in a framework where T_1 and T_2 denote the same band. Obviously, the transformation depends more and more on the knowledge of S as the overlap between $T_1(\lambda)$ and $T_2(\lambda/(1+z))$ decreases. Note that the actual spectrum of the object is generally not known, because if it were, the required flux would be extracted from this spectrum, or spectra would even be compared directly. So, we are dealing with some approximation of the spectrum, and we will now discuss how the K-correction depends on inaccuracies of this spectrum.

Let us consider a supernova at $z = 0.05$: transforming the measurements from the observer filter to the same restframe involves a filter shift of 1.05, while standard filters have a relative width (width of the bandpass over central value) of about 0.25 (see Fig 1). It means that the numerator and denominator of equation 6 overlap for about 80% of their values, and hence the correction does not depend too much on the precise knowledge of S . This is the situation that prevails for low-redshift samples (e.g. [121]). At $z \approx 0.25$, the overlap between $T_1(\lambda)$ and $T_1(\lambda/(1+z))$ becomes essentially null, but using the next redder filter as T_2 restores essentially a full overlap. For example, using the standard UBVRI filters (figure 1), $V(\bar{\lambda} = 5450)$ is a very good approximation of restframe $B(\bar{\lambda} = 4350)$ at $z = 0.25$. So, as common sense indicates, the measurement filter should follow as much as possible the red-shifted target filter. This gives rise to the cross-filter K-correction concept proposed in [202], where T_1 and T_2 are assumed to be different (in the same frame). When K-corrections are expressed in magnitudes, transforming for different filters introduces an additional term accounting for the different definition of magnitudes in the involved bands.

The worst case for K-corrections happens roughly when $T_1(\lambda)$ and $T_2(\lambda/(1+z))$ overlap by about half of their width: then about half of the flux in the target filter has to be derived from the assumed spectrum. In [203], a detailed study of K-corrections for supernovae concludes that rather than trying to obtain detailed knowledge of the SN spectrum, one should first pay attention to the spectrum broadband slope (i.e. colour), which varies from supernova to supernova. The

scheme proposed in [203] consists in tilting a template spectrum in order to reproduce a measured colour, and then using this tilted spectrum to compute K-corrections. One can note that to first order, the details of how the spectrum is tilted do not matter. In order to apply this tilting scheme, one has to measure an SN colour, which happens to be essentially mandatory for distance estimation.

The Supernova Factory survey (§ 11.1) collects spectro-photometric SN “light curves”, or photometric spectral sequence, thus eliminating the need for K-corrections of any kind when comparing supernovae.

8.2. Brighter-bluer relation and extinction

Astronomical observations in the visible are essentially *always* subject to some sort of extinction, generally by dust. For example, the Milky Way contains dust, and extragalactic observations (including supernova measurements) have to be corrected for Milky Way dust extinction, nowadays using the maps derived from dust emission in the far infrared [204].

The extinction by dust has been characterized mainly in the Milky Way [205]. By comparing colours of stars of the same spectral types, but affected by different line-of-sight extinction, the authors could derive an empirical “extinction law” (called CCM law after Cardelli, Clayton and Mathis) which relates extinction at various wavelengths. The total extinction is found by extrapolating the found wavelength dependence to a null photon energy. The first obvious parameter that characterizes a line of sight will then be its optical depth, i.e. the amount of absorbing or scattering medium. This is conventionally parametrized (and in particular in [205]) by the reddening of the $B - V$ colour (defined in §3). Naming $E(B - V)$ the colour excess attributed to dust, the extinction (in magnitude) at a given wavelength reads $A(\lambda) = E(B - V) * R(\lambda)$, where $R(\lambda)$ is the “extinction law”, directly related to the cross section of photons on the dust. Once $R(\lambda)$ is known, one may deduce the line-of-sight extinction from the reddening of colour. Identical objects extinguished by different amounts of intervening dust exhibit colours which lie along lines in colour-colour spaces.

The dust extinction law should depend on the nature of the intervening dust and [205] proposes a one-parameter family of extinction curves, parametrized by $R_V \equiv R(\lambda_V)$. The Milky Way dust is characterized on average by $R_V = 3.1$.

SNe Ia exhibit a brighter-bluer relation (see e.g. [119] and references therein), as one would expect from dust, and also exhibit a strong correlation of colour relations [109, 206], which constitutes a tantalizing analogy. However, this justifies parametrizing the colour variations of supernovae in the same way as dust extinction, but does not *impose* the assumption of CCM extinction laws. As we will discuss later, supernovae allow one to carry out a similar analysis as the one done to derive CCM extinction laws, in order to derive an average colour law for supernovae. Using then the standard candle property of SNe Ia, one can extract the equivalent of R_V from the supernova data. One should note that in order to measure an SN colour, one has to carry out measurements in at least

two bands.

8.3. Supernova empirical light curve models

We are now in a position to express some minimal requirements of supernova models used to “compress” the photometric data characterizing an event: in order to derive a distance we need a brightness (anything that scales linearly with the observed flux), some measure of the decline rate and some measure of colour.

If the measurements are dense enough along the light curve, there is no crucial need for an explicit model, which was the approach originally followed for the Δm_{15} paradigm [102]. From well-sampled light curves, one can build smooth discrete templates with different Δm_{15} values, where this quantity indexes the decline rate measured as the magnitude difference between peak and 15 (restframe) days later. An interpolation scheme (figure 1 of [207]) allows one to fit possibly sparse observations. Templates have been continuously refined [110, 208–210]. The Δm_{15} model was in particular used in the Calan-Tololo survey analysis ([8, 121], §11.1), and one of the acceleration discovery papers ([10], §11.2). Recently, the Snoopy model [211] revisited the Δm_{15} paradigm and extended it to NIR.

Light curve templates for standard visible and NIR bands were determined in [206], mainly to assess the empirical reproducibility of SNe Ia, and could then be used to fit SN photometry. In order to account for the decline-rate variation, the “stretch” paradigm [103] proposed to stretch the time axis of these templates in B and V standard bands (§3). As data improved in size and quality, these templates were refined and extended to the U -band [104, 195]. The stretch paradigm works poorly for bands redder than R . The stretch approach was used in one of the accelerated expansion discovery papers ([11], §11.2). All the models sketched above rely on light curve templates in standard bands.

The Bayesian Adapted Template Match (BATM) method [212] relies on about 20 well-measured events (spanning a decline-rate range) and about 100 spectra to predict the observed light curves in a given instrument at a given redshift, for a given extinction. Using an extinction prior, it eventually delivers a distance estimate, sensitive to the prior choice. It was used to extract cosmological constraints from the first large SN compilation [212].

Currently, there are two main streams of SNe Ia empirical models in the visible used to derive cosmological constraints: MLCS on the one hand, SALT, SALT2 and SiFTO on the other, and we will now describe those.

8.3.1. The MLCS model

The Multi Light Curve Shape (MLCS) model consists in a one-parameter family of light curve shapes for standard visible bands $BVRI$ (i.e. from 400 to 900 nm, figure 1). This complete model of SN light curves depends on three parameters (plus a reference date): a distance modulus, a brightness

offset (due to the brighter-slower relation, which indeed indexes light curve shapes), and an extinction value (in the V -band). At variance with essentially all other SN light curve models (BATM is another), MLCS incorporates the brighter-slower and brighter-bluer relations, which imposes to train it on events at known distances [95, 213]. The initial modest training sample of 12 events (by 1995) was later enlarged to about 100 events (around 2002) and the model extended towards the blue by adding the U -band (320-400 nm) [214]. This second version is named MLCS2k2. Prior to fitting, measurements have to be translated into standards restframe bands using K-corrections.

The MLCS(2k2) model assumes that extinctions follow some known distribution [95] (the “extinction prior”), which is not mandatory but improves the formal uncertainty of colour measurements (figure 4 of [95]) and enforces positive extinctions. The derivation of this prior in [214] is sometimes described as a *statistical* separation of intrinsic (internal to the supernova) and extrinsic (due to dust extinction) colour variations, which means that there is no separation on an event per event basis. This statistical separation only matters for the shape of the prior. The other assumption of the model is that after accounting for colour variations correlated with light curve shape, the average colour relations are due to extinction by dust, similar to the average Milky Way dust.

Both of these assumptions have been extensively discussed: first, the extinction prior can bias distances (as argued in, e.g., [195], appendix of [11]). Reference [200] shows from simulations that distances are unbiased if the prior faithfully reproduces the actual extinction distribution, and the accuracy of colour measurements is accurately known. This distribution is, however, not known from first principles, and one should expect some difference between the assumed and actual distributions, but in a cosmological context, a difference only matters if it is redshift-dependent. So, using a prior assumes at least that the SN population at all redshifts is drawn from the same parent population, possibly with a redshift-dependent selection function (§2.3 of [215], §5.1 of [200]). Note that as any other light curve model, MLCS can be used without any extinction prior. We will discuss the Milky Way extinction dust hypothesis in §8.3.5.

8.3.2. SALT and SALT2 models

SALT [108] models supernova light curves by integrating a spectral template (i.e. a spectral energy distribution as a function of SN phase) into properly shifted observer filters. It implements the light curve width variability mostly using the “stretch” paradigm (§8.3 and [103, 104]). The training consists in reproducing photometry of a training sample by adjusting a broadband phase-dependent correction to a spectral time series from [203]. The colour variations are modelled as an extinction factor $\exp(-cC_l(\lambda))$ multiplying the flux, where c is the colour parameter of each supernova, and $C_l(\lambda)$ is the “colour law”, common to all supernovae. It is fitted during the training, and found to be poorly compatible with extinction laws. There is no assumption on the source on colour

variations and colours that might reflect negative extinctions are accepted. Note that, even if colour variations induced by extinction are one-sided, the measured colour value is still an unbiased estimate of true colour (e.g. §5.2 in [216]). The SALT spectral template spans [300,800] nm, which covers the restframe U -band, as required to fit high-redshift data from the Supernova Legacy Survey, for which SALT was initially developed. As a spectral template, SALT incorporates K-corrections into the model. SALT does not attempt to model distances, and hence any sufficiently well-measured supernova can enter the training sample. SALT parameters are m_B^* , the peak brightness in restframe B -band, s , the stretch factor, and c , the (restframe) $B - V$ colour at maximum, plus some time reference.

SALT2 is a further development of SN spectral templates [106, 114]: the variability of spectra (and broadband light curves) of supernovae is modelled using principal component analysis (PCA), and the whole spectral model and its variability is fitted from a set of training spectra and light curves. As in SALT, the “colour law” is fitted to the data (and found again incompatible with known extinction laws). The first variability component found is extremely similar to stretch (or decline rate) and no significant further component is found. Because SALT2 does not model distances, it can incorporate high-redshift events in its training sample, and doing so allows it to go as blue as 250 nm, i.e. bluer than accessible from the ground using low-redshift events. SALT2 delivers the average spectral model and its first variability component, the colour law, the uncertainties, and some estimate of the intrinsic variability of supernovae around these averages. SALT2 finds that broadband light curve amplitudes scatter (coined “colour smearing” in [200]) by at least 2.5% around the average model, with a rapid increase when going bluer than ~ 360 nm. At variance with all other SN models, SALT2 training actually determines spectral sequences, but the large number of required parameters constitutes the main limitation of the model. This flexibility of the training process imposes the necessity to resort to some regularization scheme in order to actually define the template in regions of the phase/wavelength/decline-rate space poorly covered by the training sample. SALT2 delivers a model uncertainty.

8.3.3. The SiFTO model

SiFTO [109] models SNe light curves from a SED template, constructed through a smooth correction of the empirical template from [217]. The light curve shape variability is accounted for using the stretch paradigm, using a measured relation between stretch factors in different bands. When fitting a supernova event SiFTO adjusts a phase-independent multiplicative function of wavelength in order to match exactly the measured light curve amplitudes. The obtained mangled SED is then used to evaluate the light curve amplitudes in the standard $UBVR$ bands plus a bluer band, covering in total [250,710] nm. This set of restframe magnitudes readily provides an overall amplitude m_B^* , and a single $B - V$ colour derived from an optimal combination of all measured restframe

colours. This combination relies on restframe colour-colour diagrams obtained during the training, which also delivers a model uncertainty, used when fitting. As SALT and SALT2, SiFTO does not predict distances and can then use any well-measured event for training. Its small number of parameters makes its training easy and precise. As SALT and SALT2, SiFTO finds colour relations (e.g. $U - B$ versus $B - V$) incompatible with extinction by dust, even allowing for a coloured variation of supernovae related to stretch.

8.3.4. Tripp distance estimators

SALT, SALT2 and SiFTO do not directly deliver distances. All propose (but do not impose) to estimate distances using the most general distance estimator linear in decline rate s (e.g. stretch) and colour c :

$$\mu = m_B^* + \alpha(s - 1) - \beta c + \text{Const} \quad (7)$$

where μ is a distance modulus estimate (i.e. it varies as $5 \log_{10}(d_L)$ up to an additive constant), α and β are global parameters that characterize, respectively, the brighter-slower and brighter-bluer relationships. These parameters have to be empirically determined, typically along with the cosmological parameters, as proposed by Tripp in [119]. m_B^* refers to the peak magnitude that would be observed in the filter matching B restframe, where the choice of B is arbitrary. For most cosmological SN analyses, the measurements are actually carried out around the B restframe band and the distance uncertainty is dominated by the βc term. Assuming that colour variability at a fixed decline rate is due to Milky Way like dust sets $\beta = R_B = 4.1$.

The most common criticism to SALT, SALT2 and SiFTO is that the reported colour parameter mixes both intrinsic colour variations (slower supernovae tend to be bluer) and extrinsic ones (e.g. dust extinction), and the distance estimator defined in equation 7 conflates both effects via a single brighter-bluer coefficient β (e.g. §2.1 of [215], §2 of [136]). This is suboptimal if there are two or more sources of colour variations with different β values, but more importantly biases cosmology if the admixture building up the colour distribution evolves with redshift. Let us first assume the extra source of colour variation is entirely related to decline rate: assuming we know the relation, we can then separate the contributions to colour for each event. To first order, this separation does not change the form of equation 7, but only alters the value of α (β is unaffected, see § 4.1.1 in [108], §4.2.3 in [106]). Hence, accounting for decline rate related colour variations does not change distances evaluated using equation 7. So, this criticism assumes that there are at least two contributions to colour variations, independent of the decline rate. This is a serious concern that can only be handled via more parameters per event and hence applies to all current photometric distance estimators.

8.3.5. Comparing light curve fitters

SALT2 and MLCS2k2 were compared thoroughly in [200], which finds that they deliver systematically different distances as soon as they make use of the restframe U -band ([320,400] nm). This difference in distances has a dramatic effect on cosmological fits, and is traced to two causes: different predicted U -band peak values at given B and V and the effect of the MLCS2k2 extinction prior on high-redshift ground-based events from the SNLS sample (see §11 of [200]). When MLCS2k2 uses SALT2 light curve templates, and does not apply any extinction prior, the cosmological results become essentially as when using SALT2 right away. So, [200] argues that some unidentified issue with the low-redshift observer-frame U -band seriously affects MLCS2k2, and accounts for the difference with SALT2 as a systematic uncertainty. On a similar data set, [218] identifies that observer-frame U -band SN data are incompatible with higher redshift measurements of the same restframe spectral region, and ignores this chunk of data.

Regarding restframe U -band, the difference between MLCS2k2 and SALT2 models lies in their training strategy: while MLCS2k2 has to train restframe U from observer-frame U SN data, SALT2 (and SiFTO) use higher redshift events (typically at $z \sim 0.2 - 0.5$) to model restframe U -band. Observer-frame U is notoriously difficult to calibrate because the actual shape of the bandpass is determined by the variable atmospheric absorption⁵. This difficulty is illustrated, in the supernova framework, by the observed dispersion of the restframe U -band light curve amplitude, which is much larger for nearby events (where restframe U is measured from observer U) than for higher redshift events (where redshift pushes restframe U into regions unaffected by the atmosphere (see figure 11 in [196], §2.6 in [218]). For MLCS2k2, dropping the observer-frame U -band at training implies that the resulting model misses restframe U -band, which is unacceptable: all modern SN models insist on modelling near UV SED of supernovae, because distances to many high-redshift events rely on this modelling.

In [200], the second source of MLCS2k2/SALT2 difference is traced to the use of an extinction prior for high-redshift SNLS events. The fact that applying or not the extinction prior to a measurable quantity (the event colour) questions the prior (as discussed in §8.3.1), and dropping the prior is technically possible. We also note that for samples of several hundred events, the uncertainties associated with the choice of the prior (table 7 of [215], figure 32 of [200]) are larger than the statistical uncertainties. Finally, as events are better and better measured, the statistical benefit from constraining their parameters a priori is vanishing.

Colour variations independent from decline rate are typically assumed to be due to extinction by dust or not. In this second case, both colour relations (the colour law) and

⁵ Correction of the absorption by the Milky Way dust might also be large in observer U -band, and correspondingly uncertain [204].

the brighter-bluer coefficient (β of equation 7) should be extracted from the data. In [200] (§11), it is shown that inserting the fitted SALT2 colour law into MLCS2k2 has no sizable effect on MLCS2k2 distances. Fitted brighter-bluer coefficients are generally smaller than those for Milky Way dust (see e.g. [119] and references therein, [108]). The finding from MLCS2k2 distances that we might be at the centre of a “Hubble bubble” [214] (i.e. a spherically symmetric under-density) was shown to be a consequence of assuming rather than fitting the brighter-bluer relation [136, 219].

In [136], one can find a comparison of SALT, SALT2 and MLCS, but the SALT and SALT2 packages were probably not used properly: using the same photometric data, supernova fits differ from the ones published by the authors of the packages. In [215] SALT and MLCS2k2 were compared and found to agree very well. This is not very surprising as their training samples vastly overlap. In [106], SALT2 and SiFTO are compared using exactly the same event sample and the found differences are acceptable for a few hundred events.

Comparing the scatter of the resulting Hubble diagram yields useful comparisons of distance estimation strategies. For large and similar samples, table 11 in [200] exhibits rms Hubble residuals of 0.21 mag (about 10% in distance) using MLCS2k2, while SALT2/SiFTO combined distances deliver about 0.17 mag (table 4 of [218]).

SALT2 and SiFTO are compared in [106] on exactly the same distant events, and SiFTO outperforms SALT2 by a small but significant amount, 0.150 versus 0.173 mag.

8.4. Other distance estimators

Most distance estimators proposed for SNe Ia follow the form of equation 7. We review here two notable exceptions.

The so-called “Bailey ratio” [220] was optimized to obtain the best distance estimator from a sample of 58 photometric spectra from the SuperNova Factory (§11.1). It uses the flux ratio of two narrow spectral regions $F(642 \text{ nm})/F(443 \text{ nm})$ as a single intrinsic luminosity estimator, and achieves a smaller Hubble diagram scatter than all other known distance estimators on the same sample. This good performance remains unexplained, and was confirmed using long slit spectra of nearby events [113]. Note that at $z > 0.6$, most of the current SN spectra do not cover the 642 nm region, although the Si line characteristic of SNe Ia is around 615 nm.

The CMagic distance estimator [221] makes use of the post-maximum trajectory of SNe Ia in the colour-magnitude ($B-V, B$) plane, in order to evaluate the brightness when a given colour is reached. The obtained brightness is then corrected for brighter-slower relation to yield distances, which exhibit a reduced scatter with respect to other distances, on the nearby training sample. The technique was applied to a cosmological analysis [222] and proved to be applicable to high-redshift events, provided that the latter are measured in bands close to restframe B and V , a demanding constraint. The performance improvement on this sample is not large enough to compensate for the loss in event statistics due to the requirements in phase and wavelength coverage.

9. PHOTOMETRIC CALIBRATION

9.1. The traditional way

Stellar fluxes are essentially always measured relative to some other star. The ratio of the studied object flux to a standard star is commonly reported as a magnitude. In order to measure luminosity distances, one has to convert magnitudes into fluxes, relying on a star that has both magnitudes (in the same system as the standard) and a spectrum in physical units; one also needs to know the pass bands of all involved photometric measurements.

In order to report fluxes from relative measurements, one obviously needs primary calibrators, in practice non-variable stars with known spectrum. Establishing the spectrum of Vega (or α -Lyrae) is described in [223], where the astronomical instrument is calibrated against artificial black bodies (or sources themselves calibrated to black bodies). As Vega is far too bright to be measured in most modern instruments⁶, anchoring photometry of $m \simeq 20$ objects to Vega ($m = 0$) goes in practice (see §8.1 in [224]) through two steps: the Landolt star network [225, 226] ($< m > \simeq 12$), referenced to Johnson [227] and Cousins [228] standards ($< m > \simeq 5$), themselves referenced to Vega [229]. Although this lengthy sequence was not conducted to ensure a robust conversion of magnitude to fluxes, all supernova cosmology works until 2006 calibrate supernova magnitudes against Landolt stars and convert those to fluxes using the Vega spectrum (usually from [223]), because they had no alternative. One should note that the Landolt system is not a natural system (§8.1 in [224]), meaning that the reported magnitudes are not directly measured, but rather derived from actual measurements and colours, and hence that the filters defining the reported magnitudes are unclear. The networks of standard stars were designed to allow astronomers to precisely compare magnitudes of stars, but allowing one to convert these magnitudes to high precision fluxes was not a primary goal.

A new and shorter path to convert magnitudes into fluxes was designed in the framework of the HST flux calibration: the Calspec project⁷ reports spectra measured from the HST and carefully cross-calibrated. The instruments used to gather these spectra are flux-calibrated from stellar models of pure hydrogen white dwarfs (references in [230]). The models make use of temperatures and gravity obtained from Balmer line shapes from ground-based high-resolution spectroscopy. The consistency with the calibration route sketched in the above section was checked by bravely measuring Vega in the same programme [231]. As a few Calspec standards now have broadband magnitudes in the widely used Landolt system [232], the numerous SNe Ia distances calibrated on this system now have a direct link to this spectral library. The overall flux scale of the Calspec library is set to match ground-based photometry, and dominates the uncertainty budget at

⁶ A SN Ia at $z \sim 0.1$ typically peaks at $m_B \simeq 20$, i.e. 10^{-8} times Vega.

⁷ <http://www.stsci.edu/hst/observatory/cdbs/calspec.html>

about 2% [233], but is irrelevant for cosmology with SNe Ia. Because the ratio of fluxes of supernovae at different redshifts depend on the ratio of fluxes of the standards at different wavelengths, the “colour uncertainty” of the spectral library is, in contrast, extremely relevant to our subject. Two terms dominate this uncertainty: the model slope (dominated in the visible by temperature uncertainty), and the reproducibility of the Calspec measurements. Both terms are estimated to typically 0.5% or less (table 12 in [224]) for the measurement of the star BD +17 4708 from [234].

9.2. Instrumental calibration from calibrated laboratory sources

Using artificial sources to calibrate instruments is not a modern idea (see e.g. [223] and references therein). Suggestions to calibrate imagers from artificial light sources have been recently formulated [235], relying on photo-diodes calibrated by the US NIST. Results from a setup delivering a monochromatic illumination of a screen in the telescope dome are provided in [236]. However, reflections on the numerous optical surfaces in front of wide-field imagers (typically at least three lenses, one filter and the cold chamber window) contribute to the image obtained with a flat-field screen, but not to star photometry. For the specific case of the MegaPrime instrument on CFHT, direct evidence for these internal reflections is provided in [237]; [224] evaluates to about 10% or more their contribution to twilight images. This justifies proposing a different artificial light source setup in [237, 238]. The most recent results presenting calibration from an artificial source [239] are encouraging but do not yet outperform the stellar approach.

There are great expectations from these illumination devices since most ground-based wide-field survey instruments either own one or plan to install one. We can sketch plausible outcomes of current efforts roughly ordered in increasing difficulty and reward: daily monitoring of the instrument response, measuring the bandpass profiles in situ, establishing a flat-field correction, measuring the relative transmission of photometric bands, or even absolute transmission of photometric bands.

9.3. Ground-based observations and atmospheric extinction.

The canonical procedure to evaluate atmospheric extinction consists in following sources at various elevations and extrapolating above the atmosphere, or more commonly around zenith. One then relies on repetition to beat down atmospheric variability. A more precise technique, relying on spectroscopy and atmospheric extinction models is implemented in [240].

Atmospheric extinction is less critical when calibrating from stellar standards, and again, repeating the calibration of stars around supernovae over tens of nights allows one to mitigate the atmospheric variability (e.g. [224]). Ground-based rolling supernovae searches incorporate these calibration observations in their programme.

9.4. Linearity issues

Since standard stars are much brighter than tertiary stars, themselves often brighter than supernovae, one should wonder whether the reported signals scale as fluxes. One first varies the exposure time from typically 1 s to a few hundred seconds, in order to compare different brightnesses in the same electronic range. Precise shutter timing is required for CCDs and can be obtained (see e.g. §12.1 in [224]). The overall linearity of CCDs and their readout electronics can be checked on the sky (App. C in [224]), alleviating concerns that quasi-uniform illumination (“flat fields”) might not be representative of the instrument response to stars. CCDs in space suffer from charge transfer inefficiency that builds up with the integrated radiation dose, alters linearity, and should be corrected for (e.g. [195, 241]). Observations with the NICMOS NIR instrument on HST suffer from a poorly understood non-linearity issue, which adversely affects fluxes, and hence distances to high-redshift supernovae obtained with this instrument (see § 5.1.3 in [218]).

9.5. Prospects for improvements

As calibration constitutes the leading systematic uncertainty of current supernova cosmology results [218, 242], improving over the present situation is mandatory. The weaknesses of the Landolt system [218, 224] have a decreasing impact as new supernovae calibrated via alternative paths are published: for example, the SDSS [197] directly ties its magnitudes to solar analogues with CALSPEC spectra. Some pass bands of the CSP nearby sample [98, 243] are calibrated to the Smith magnitude catalogue [244], which is now anchored as well to CALSPEC standards. The calibration of instruments against laboratory standards can provide a significant breakthrough, provided that parasitic reflections in the optics are controlled well enough and atmospheric extinction accurately measured. These two complications vanish if the artificial light source is mounted on a satellite, as proposed in [245].

10. ASTROPHYSICAL SYSTEMATIC UNCERTAINTIES AFFECTING SN DISTANCES

10.1. Evolution of supernovae

Evolution of supernovae refers to the concept that supernovae could be different at high redshift (i.e. early in the stellar history) than at low redshift. We already know that a demographic evolution exists (§5.3), and our concern here is to constrain if supernovae exhibiting the same observables could have a different average brightness at low and high redshifts: the derivation of distances used for the cosmological analysis makes the hypothesis that it is not the case. One set of tests compares properties of nearby and distant samples, and the other set compares properties of events at similar redshifts in different environments, i.e. different stellar ages.

10.1.1. Light curve rise time

Reference [161] proposes the approximate rule that the maximum (bolometric) luminosity equals the instantaneous energy released by β and γ decays. This relates the rise time, peak luminosity and produced ^{56}Ni mass, so that a change in rise time at a given nickel mass implies a change in peak brightness. Rise times at a given decline rate hence constitute a plausible handle on intrinsic peak brightness. Even without theoretical guidance, the rise time of the light curve is sensitive to the explosion energy and the evolution of the opacity of the ejecta, and any evolution of rise time with redshift unrelated to usual decline-rate indicators is a direct threat to relative distances, as they are evaluated from a single light curve shape modelling.

In order to measure rise times accurately, authors devise methods that scale the actual measurement of the rise time to that of the fall time, so that variations of the decline rate do not smear out the measurement. Three studies [89, 104, 105] do not detect any sizable difference between distant and nearby samples. One might note, however, that different studies find different average rise time values because of different definitions, and/or different fiducial supernova. Reference [246] discusses some difficulties of the measurement and closes a dispute caused by the troublesome comparison of rise time determinations obtained through different estimators. Rise times are also compared as a function of the “stellar age” of the host galaxy and they turn out to be in excellent agreement (table 2 in [89]).

10.1.2. Spectroscopic evolution tests

Comparisons of supernova spectra across redshifts appear in the very first SN cosmology papers (e.g. figure 11 in [10]). Quantitative comparisons involving line velocities [247], line velocities and profiles [248], line velocities and strengths [249] did not reveal compelling differences.

More detailed comparisons with increasing statistics are presented in [250], where global agreement is found, with perhaps some small differences in line strengths, however, without subtraction of the host galaxy light. Studies of samples of similar size [115, 116, 251] do not confirm these small differences, but they carry out galaxy light subtraction.

High-redshift samples allow one to study the UV part of the spectrum (below ~ 350 nm) absorbed by the Earth’s atmosphere for nearby events, and deemed to encode metallicity of the progenitor, although theoretical predictions disagree on the sense of the effect [252, 253]. These high-redshift studies agree on a event-to-event scatter increasing towards blue wavelengths (figure 7 in [114] shows the same trend using photometry only), and stress that comparison at wavelengths below ~ 350 nm lack a nearby counterpart, which is nowadays being collected from space. A first sample of 12 events [254] shows reasonable agreement in the UV part with events at $z \sim 0.5$ and mildly suggests that the observed differences might reflect sampling variance. The large observed variability in UV, probably due to metallic features [254], suggests

that cosmological analyses aiming at higher and higher precision limit their use of restframe UV (below ~ 350 nm) to measure distances to high-redshift supernovae.

To summarize, when differences between nearby and distance spectra are observed, they can usually be interpreted as the already known demographic evolution, i.e. that explosions tend to be more energetic as redshift grows.

10.1.3. Segregation according to host galaxy types

In order to compare brightnesses (or even derived distances) of events at different stellar ages, one can take advantage that varying stellar ages cohabit at the same cosmological age. For example, the local Universe hosts both young stellar systems (and even galaxies producing stars), as well as old evolved heavy elliptical galaxies. One can then question whether we derive identical average distances to events at the same redshift but in different environments, thus directly addressing the heart of the evolution question without strong assumptions on the distance-redshift relationship. Comparisons between spiral and elliptical galaxies reported null differences (e.g. §5.3 in [199], [255]). Many works test the effects of host galaxy metallicity (see §1. in [256]), and report null results, with the exception of [257] which only tests a small sample of early-type hosts. A first indication of systematic difference of distances as a function of the host galaxy stellar mass was proposed in [258], and confirmed on independent samples by [128, 132], and could perhaps be attributed to systematic differences in metallicity. Note that the galaxy stellar mass is inferred from the wide-band photometry of the host galaxy, a by-product of light curve measurements, and hence the effect is easily corrected for. Ignoring this brightness difference of $\sim 8\%$ between low and high stellar-mass hosts would bias the dark energy equation of state w by ~ 0.04 to 0.08 (table 9 in [132]).

10.2. Gravitational lensing of supernovae

Gravitation bends light rays along the transverse component of the gravitational potential gradient (e.g. [259, 260]). Mass concentrations act somehow as lenses, which coined this class of phenomena. Cosmic bending of light rays re-maps the image plane, which alters the brightness, shape, size and position of sources. In the framework of supernova observations, the gravitational lensing of supernova light by foreground mass contrasts induces two main effects: an increased scatter of the observed brightness, and when going through strong lenses, the possibility of multiple images of the same event, usually with different time delays. Strong lenses are characterized by a singular mapping of the source plane onto the image plane, leading to an infinite magnification on critical lines, and the possibility of multiple images (see e.g. [259, 261]). The lines of sight subject to critical lines are very scarce and the vast majority of supernovae incur asymptotically weak lensing. Because supernovae are point sources, their geometrical

shape is unaffected by lensing, but their brightness follows the optical magnification.

Lensing of supernovae causes an extra scatter of their apparent brightness: the rare events observed through a mass concentration will appear brighter, while the bulk of the events (going through under-dense regions) will be slightly fainter than the average. Lensing conserves the average intensity [262], and does not constitute a first-order threat on luminosity distance measurements [263]: the mass density that is probed through these measurements is the actual average density, rather than that of a smooth component⁸. Strong lensing might violate flux conservation in the case of several images where one or more escapes detection. This is commonly investigated through numerical simulations (e.g. [264–266]), and as expected, the result strongly depends on the assumptions on the “clumpiness” of matter distribution. Monte-Carlo techniques also face practical difficulties in re-summing multiple images that would be merged by an observer [265, 266]. Fortunately, one may use systematical searches for multiple images of distant radio sources [267], in order to evaluate an upper bound to the average amount of flux lost in faint secondary images of supernovae: in [196] (§7.6), it is found that at $z = 1$, less than 0.3% of the flux is lost to secondary images. This is far below other systematic uncertainties, both for present and foreseen SN surveys. Note that for very large statistics SN surveys, the frequency of multiple images becomes measurable and this very small effect could even be estimated and corrected for.

The expected magnification distribution is significantly skewed [262, 264–266, 268, 269], because the magnification decays very rapidly with the impact parameter to a lens. So, even if the average flux is not altered by lensing, the average magnitude is, and its distribution is no longer Gaussian: least-squares estimates from high-statistics Hubble diagram fits made in magnitude space can be biased. In [269], it is shown that the maximum likelihood (rather than least squares) delivers unbiased cosmological parameters, even for several thousands of events up to $z \sim 1.7$.

The extra brightness scatter due to lensing also broadens distance residuals and degrades the cosmological inferences. Again, different simulations using different assumptions on the clumpiness of matter lead to different conclusions: while [270] find an extra magnitude scatter of $\sim 0.09 \times z$, [265] find 0.04 at $z = 1$ for smooth halo profiles.

Evidence of weak lensing of supernovae by foreground structures was obtained recently, by correlating the Hubble line residuals of individual events with the magnification expected from the foreground galaxies [271], and also shows that the amplifications agree with the expectations from measured mass contrasts. Stronger detections are only expected from increased statistics. From the same sample of events, [272] extracts weak constraints on dark matter halos. We also have evidence for a supernova at $z \simeq 0.6$ experiencing strong

magnification by ~ 3.6 (1.4 mag.) through a foreground galaxy cluster at $z = 0.18$ [273].

Lensing of supernovae will not probably limit the cosmological accuracy of future high-statistics and high-precision SN surveys. For large-scale SN surveys (typically targeting 10^4 to 10^5 events) lensing will open two new avenues: constraining the shape of dark matter halo from correlation of Hubble residuals with properties of the line of sight (see [271, 272] and references therein); large surveys will also detect multiple images of strongly lensed events, where an accurate measurement of the distance, flux ratio and time delay of the images provides valuable cosmological information, assuming the lenses can be accurately modelled (e.g [274] and references therein). One should note here that any kind of high-redshift time-variable source is eligible for this type of study, typically any type of bright enough supernova, and to a lesser extent quasars. However, the “standard candle” property of SNe Ia allows one to determine the lensing magnification factors (rather than their sole ratio), which breaks some degeneracy between the lens potential and the Hubble constant [275]. Simulations conducted in [276] indicate that the prospect for finding multiply imaged supernovae are modest for a possible space mission (about 10 events), where the ground-based LSST project would find $O(100)$ events in its 10-year mission; the same space mission would measure time delays of about 20 multiply imaged quasars, while LSST would measure several thousands.

11. SN SURVEYS AND THEIR COSMOLOGICAL FINDINGS

We review here the main SNe Ia surveys. Table I lists the main event samples we will present in the following sections. We will start with nearby SN samples (typically $z < 0.1$) used in essentially all analyses. Most analyses presenting new events also incorporate events from pre-existing samples. For exhaustive lists of SNe Ia samples, we refer to compilations, rapidly presented in §11.6.

11.1. Nearby samples

“Nearby” here broadly refers to samples at $z \lesssim 0.1$, but at $z \gtrsim 0.01$, because smaller redshifts are too contaminated by Doppler shifts due to proper motions. Practically, the photometry and spectroscopy of these events are mostly carried out using respectively, 1 and 2 m class telescopes. There are no practical examples of cosmological constraints derived without a nearby sample, because it increases the redshift lever arm, and decouples the nuisance parameter $\mathcal{L}H_o^2$ (see §2.3) from cosmological parameters.

While wide-field imagers make it easier and easier to find and measure distant supernovae, nearby events are still difficult to find. As discussed above, the Calan-Tololo nearby survey delivered the first well-measured sample [9] found from photographic plates. The Lick Observatory Supernova Search (LOSS) [283] has been a key provider of nearby events for

⁸ The most common parametrizations of gravitational magnification are obtained perturbatively, thus miss the large-angle de-magnification, and hence do not conserve the average brightness.

Name	z range	N_{events}	Dates	N_{bands}	$\$$	References
Calan-Tololo	< 0.1	29	90-93	4	11.1	[8, 9, 121]
HZT	[0.2,0.6]	10	95-97	2	11.2	[10, 199, 277]
SCP	[0.2,0.8]	42	92-97	1-2	11.2	[11]
SCP (HST)	[0.4,0.8]	11	97-00	2	11.3	[195]
SN-Goods (1&2)	[0.3,1.5]	37	02-05	2-3	11.4	[29, 278]
SNLS (1&3)	[0.2,1.0]	242 (~400)	03-08	3-4	11.5	[106, 196, 218, 242]
ESSENCE	[0.3,0.7]	60 (~200)	02-06	2	11.5	[215]
SN-SDSSII	[0.1,0.4]	103 (~500)	05-07	3-5	11.5	[200, 279]
CFA (1,2 & 3)	<0.1	185	01-08	4-5	11.1	[280-282]
CSP nearby	<0.1	85 (129)	04-09	5-8	11.1	[98, 243]

TABLE I. SN surveys presented in the following sections. N_{events} is the number of reported events, possibly followed by the anticipated size of the final sample, in parentheses. N_{bands} indicates the number of different bands these events were measured in. A fair fraction of CSP events was measured in NIR, which makes 8 bands in total.

about 15 years, and mostly targets galaxies not in the Hubble flow, but also delivers events in the Hubble flow.

The Harvard Center for Astrophysics (CfA) has produced three releases [280–282] of spectra and light curves of nearby events discovered by both professionals and amateurs. With 185 events, the last release (CfA3) constitutes the largest homogeneous sample to date, with systematic calibration uncertainties evaluated to 3% (a probably pessimistic value according to [218]). The CfA data set has recently been complemented by a massive release of spectra [284], which will significantly contribute to training of light curve fitters.

The Carnegie Supernova Project (CSP) also follows up detections from professionals and amateurs. It released two batches [98, 243] of high-quality light curves reaching a total of 85 events among which 70 have NIR light curves.

Regarding distance measurements the merits of the various samples are evaluated in detail in [218] (§2.3 and 5.1.2), and turn out to be comparable after strict quality cuts. The issues related to the U-band of nearby supernovae are discussed as well in the same work (§2.6) and the conclusion is that the U-band measurements of the CfA and the CSP are incompatible, and the latter agree with colours of higher redshift events.

The SuperNova Factory aims at collecting several hundreds of spectro-photometric spectral sequences of SNe Ia [285], using its own blank-field search. The reduction of spectra is very involved and sequences have not yet been released. A low-scatter distance estimator relying on photometric spectra has been proposed (§8.4 and [220]).

When events are used for cosmology, one should evaluate the distance bias caused by the search and identification steps possibly missing faint events (the so-called Malmquist bias). For a nearby sample, only the average distance bias matters for cosmology, and when caused by a sharp flux limit, its value does not depend on the value of this limit and only mildly depends on the shape of the cut (§7.4 in [196] and §2.7.1 in [218]). Different works find slightly different bias values, from 4% ([11]) down to 2.7% ([196])) mainly because of different assumed values of the brighter-bluer relation. Whether this flux limit model applies to a given sample can be tested through the phase of the first measurement of the found events

[11, 218].

11.2. The SCP and HZT pioneers: the twin papers

In the mid 1990s, two groups embarked on the measurement of distances to high-redshift supernovae (typically $z \sim 0.5$), the Supernova Cosmology Project (SCP) and the High-Z team (HZT). The first campaigns allowed the teams to refine the search strategy, and the “batch discoveries” of 1995 (§7.1) define the start of systematic programmes. From there on, time allocation committees awarded observing time to both teams on a regular basis. Both teams even gained access to the HST for photometric follow-up of their supernovae.

The SCP produced an early analysis of 7 high-redshift events [103], which when compared with the Calan-Tololo nearby sample mildly favoured a matter-dominated Universe assumed to be flat. The quality of distances was very poor, and some events lacked spectroscopic identification. The HZT presented an early sample of 4 distant events among which 3 are measured by the HST [286], and found $\Omega_M \simeq 0.3 \pm 0.3$.

Both teams were in fact building up larger samples, and published their twin analyses [10, 11] a few months apart. The SCP analysis [11] presents 42 distant events, mostly with poor colour measurements, and uses 17 nearby events (from the Calan-Tololo survey [9]). The used distance estimator ignores colour, however, after eliminating reddened events and having checked that the distant and nearby samples have the same average colour and understood spreads. The HZT analysis [10] makes use of 10 distant events and has colour measurements for 9 of them, but colours are used through an extinction prior, which limits their impact⁹. It also makes use of 27 nearby

⁹ The average distance modulus uncertainty without a prior would be ~ 0.38 from the uncertainty of peak magnitudes, while the average reported the uncertainty of distance modulus is 0.18 (without intrinsic dispersion). This together with the fact that more than half of the events hit the prior hard limit $A_V = 0$ indicates that the weight of the colour measurements in the distance estimation is modest.

events mostly from the Calan-Tololo survey, and finds similar results using two different distance estimators (which, however, share the same extinction prior). Both distant samples exhibit similar photometric quality in restframe B -band with an average photometric uncertainty of the light curve amplitude of 0.07 mag. The SCP sample has poor or even missing restframe V -band measurements. Those from the HZT compare well with their restframe B -band, but however do not deliver a precise enough colour that might enter a distance estimator without a prior. A Hubble diagram combining both sets is shown in figure 6.

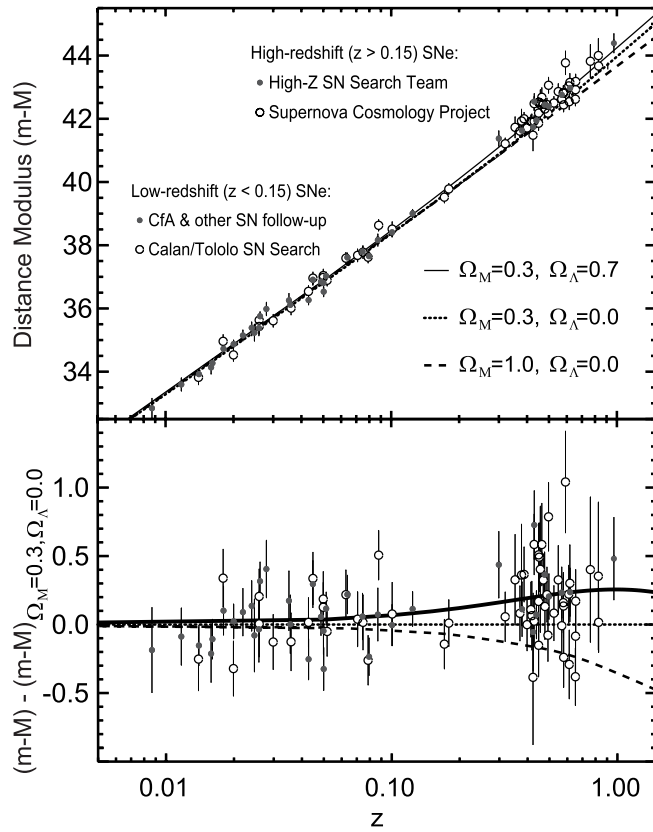


FIG. 6. Combined Hubble diagram (logarithm of a distance versus z) from the twin papers (top), and residuals to a $\Omega_M = 0.3, \Omega_\Lambda = 0$ cosmology (bottom). The fit favours the thick line over the two other proposed hypotheses. Note that the HZT events have more precise distances than those from the SCP. Reproduced from [287], with permission.

Both teams fitted their data to an Ω_M, Ω_Λ Universe and found extremely similar best fits and contours: $Prob(\Omega_\Lambda > 0) > 99\%$, a flat matter-dominated Universe was excluded at more than 7σ , $\Omega_M = 0.28 \pm 0.10$ for a flat Universe. Fitting a matter density with $\Omega_\Lambda = 0$ drives Ω_M negative for both analyses, a certainly uncomfortable situation, which strongly suggests acceleration. Both teams reported a long study of systematic uncertainties, and did not find room for large offsets: the SCP reported a systematic uncertainty roughly half of the statistical one.

The significance of a non-zero cosmological constant was

in fact modest, typically 3σ or less, but there were two of them, however statistically correlated because they share a great part of their nearby samples. The significance of acceleration is even smaller. But taking the confidence levels at face value, matter-dominated universes with $\Omega_M > 0.2$ were excluded at more than 4σ by each analysis.

Both teams also explored variants of the cosmological constant by replacing it by a fluid X with unknown equation of state w (i.e. w is the ratio of pressure to density, see §2.1), so that $\rho_X(z) = \rho_X(0)(1+z)^{3(w+1)}$. In a flat Universe, both analyses [11, 277] found similar and almost degenerate contours, which can be roughly approximated by $\Omega_X w = (1 - \Omega_M)w \simeq -0.72 \pm 0.1$.

These twin papers are usually regarded as the original key evidence for an accelerated expansion, and Saul Perlmutter (SCP), Adam Riess and Brian Schmidt (HZT) were awarded the 2011 Nobel Price in Physics for this discovery.

11.3. First Hubble Space Telescope samples

Both pioneering analyses illustrate that the colour measurement quality is the Achilles' heel of distance measurements, because both teams could not use the bare colour measurements in their distance estimation. Measuring accurate light curves and accurate colours with the HST seems an efficient response to this limitation and HST photometric follow-up of ground-based searches started in 1997. One event from the SCP sample has HST measurements and three events from the HZT sample [286].

The SCP team delivered [195] the first cosmological analysis in 2003 where distances to high-redshift events use bare measured colours, from a mixture of 11 new HST well-measured events and ground-based ones. Interestingly, three ways of inserting colours in the distance estimator are compared (figure 9 of [195]):

1. ignoring colours on a low reddening sample (as in the SCP original paper);
2. applying a one-sided extinction prior (as in the HZT original paper);
3. using bare measured colours.

One realizes that with the third approach, the events with HST colour measurements totally dominate the obtained cosmological constraints, which are slightly worse than the ones drawn in each of the twin papers. The “ground-based” events alone deliver very poor constraints if their bare colour measurements are used.

Among these different approaches, one is not necessarily right and the others wrong; the different obtained cosmological constraints rather reflect different hypotheses. In the first method, one should check (as done in SCP original analysis [11]) that the average colour of distant and nearby events agrees, but if the uncertainty in the difference between the average colour of both samples is propagated to the end of the analysis, one gets the same uncertainties as with the third

method. So, not propagating this uncertainty relies on the assumption that both samples have the same average colour, and that the measured difference reflects sampling variance, provided however that it is compatible with zero. The second method assumes that the colour distribution itself does not vary with redshift, i.e. that events at all redshifts are drawn from the same parent population (possibly with selection biases, see §8.3.1). So, the first method assumes identical colour averages, the second identical (or known) colour distributions and the third makes no assumption. The third method is robust to unknown redshift-dependent selection biases or demographic evolution, which should generally be expected to some level.

This 11-event sample of [195] also illustrates wavelength coverage issues: these events were measured in R and I filters (namely F675W and F814W of WFPC2), which map almost exactly on restframe B and V at $z \simeq 0.5$ but on U and B at $z \sim 0.75$. The colours of three events at $z > 0.7$ could only be measured by a comparison with $U - B$ of nearby events, but there were very few nearby events to compare, and the restframe $U - B$ versus $B - V$ colour relation was logically the dominant uncertainty of the study (table 9. of [195]). Later, the $U - B$ versus $B - V$ restframe relation was first established in [108] from nearby events from [281], and then using distant events [109, 114, 196].

11.4. HST searches

In 2002, the Advanced Camera for Surveys (ACS) was installed on HST, and opened the possibility of finding faint high-redshift events with HST. The first harvest of supernovae detected with this instrument reported 16 events [29] (complemented by 2 from [288]) among which 8 at $z > 1$. The identification came from a mixture of ground-based spectroscopy, ACS low-resolution slit-less spectroscopy, and typing from light curves. The highest redshift light curves are measured in the NIR using NICMOS aboard HST, using the F110W ($[0.8, 1.4]\mu\text{m}$) and the F160W ($[1.4, 1.8]\mu\text{m}$) filters. This work gathers all SN Ia events available by late 2003, selects a “gold” sample and estimates distances in a consistent way, using MLCS2k2 (§8.3.1) with an extinction prior. Taking advantage of the increase in the redshift lever arm offered by the $z > 1$ events, the key conclusion of the paper is to provide evidence for past deceleration, a distinctive feature of dark energies similar to Λ . The analysis thus eliminated some dust models as alternatives to the cosmological constant. A standard cosmological fit yield an the equation of state parameter w very close to -1 (i.e. Λ) with a precision of ~ 0.16 .

A second round with 22 more events was published 3 years later [278], using a better characterization of NICMOS (the key instrument for events at $z > 1$), establishing that the photometric response of the instrument is non-linear. Uncertainties on corrections are not propagated in the analysis, but however cause sizable distance uncertainties common to all high-redshift events (see e.g. §5.1.3 of [218] for details). The cosmological analysis concentrates on variable equation of state fits, concludes that the data do not require $w \neq -1$, and also

indicates that $w(z > 1) < 0$ at $\sim 98\%$ CL. However, the determination of $w(z > 1)$ still has a variance of order 1 or more.

More HST events have been collected or published in the last few years within different programmes. The six events (two at $z > 1$) presented in [289] have HST data. The HST Cluster Supernova survey targets high-redshift galaxy clusters in rolling search mode, in order to increase the SN yield with respect to blank fields [290]. Recently, the programme delivered accurate distances to 14 SNe [291] among which 10 are at $z > 1$. The CLASH+CANDELS SN programme runs a rolling search with the new WFC3-IR imager, targeting high-redshift events mostly in galaxy clusters. It recently delivered an accurate distance to an event at $z = 1.55$ [292].

Although the redshift coverage of HST samples is unique, they now have a modest weight in cosmological fits of the latest compilations, which typically gather several hundred events (see e.g. [242], and §11.6).

11.5. Ground-based rolling searches: ESSENCE, SNLS, and SDSS-II

The ESSENCE, SNLS and SDSS-II SN surveys are second-generation “high-redshift” surveys. They all aim at a significant increase in both the amount and the quality of well-measured high-redshift SNe Ia, in order to constrain the dark energy equation of state. They all worked in the rolling search mode (§7.1), i.e. image repeatedly the same pointings and extract detections and photometry of the events from the same image sequence. All three surveys benefited from large guaranteed multi-year allocations for their imaging data. They spectroscopically identified their candidates and measured redshifts using 4 and 8 m class telescopes.

The ESSENCE survey [293] ran at the CTIO 4-m (Northern Chile) on the 0.36 deg^2 Mosaic-II imager. It monitored in R and I bands 36 pointings (i.e. $\sim 10\text{deg}^2$) every fourth night, for a 3-month observing season, over 5 years (2003-2008). The 2002 season was essentially lost to weather and technical problems.

The SNLS survey [196] ran at the CFHT 3.6 m in Hawaii, equipped with the Megacam 1 deg^2 imager. It monitored 4 pointings in g, r, i and z bands every fourth to fifth night, as long as they remained visible from 2003 to 2008. The observations were part of the CFHT Legacy Survey¹⁰ (CFHTLS) and were aiming also at galaxy studies in the very deep stacked images.

The SDSS-II Supernova Survey [197] used the SDSS 2.5-m telescope at Apache Point (new Mexico), with its original 1.52 deg^2 imaging camera. It monitored a 300 deg^2 equatorial stripe every second night for 3 months per year in u, g, r, i and z bands.

The deepest survey is SNLS, which delivered usable light curves at $z > 1$, thanks to ~ 40 mn exposures in the red bands, with good IQ. Then comes ESSENCE, which used 200- and

¹⁰ <http://www.cfht.hawaii.edu/CFHTLS>

400-s exposures at a similar cadence, and is thus limited to $z \lesssim 0.7$. SDSS took advantage of its fast scanning camera and used 54 s exposures and thus efficiently addresses the $0.1 \lesssim z \lesssim 0.4$ “redshift desert” where regular point-and-stare imaging with large telescopes is inefficient. ESSENCE and SNLS use similar instrumentation and have made opposite choices: ESSENCE went for a wide survey in order to obtain the smallest statistical uncertainty on w [293], while SNLS was limited to four deep pointings by the observing time allocation mechanism. It turned out that both surveys found about twice as many events than they could possibly identify within their sizable spectroscopic observing time allocations.

SNLS has produced its first [196] and third [106, 218, 224, 242] year analyses. The first year analysis gathers 44 high quality nearby events and compares those to 71 SNLS distant events, using distances estimated with SALT (§8.3.2). Constraining supernova restframe $U - B$ versus $B - V$ colour relation is performed using the distant sample (measured in more than 2 bands), where it is found to be much better defined than in nearby samples. A constant equation of state fit to this data set yields $w = -1.02 \pm 0.09(\text{stat}) \pm 0.054(\text{syst})$, a result compatible with Λ and systematic uncertainties dominated by photometric calibration issues. The third year SNLS analysis uses a much larger sample of strictly selected events (table 1. in [218]): 123 nearby events, 242 SNLS events, 93 from the first year SDSS sample, and 14 HST events (see figure 7). The systematic uncertainties correlate events and the introduced covariances are propagated to the cosmological fits, and delivered with the data [218]. The light curve fitters (SALT2 and SiFTO §8.3.2 & 8.3.3) training uses distant events in order to model the UV behaviour of supernovae [109, 114], which improves the distance scatter at $z > 0.8$ by about a factor of 2. For a flat Universe, a constant equation of state fit to the supernovae data, CMB, and BAO yields [242] $w = -1.068 \pm 0.08(\text{stat} + \text{sys})$, where statistics contributes 0.054. Again, systematics are totally dominated by several photometric calibration limitations (table 3 of [242]). Some could be overcome in a joint analysis with the SDSS full sample. Fits allowing a variable equation of state $w(z) = w_0 + zw_a/(1+z)$ yield $w_a = -0.98 \pm 1.1$ compatible with 0. These cosmological fits are fully compatible with the cosmological constant hypothesis (figures 8 and 9).

ESSENCE has produced its fourth year analysis [215, 293] which presents 60 new events at $z \lesssim 0.7$. These events are analysed using MLCS2k2 (§8.3.1), and considerable care is devoted to choosing the prior¹¹, which incorporates provision to compensate selection biases, because the images are shallow. A constant equation of state fit yields $w = -1.05 \pm 0.12(\text{stat}) \pm 0.13(\text{syst})$. The uncertain choice of the extinction prior dominates systematics (0.08), followed by the possible existence of a “Hubble bubble” (0.06) and the restframe $U - B$ versus $B - V$ relation (0.06). These three main contributions could be reduced.

The SDSS-II SN survey has produced its first year analysis [197, 200] with 103 new events at $0.04 < z < 0.42$. The pre-

sented analysis gathers nearby samples, the SNLS first year, ESSENCE and HST samples. As already discussed (§8.3.5), the core of the cosmology paper [200] is a comparison of the outcome of MLCS2k2 and SALT2 frameworks, which finds alarmingly different cosmologies. We just repeat here (§8.3.5) that the main causes of the discrepancy are identified as the restframe $U - B$ versus $B - V$ relation (likely induced by photometric calibration issues of the training sample), and the effect of applying or not an extinction prior to the SNLS sample. Both can be settled (and indeed are), and hence do not threaten the use of supernovae as distance indicators. This detailed and alarming comparison of approaches was sometimes interpreted as a general failure of supernova cosmology. Alternatively, one might argue that both the ESSENCE [215] and SDSS [200] analyses have convincingly demonstrated that uncertainties associated with the choice of an extinction prior are now too large for the present sample sizes.

Distances to 35 SDSS, ESSENCE and SNLS supernovae at $0.2 < z < 0.7$ were measured in the restframe I-band (i.e. in NIR for observers) and with different systematics, confirm the findings of the parent surveys [216]: $w = -1.05 \pm 0.13(\text{stat}) \pm 0.09(\text{sys})$.

None of these second-generation surveys has finalised its full-sample analysis yet, but efforts on cross-calibrating the surveys are on-going, in order to tighten the relative flux scales. Because of their multi-band coverage, SNLS and SDSS are expected to produce a precisely cross-calibrated sample. In this scenario, nearby samples will not benefit from an improved SNLS-SDSS cross-calibration and their weight in the determination of cosmological parameters will be diminished.

11.6. Supernova compilations

There is no example of a single survey delivering interesting supernova constraints on its own: covering a large redshift range requires different instruments generally operated within different projects. Compilations of supernovae primarily target the production of cosmological constraints and mainly consist in producing a coherent set of distances, possibly with their systematic uncertainties. In most of the cases, compilations present some new events. By delivering state-of-the-art and homogenized collections of events, these compilations receive a lot of attention from users primarily interested in cosmology constraints.

In [212], a new distance estimation method (BATM) is compared to MLCS2k2 and two versions of Δm_{15} , and found to be “generally consistent”. Using a combined distance, 172 events are then placed on a Hubble diagram, and the cosmological conclusions strengthen earlier findings. In [29], events found and measured with the HST (see §11.4) are merged into a large compilation, ranking events into gold and silver samples, analysed using MLCS2k2. The *Union* sample [294] consists of 307 events selected from more than 10 sources and analysed using SALT. The analysis accounts for systematic uncertainties, in particular photometric calibration, and delivers correlated uncertainties. This compilation was augmented

¹¹ The same data set is analysed with a different extinction prior in [200]

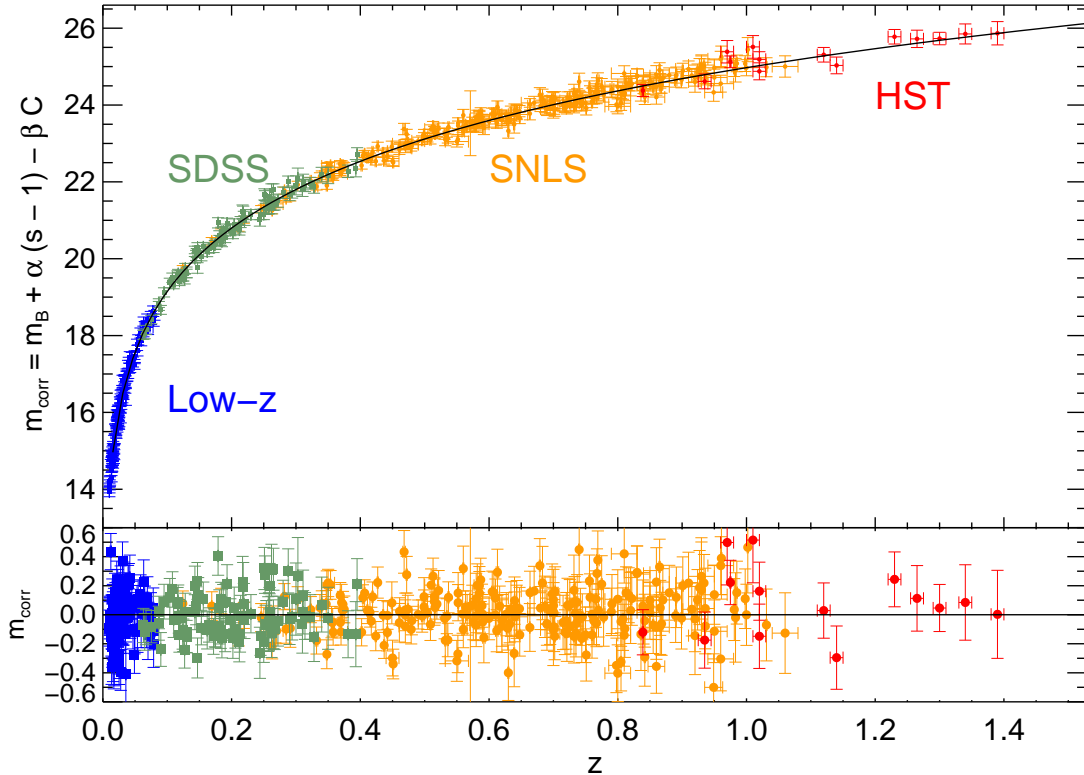


FIG. 7. One of the latest SNe Ia Hubble diagrams (logarithm of distance versus z), which gathers well-measured events by 2010. The lower plot displays residuals to the best fit cosmology. A comparison with figure 6 shows that distance uncertainties and scatter of high-redshift events were almost halved in about 10 years. Reproduced from [218], with permission.

into the *Union 2* compilation [289], mainly adding the SDSS (§11.5) and CFA3 (§11.1) samples, and reaches 557 events fitted using SALT2, again evaluating systematic uncertainties in a correlated fashion. The *Union 2.1* compilation [291] adds 23 events, in particular 14 HST events among which 10 are at $z > 1$. The *Union (1)* compilation was also augmented into the *Constitution* compilation [136] by the addition of the CFA 3 nearby SNe sample, analysed using MLCS2k2, SALT and SALT2. As noted in §8.3.5, the comparison of light curve fitters conducted there is very likely affected by an improper use of SALT and SALT2.

12. PROSPECTS FOR SUPERNOVA COSMOLOGY

The fact that statistical and systematic uncertainties contribute similar amounts to current cosmological constraints from supernovae forces new supernova survey projects to rely on new setups. Three fronts are usually simultaneously pursued: increasing the number and quality of events, improving the quality of the photometric calibration and collecting higher redshift events.

One should note that essentially all supernovae events in-

volved in cosmological analyses to date have been spectroscopically confirmed. Given that samples already on disk amount today to about 1000 events usable for cosmology, future SN imaging surveys should target at least a few thousand well-measured events. Spectroscopic identification of such a large sample lies beyond likely allocations on large-aperture telescopes. Recent practical studies of photometric identification (i.e. from light curves) propose techniques to reach a purity of about 95%, with an efficiency still greater than that of spectroscopic identification [295–297]. The required quality of redshifts is still debated, and “after the fact” multi-object spectroscopy of host galaxies constitutes the most obvious way to secure high-quality redshifts. So, broadband photometry of supernovae should aim in the future at providing both distances and identification, and possibly even redshifts [298, 299]. Regarding dark energy constraints, all current wide-field imaging large-scale projects aim at combining probes, typically cluster counts, weak shear correlations, BAOs, and distances to supernovae. Two reports [300, 301] have reviewed in detail the scientific and technical merits of these probes and note that distances to supernovae is the most mature. Both reports also stress that the potential reach of each probe at constraining dark energy primarily depends

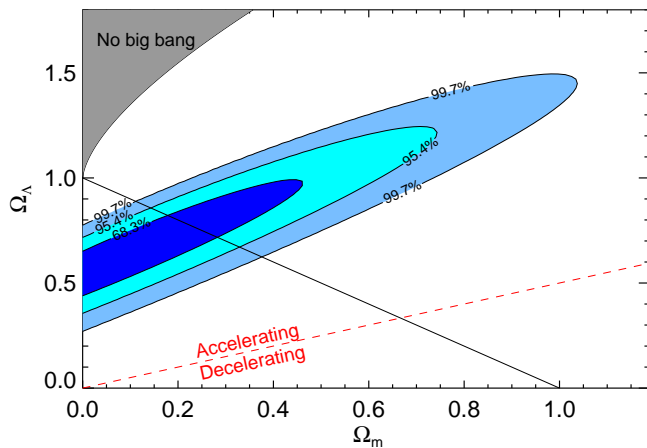


FIG. 8. Statistical constraints from supernovae alone (figure 7) on $(\Omega_m, \Omega_\Lambda)$ cosmological models, including systematic uncertainties. Reproduced from [218], with permission.

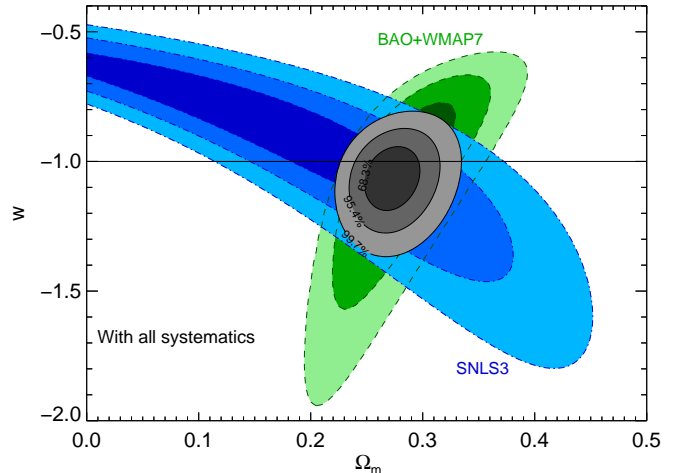


FIG. 9. Statistical joint constraints on (Ω_m, w) flat cosmological models from supernovae of figure 7 (blue contours including systematics), CMB and BAOs (green). The joint contours (grey) favour models close to a cosmological constant, i.e. $w = -1$. Reproduced from [242], with permission.

on systematic uncertainties, which especially for forecasts are highly uncertain, and strongly suggest a multi-probe approach. Coming back to results, one might note that five years after these reports, dark energy constraints are still dominated by supernova distances.

12.1. Space missions concepts

Although several mission concepts to measure supernovae from space were developed in the last decade, none has yet passed the selection processes. Working from space is mandatory at $z \gtrsim 1$, because reliable distances should then be measured in the NIR, in order to allow a direct comparison with nearby events measured in blue bands. Ground-based measurements in the NIR suffer from both a very bright atmospheric emission and a sizable and time-variable atmospheric extinction. Space also offers a very good image quality and a stable environment, which both significantly improve photometric measurements with respect to ground.

Euclid at ESA is an approved dark energy project, to be launched in 2019, but has no compelling supernova programme yet: regarding dark energy, the project concentrates on measuring galaxy shapes for weak lensing and conducting a (spectroscopic) galaxy redshift survey in NIR for BAOs [47], on about one third of the sky. It will also deliver NIR imaging in three bands of the surveyed fields. The WFIRST project at NASA is not yet approved and contains a high-redshift supernova programme, targeting a few thousand events.

Project	Mirror ϕ (m)	Area (deg 2)	First light	Large survey (nights)
CFHT/Megacam	3.6	1.	2002	500
Pan-STARRS	1.8	7.	2009	>1000
Blanco/DEC	4.0	3.	2012	500
Subaru/HSC	8.2	1.8	2013	~500
LSST	6.5	10.	2019	3500

TABLE II. Key figures for the major past and future wide-field imaging facilities. The SNLS survey was part of the CFHTLS large survey. Pan-STARRS is currently constructing a second telescope and aims at eventually operating four of them. The 500-night survey to be run at the CTIO-Blanco is called Dark Energy Survey (DES). LSST real diameter is 8.2 m but suffers from a 5 m central occultation. This facility will almost entirely observe in survey mode during its anticipated 10-year lifetime.

12.2. Ground-based SN projects

Planned ground-based SN surveys will enlarge the redshift span of Hubble diagrams (in particular compared with SNLS) by using thick high-resistivity CCD sensors (e.g. [302]), which typically deliver quantum efficiencies above 50% at 1 μm (while the silicon cutoff lies at 1.1 μm). Ground-based projects are including the four canonical dark energy probes in their science agenda. High-statistics Hubble diagrams with a high efficiency up to high redshifts ($z \sim 1$) is reserved to 4 and 8 m class telescopes. Table II summarizes the key figures of these projects.

For DES, the promises of the SN survey were published recently [303]: the available observing time will allow one to measure distances to about 4000 events at $z < 1.2$, and tentatively relying on photometric redshift of both host galaxies

and supernovae to build a Hubble diagram.

13. SUMMARY AND CONCLUSIONS

During the 1990s, distances to SNe Ia allowed observers to map the expansion history of the Universe, and led to the discovery that this expansion is currently accelerating. Dark energy has been inserted in the standard cosmological model as the fluid causing the acceleration, which has been confirmed independently of supernovae. Second-generation supernova surveys have delivered precise constraints on the “nature” of dark energy: the cosmological constant paradigm, corresponding to a dark energy of constant density, describes the data very well and leaves little room for dark energy density evolution. The Λ CDM cosmological model successfully describes large-scale cosmological observables, including those involving structure formation.

The nature of SNe Ia explosion is still questioned, and both progenitor scenarios have supporting evidence and face difficulties. The paradigm of a WD exploding when reaching the Chandrasekhar mass fulfills observational constraints, but is accepted by default of an alternative rather than observational evidence, the lack thereof being perfectly understood. Numerical explosion models broadly match observations, even if they still cannot replace empirical models used to fit observed light curves. Cosmology is expecting to gain insight into possible distance biases from the steady improvement of numerical SN models.

Several second-generation surveys have collected samples of a few hundred spectroscopically confirmed and well-measured SNe Ia events up to $z \sim 1$ over the last decade. This world sample amounts in total to about 1000 events and the

dark energy constraints already extracted from about one half of it ([242]) show that calibration and statistical uncertainties contribute similar amounts. Improving the photometric calibration, improving the survey design to make it less sensitive to calibration errors and increasing the statistics (in particular at the highest possible redshift) are the three main handles to improve over present constraints. Since spectroscopic identification of several thousand events involves too much observing time, broadband photometry should now also deliver identification of the events, which pushes for increased quality measurements. Constraints from other dark energy probes will, hopefully, soon become available and crossing results will tighten and secure the obtained dark energy constraints.

Future SN surveys are planned but only secured on ground-based facilities, although observing from space opens the possibility of measuring precise distances to supernovae at $z > 1$, a key handle on dark energy constraints. Ground-based imaging surveys and space-based imaging and spectroscopy surveys target high-quality dark energy constraints. For the next decade, the LSST (ground) and Euclid (space) projects are aiming at surveying most of the extragalactic sky, and expect to see their first light around 2020. Currently, only LSST plans to constrain dark energy from supernovae distances.

ACKNOWLEDGMENTS

Writing this review would have been impossible without numerous discussions with many colleagues, in particular C. Balland, S. Beaumont, M. Betoule, S. Bongard, J. Guy, D. Hardin, R. Pain and N. Regnault. It also benefited a lot from the remarks from the two anonymous referees. Several illustrations were borrowed from published papers and we are grateful to the original authors and publishers for granting their authorization to reproduce these figures.

-
- [1] Lemaître, G. Un Univers homogène de masse constante et de rayon croissant rendant compte de la vitesse radiale des nébuleuses extra-galactiques. *Annales de la Société Scientifique de Bruxelles*, 47:49–59, 1927 ([ADS](#)).
- [2] Lemaître, G. Expansion of the universe, A homogeneous universe of constant mass and increasing radius accounting for the radial velocity of extra-galactic nebulae. *MNRAS*, 91:483–490, March 1931 ([ADS](#)).
- [3] Hubble, E. A Relation between Distance and Radial Velocity among Extra-Galactic Nebulae. *Proceedings of the National Academy of Science*, 15:168–173, March 1929 ([ADS](#)).
- [4] Ostriker, J. P. & Tremaine, S. D. Another evolutionary correction to the luminosity of giant galaxies. *ApJ Lett.*, 202:L113–L117, December 1975 ([ADS](#)).
- [5] Kowal, C. T. Absolute magnitudes of supernovae. *AJ*, 73:1021–1024, December 1968 ([ADS](#)).
- [6] Kirshner, R. P. & Kwan, J. Distances to extragalactic supernovae. *ApJ*, 193:27–36, October 1974 ([ADS](#)).
- [7] Wagoner, R. V. Determining q_0 from Supernovae. *ApJ Lett.*, 214:L5+, May 1977 ([ADS](#)).
- [8] Hamuy, M., Phillips, M. M., Suntzeff, N. B., et al. The Hubble Diagram of the Calan/Tololo Type IA Supernovae and the Value of HO . *AJ*, 112:2398–+, December 1996, arXiv:astro-ph/9609062 ([ADS](#)).
- [9] Hamuy, M., Phillips, M. M., Suntzeff, N. B., et al. BVRI Light Curves for 29 Type IA Supernovae. *AJ*, 112:2408–+, December 1996 ([ADS](#)).
- [10] Riess, A. G., Filippenko, A. V., Challis, P., et al. Observational Evidence from Supernovae for an Accelerating Universe and a Cosmological Constant. *AJ*, 116:1009–1038, September 1998 ([ADS](#)).
- [11] Perlmutter, S., Aldering, G., Goldhaber, G., et al. Measurements of Omega and Lambda from 42 High-Redshift Supernovae. *ApJ*, 517:565–586, June 1999 ([ADS](#)).
- [12] Efstathiou, G., Sutherland, W. J., & Maddox, S. J. The cosmological constant and cold dark matter. *Nature*, 348:705–707, December 1990 ([ADS](#)).
- [13] White, S. D. M., Navarro, J. F., Evrard, A. E., & Frenk, C. S. The baryon content of galaxy clusters: a challenge to cosmological orthodoxy. *Nature*, 366:429–433, December 1993 ([ADS](#)).
- [14] Spergel, D. N., Bean, R., Doré, O., et al. Three-Year Wilkinson Microwave Anisotropy Probe (WMAP) Observations: Implications for Cosmology. *ApJS*, 170:377–408, June 2007,

- arXiv:astro-ph/0603449 ([ADS](#)).
- [15] Komatsu, E., Smith, K. M., Dunkley, J., et al. Seven-year Wilkinson Microwave Anisotropy Probe (WMAP) Observations: Cosmological Interpretation. *ApJS*, **192**:18–+, February 2011, 1001.4538 ([ADS](#)).
- [16] Goobar, A. & Leibundgut, B. Supernova Cosmology: Legacy and Future. *Annual Review of Nuclear and Particle Science*, **61**:251–279, November 2011, 1102.1431 ([ADS](#)).
- [17] Hillebrandt, W. & Niemeyer, J. C. Type IA Supernova Explosion Models. *ARA&A*, **38**:191–230, 2000, arXiv:astro-ph/0006305 ([ADS](#)).
- [18] Howell, D. A. Type Ia supernovae as stellar endpoints and cosmological tools. *Nature Communications*, **2**, June 2011, 1011.0441 ([ADS](#)).
- [19] Freedman, W. L. & Madore, B. F. The Hubble Constant. *ARA&A*, **48**:673–710, September 2010, 1004.1856 ([ADS](#)).
- [20] Frieman, J. A., Turner, M. S., & Huterer, D. Dark Energy and the Accelerating Universe. *ARA&A*, **46**:385–432, September 2008, 0803.0982 ([ADS](#)).
- [21] Weinberg, D. H., Mortonson, M. J., Eisenstein, D. J., et al. Observational Probes of Cosmic Acceleration. *ArXiv e-prints*, January 2012, 1201.2434 ([ADS](#)).
- [22] Smoot, G. F., Bennett, C. L., Kogut, A., et al. Preliminary results from the COBE differential microwave radiometers - Large angular scale isotropy of the cosmic microwave background. *ApJ Lett.*, **371**:L1–L5, April 1991 ([ADS](#)).
- [23] Hogg, D. W., Eisenstein, D. J., Blanton, M. R., et al. Cosmic Homogeneity Demonstrated with Luminous Red Galaxies. *ApJ*, **624**:54–58, May 2005, arXiv:astro-ph/0411197 ([ADS](#)).
- [24] Friedmann, A. Über die möglichkeit einer welt mit konstanter negativer krümmung des raumes. *Zeitschrift für Physik A Hadrons and Nuclei*, **21**:326–332, 1924. 10.1007/BF01328280.
- [25] Carroll, S. M., Press, W. H., & Turner, E. L. The cosmological constant. *ARA&A*, **30**:499–542, 1992 ([ADS](#)).
- [26] Etherington, I. M. H. On the Definition of Distance in General Relativity. *Philosophical Magazine*, **15**:761–773, 1933 ([ADS](#)).
- [27] Riess, A. G., Macri, L., Casertano, S., et al. A 3% Solution: Determination of the Hubble Constant with the Hubble Space Telescope and Wide Field Camera 3. *ApJ*, **730**:119, April 2011, 1103.2976 ([ADS](#)).
- [28] Goobar, A. & Perlmutter, S. Feasibility of Measuring the Cosmological Constant Lambda and Mass Density Omega Using Type IA Supernovae. *ApJ*, **450**:14, September 1995, arXiv:astro-ph/9505022 ([ADS](#)).
- [29] Riess, A. G., Strolger, L., Tonry, J., et al. Type Ia Supernova Discoveries at $z > 1$ from the Hubble Space Telescope: Evidence for Past Deceleration and Constraints on Dark Energy Evolution. *ApJ*, **607**:665–687, June 2004 ([ADS](#)).
- [30] Cattoën, C. & Visser, M. The Hubble series: convergence properties and redshift variables. *Classical and Quantum Gravity*, **24**:5985–5997, December 2007, 0710.1887 ([ADS](#)).
- [31] Durrer, R. The theory of CMB anisotropies. *Journal of Physical Studies*, **5**:177–215, 2001, arXiv:astro-ph/0109522 ([ADS](#)).
- [32] Seo, H.-J. & Eisenstein, D. J. Probing Dark Energy with Baryonic Acoustic Oscillations from Future Large Galaxy Redshift Surveys. *ApJ*, **598**:720–740, December 2003, arXiv:astro-ph/0307460 ([ADS](#)).
- [33] Blake, C., Kazin, E. A., Beutler, F., et al. The WiggleZ Dark Energy Survey: mapping the distance-redshift relation with baryon acoustic oscillations. *MNRAS*, **418**:1707–1724, December 2011, 1108.2635 ([ADS](#)).
- [34] Eisenstein, D. J., Zehavi, I., Hogg, D. W., et al. Detection of the Baryon Acoustic Peak in the Large-Scale Correlation Function of SDSS Luminous Red Galaxies. *ApJ*, **633**:560–574, November 2005, arXiv:astro-ph/0501171 ([ADS](#)).
- [35] Peebles, P. J. & Ratra, B. The cosmological constant and dark energy. *Reviews of Modern Physics*, **75**:559–606, April 2003, arXiv:astro-ph/0207347 ([ADS](#)).
- [36] Carroll, S. M. The Cosmological Constant. *Living Reviews in Relativity*, **4**:1, February 2001, arXiv:astro-ph/0004075 ([ADS](#)).
- [37] Weinberg, S. The cosmological constant problem. *Reviews of Modern Physics*, **61**:1–23, January 1989 ([ADS](#)).
- [38] Odom, B., Hanneke, D., D’Urso, B., & Gabrielse, G. New Measurement of the Electron Magnetic Moment Using a One-Electron Quantum Cyclotron. *Physical Review Letters*, **97**(3):030801–+, July 2006 ([ADS](#)).
- [39] Caldwell, R. R., Dave, R., & Steinhardt, P. J. Cosmological Imprint of an Energy Component with General Equation of State. *Physical Review Letters*, **80**:1582–1585, February 1998, arXiv:astro-ph/9708069 ([ADS](#)).
- [40] Wetterich, C. Cosmology and the fate of dilatation symmetry. *Nuclear Physics B*, **302**:668–696, June 1988 ([ADS](#)).
- [41] Ratra, B. & Peebles, P. J. E. Cosmological consequences of a rolling homogeneous scalar field. *Phys. Rev. D*, **37**:3406–3427, June 1988 ([ADS](#)).
- [42] Ferreira, P. G. & Joyce, M. Cosmology with a primordial scaling field. *Phys. Rev. D*, **58**(2):023503–+, July 1998, arXiv:astro-ph/9711102 ([ADS](#)).
- [43] Wetterich, C. Naturalness of exponential cosmon potentials and the cosmological constant problem. *Phys. Rev. D*, **77**(10):103505–+, May 2008, 0801.3208 ([ADS](#)).
- [44] Brax, P. H. & Martin, J. Quintessence and supergravity. *Physics Letters B*, **468**:40–45, November 1999, arXiv:astro-ph/9905040 ([ADS](#)).
- [45] Linder, E. V. Paths of quintessence. *Phys. Rev. D*, **73**(6):063010–+, March 2006, arXiv:astro-ph/0601052 ([ADS](#)).
- [46] Guzzo, L., Pierleoni, M., Meneux, B., et al. A test of the nature of cosmic acceleration using galaxy redshift distortions. *Nature*, **451**:541–544, January 2008, 0802.1944 ([ADS](#)).
- [47] Laureijs, R., Amiaux, J., Arduini, S., et al. Euclid Definition Study Report. *ArXiv e-prints*, October 2011, 1110.3193 ([ADS](#)).
- [48] Linder, E. V. & Huterer, D. Importance of supernovae at $z > 1.5$ to probe dark energy. *Phys. Rev. D*, **67**(8):081303–+, April 2003, arXiv:astro-ph/0208138 ([ADS](#)).
- [49] Jaekel, M.-T. & Reynaud, S. Tests of gravity at the solar system scale. *ArXiv e-prints*, July 2011, 1107.4987 ([ADS](#)).
- [50] Anderson, J. D., Laing, P. A., Lau, E. L., et al. Study of the anomalous acceleration of Pioneer 10 and 11. *Phys. Rev. D*, **65**(8):082004–+, April 2002, arXiv:gr-qc/0104064 ([ADS](#)).
- [51] Levy, A., Christophe, B., Béria, P., et al. Pioneer 10 Doppler data analysis: Disentangling periodic and secular anomalies. *Advances in Space Research*, **43**:1538–1544, May 2009, 0809.2682 ([ADS](#)).
- [52] Francisco, F., Bertolami, O., Gil, P. J. S., & Páramos, J. Modelling the reflective thermal contribution to the acceleration of the Pioneer spacecraft. *ArXiv e-prints*, March 2011, 1103.5222 ([ADS](#)).
- [53] Dvali, G., Gabadadze, G., & Porrati, M. 4D gravity on a brane in 5D Minkowski space. *Physics Letters B*, **485**:208–214, July 2000, arXiv:hep-th/0005016 ([ADS](#)).
- [54] Deffayet, C., Landau, S. J., Raux, J., Zaldarriaga, M., & Astier, P. Supernovae, CMB, and gravitational leakage

- into extra dimensions. *Phys. Rev. D*, 66(2):024019–+, July 2002 (ADS).
- [55] Fairbairn, M. & Goobar, A. Supernova limits on brane world cosmology. *Physics Letters B*, 642:432–435, November 2006, arXiv:astro-ph/0511029 (ADS).
- [56] Fang, W., Wang, S., Hu, W., et al. Challenges to the DGP model from horizon-scale growth and geometry. *Phys. Rev. D*, 78(10):103509–+, November 2008, 0808.2208 (ADS).
- [57] Amendola, L., Polarski, D., & Tsujikawa, S. Are f(R) Dark Energy Models Cosmologically Viable? *Physical Review Letters*, 98(13):131302–+, March 2007, arXiv:astro-ph/0603703 (ADS).
- [58] Bean, R., Bernat, D., Pogosian, L., Silvestri, A., & Trodden, M. Dynamics of linear perturbations in f(R) gravity. *Phys. Rev. D*, 75(6):064020–+, March 2007, arXiv:astro-ph/0611321 (ADS).
- [59] Amendola, L., Gannouji, R., Polarski, D., & Tsujikawa, S. Conditions for the cosmological viability of f(R) dark energy models. *Phys. Rev. D*, 75(8):083504–+, April 2007, arXiv:gr-qc/0612180 (ADS).
- [60] Buchert, T. On Average Properties of Inhomogeneous Fluids in General Relativity: Dust Cosmologies. *General Relativity and Gravitation*, 32:105–126, January 2000, arXiv:gr-qc/9906015 (ADS).
- [61] Marra, V., Kolb, E. W., & Matarrese, S. Light-cone averages in a Swiss-cheese universe. *Phys. Rev. D*, 77(2):023003–+, January 2008, 0710.5505 (ADS).
- [62] Vanderveld, R. A., Flanagan, É. É., & Wasserman, I. Luminosity distance in “Swiss cheese” cosmology with randomized voids. I. Single void size. *Phys. Rev. D*, 78(8):083511–+, October 2008, 0808.1080 (ADS).
- [63] Mukhanov, V. F., Abramo, L. R. W., & Brandenberger, R. H. Backreaction Problem for Cosmological Perturbations. *Physical Review Letters*, 78:1624–1627, March 1997, arXiv:gr-qc/9609026 (ADS).
- [64] Nambu, Y. Back reaction and the effective Einstein equation for the universe with ideal fluid cosmological perturbations. *Phys. Rev. D*, 65(10):104013–+, May 2002, arXiv:gr-qc/0203023 (ADS).
- [65] Ishibashi, A. & Wald, R. M. Can the acceleration of our universe be explained by the effects of inhomogeneities? *Classical and Quantum Gravity*, 23:235–250, January 2006, arXiv:gr-qc/0509108 (ADS).
- [66] Behrend, J., Brown, I. A., & Robbers, G. Cosmological back-reaction from perturbations. *J. Cosm. Astropart. P.*, 1:13–+, January 2008, 0710.4964 (ADS).
- [67] Buchert, T. Dark Energy from structure: a status report. *General Relativity and Gravitation*, 40:467–527, February 2008, 0707.2153 (ADS).
- [68] Léna, P., Lebrun, F., & Mignard, F. *Observational astrophysics*. Springer, Berlin (Germany), 1998.
- [69] Bessell, M. S. UVRI passbands. *PASP*, 102:1181–1199, October 1990 (ADS).
- [70] Fukugita, M., Ichikawa, T., Gunn, J. E., et al. The Sloan Digital Sky Survey Photometric System. *AJ*, 111:1748–+, April 1996 (ADS).
- [71] Oke, J. B. & Gunn, J. E. Secondary standard stars for absolute spectrophotometry. *ApJ*, 266:713–717, March 1983 (ADS).
- [72] Gunn, J. E., Siegmund, W. A., Mannery, E. J., et al. The 2.5 m Telescope of the Sloan Digital Sky Survey. *AJ*, 131:2332–2359, April 2006, arXiv:astro-ph/0602326 (ADS).
- [73] de Zeeuw, P. T., Allington-Smith, J. R., Bacon, R., et al. The One Eye that Sees All: Integral Field Spectroscopy with SAURON on the WHT. *The Newsletter of the Isaac Newton Group of Telescopes*, 2:11–15, March 2000 (ADS).
- [74] Lantz, B., Aldering, G., Antilogus, P., et al. SNIFS: a wide-band integral field spectrograph with microlens arrays. In L. Mazuray, P. J. Rogers, & R. Wartmann, editor, *Society of Photo-Optical Instrumentation Engineers (SPIE) Conference Series*, volume 5249 of *Society of Photo-Optical Instrumentation Engineers (SPIE) Conference Series*, pages 146–155, February 2004 (ADS).
- [75] Hodapp, K.-W., Hora, J. L., Hall, D. N. B., et al. The HAWAII Infrared Detector Arrays: testing and astronomical characterization of prototype and science-grade devices. *New A*, 1:177–196, October 1996 (ADS).
- [76] Leinert, C., Bowyer, S., Haikala, L. K., et al. The 1997 reference of diffuse night sky brightness. *A&AS*, 127:1–99, January 1998 (ADS).
- [77] Baade, W. & Zwicky, F. On Super-novae. *Proceedings of the National Academy of Science*, 20:254–259, May 1934 (ADS).
- [78] Minkowski, R. Spectra of Supernovae. *PASP*, 53:224–+, August 1941 (ADS).
- [79] Wheeler, J. C. & Levreault, R. The peculiar Type I supernova in NGC 991. *ApJ Lett.*, 294:L17–L20, July 1985 (ADS).
- [80] da Silva, L. A. L. The classification of supernovae. *Ap&SS*, 202:215–236, April 1993 (ADS).
- [81] Filippenko, A. V. Optical Spectra of Supernovae. *ARA&A*, 35:309–355, 1997 (ADS).
- [82] Wheeler, J. C. Resource Letter: OTS-1: Observations and theory of supernovae. *American Journal of Physics*, 71:11–22, January 2003, arXiv:astro-ph/0209514 (ADS).
- [83] Woosley, S. E. & Weaver, T. A. The physics of supernova explosions. *ARA&A*, 24:205–253, 1986 (ADS).
- [84] Smartt, S. J. Progenitors of Core-Collapse Supernovae. *ARA&A*, 47:63–106, September 2009, 0908.0700 (ADS).
- [85] Woosley, S. & Janka, T. The physics of core-collapse supernovae. *Nature Physics*, 1:147–154, December 2005, arXiv:astro-ph/0601261 (ADS).
- [86] Richardson, D., Branch, D., Casebeer, D., et al. A Comparative Study of the Absolute Magnitude Distributions of Supernovae. *AJ*, 123:745–752, February 2002 (ADS).
- [87] Li, W., Leaman, J., Chornock, R., et al. Nearby supernova rates from the Lick Observatory Supernova Search - II. The observed luminosity functions and fractions of supernovae in a complete sample. *MNRAS*, 412:1441–1472, April 2011, 1006.4612 (ADS).
- [88] Minkowski, R. Supernovae and Supernova Remnants. *ARA&A*, 2:247–+, 1964 (ADS).
- [89] Conley, A., Howell, D. A., Howes, A., et al. The Rise Time of Type Ia Supernovae from the Supernova Legacy Survey. *AJ*, 132:1707–1713, October 2006, arXiv:astro-ph/0607363 (ADS).
- [90] Colgate, S. A. & McKee, C. Early Supernova Luminosity. *ApJ*, 157:623, August 1969 (ADS).
- [91] Colgate, S. A., Petschek, A. G., & Kriese, J. T. The luminosity of type I supernovae. *ApJ Lett.*, 237:L81–L85, May 1980 (ADS).
- [92] Ruiz-Lapuente, P. & Spruit, H. C. Bolometric Light Curves of Supernovae and Postexplosion Magnetic Fields. *ApJ*, 500:360–+, June 1998, arXiv:astro-ph/9711248 (ADS).
- [93] Stritzinger, M., Leibundgut, B., Walch, S., & Contardo, G. Constraints on the progenitor systems of type Ia supernovae. *A&A*, 450:241–251, April 2006, arXiv:astro-ph/0506415 (ADS).
- [94] Branch, D. & Tammann, G. A. Type IA supernovae as standard candles. *ARA&A*, 30:359–389, 1992 (ADS).
- [95] Riess, A. G., Press, W. H., & Kirshner, R. P. A Precise Dis-

- tance Indicator: Type IA Supernova Multicolor Light-Curve Shapes. *ApJ*, 473:88–+, December 1996 ([ADS](#)).
- [96] Branch, D., Drucker, W., & Jeffery, D. J. Differences among expansion velocities of Type IA supernovae. *ApJ Lett.*, 330:L117+, July 1988 ([ADS](#)).
- [97] Benetti, S., Cappellaro, E., Mazzali, P. A., et al. The Diversity of Type Ia Supernovae: Evidence for Systematics? *ApJ*, 623:1011–1016, April 2005, arXiv:astro-ph/0411059 ([ADS](#)).
- [98] Contreras, C., Hamuy, M., Phillips, M. M., et al. The Carnegie Supernova Project: First Photometry Data Release of Low-Redshift Type Ia Supernovae. *AJ*, 139:519–539, February 2010, 0910.3330 ([ADS](#)).
- [99] Stanishev, V., Goobar, A., Benetti, S., et al. SN 2003du: 480 days in the life of a normal type Ia supernova. *A&A*, 469:645–661, July 2007, 0704.1244 ([ADS](#)).
- [100] Pskovskii, I. P. Light curves, color curves, and expansion velocity of type I supernovae as functions of the rate of brightness decline. *Soviet Astronomy*, 21:675–682, December 1977 ([ADS](#)).
- [101] Pskovskii, Y. P. Photometric classification and basic parameters of type I supernovae. *Soviet Astronomy*, 28:658–+, December 1984 ([ADS](#)).
- [102] Phillips, M. M. The absolute magnitudes of Type Ia supernovae. *ApJ Lett.*, 413:L105–L108, August 1993 ([ADS](#)).
- [103] Perlmutter, S., Gabi, S., Goldhaber, G., et al. Measurements of the Cosmological Parameters Omega and Lambda from the First Seven Supernovae at $z > 0.35$. *ApJ*, 483:565–+, July 1997 ([ADS](#)).
- [104] Goldhaber, G., Groom, D. E., Kim, A., et al. Timescale Stretch Parameterization of Type Ia Supernova B-Band Light Curves. *ApJ*, 558:359–368, September 2001, arXiv:astro-ph/0104382 ([ADS](#)).
- [105] Hayden, B. T., Garnavich, P. M., Kessler, R., et al. The Rise and Fall of Type Ia Supernova Light Curves in the SDSS-II Supernova Survey. *ApJ*, 712:350–366, March 2010, 1001.3428 ([ADS](#)).
- [106] Guy, J., Sullivan, M., Conley, A., et al. The Supernova Legacy Survey 3-year sample: Type Ia supernovae photometric distances and cosmological constraints. *A&A*, 523:A7+, November 2010, 1010.4743 ([ADS](#)).
- [107] González-Gaitán, S., Perrett, K., Sullivan, M., et al. Subluminous Type Ia Supernovae at High Redshift from the Supernova Legacy Survey. *ApJ*, 727:107–+, February 2011, 1011.4531 ([ADS](#)).
- [108] Guy, J., Astier, P., Nobili, S., Regnault, N., & Pain, R. SALT: a spectral adaptive light curve template for type Ia supernovae. *A&A*, 443:781–791, December 2005, arXiv:astro-ph/0506583 ([ADS](#)).
- [109] Conley, A., Sullivan, M., Hsiao, E. Y., et al. SiFTO: An Empirical Method for Fitting SN Ia Light Curves. *ApJ*, 681:482–498, July 2008, 0803.3441 ([ADS](#)).
- [110] Phillips, M. M., Lira, P., Suntzeff, N. B., et al. The Reddening-Free Decline Rate Versus Luminosity Relationship for Type IA Supernovae. *AJ*, 118:1766–1776, October 1999, arXiv:astro-ph/9907052 ([ADS](#)).
- [111] Riess, A. G., Press, W. H., & Kirshner, R. P. Is the Dust Obscuring Supernovae in Distant Galaxies the Same as Dust in the Milky Way? *ApJ*, 473:588–+, December 1996 ([ADS](#)).
- [112] Nobili, S. & Goobar, A. The colour-lightcurve shape relation of type Ia supernovae and the reddening law. *A&A*, 487:19–31, August 2008, 0712.1155 ([ADS](#)).
- [113] Blondin, S., Prieto, J. L., Patat, F., et al. A Second Case of Variable Na I D Lines in a Highly Reddened Type Ia Supernova. *ApJ*, 693:207–215, March 2009, 0811.0002 ([ADS](#)).
- [114] Guy, J., Astier, P., Baumont, S., et al. SALT2: using distant supernovae to improve the use of type Ia supernovae as distance indicators. *A&A*, 466:11–21, April 2007, arXiv:astro-ph/0701828 ([ADS](#)).
- [115] Ellis, R. S., Sullivan, M., Nugent, P. E., et al. Verifying the Cosmological Utility of Type Ia Supernovae: Implications of a Dispersion in the Ultraviolet Spectra. *ApJ*, 674:51–69, February 2008, 0710.3896 ([ADS](#)).
- [116] Balland, C., Baumont, S., Basa, S., et al. The ESO/VLT 3rd year Type Ia supernova data set from the supernova legacy survey. *A&A*, 507:85–103, November 2009, 0909.3316 ([ADS](#)).
- [117] Milne, P. A., Brown, P. J., Roming, P. W. A., et al. Near-ultraviolet Properties of a Large Sample of Type Ia Supernovae as Observed with the Swift UVOT. *ApJ*, 721:1627–1655, October 2010, 1007.5279 ([ADS](#)).
- [118] Foley, R. J. & Kasen, D. Measuring Ejecta Velocity Improves Type Ia Supernova Distances. *ApJ*, 729:55, March 2011, 1011.4517 ([ADS](#)).
- [119] Tripp, R. A two-parameter luminosity correction for Type IA supernovae. *A&A*, 331:815–820, March 1998 ([ADS](#)).
- [120] Chotard, N., Gangler, E., Aldering, G., et al. The reddening law of type Ia supernovae: separating intrinsic variability from dust using equivalent widths. *A&A*, 529:L4, May 2011, 1103.5300 ([ADS](#)).
- [121] Hamuy, M., Phillips, M. M., Suntzeff, N. B., et al. The Absolute Luminosities of the Calan/Tololo Type IA Supernovae. *AJ*, 112:2391, December 1996, arXiv:astro-ph/9609059 ([ADS](#)).
- [122] Krisciunas, K., Phillips, M. M., & Suntzeff, N. B. Hubble Diagrams of Type Ia Supernovae in the Near-Infrared. *ApJ Lett.*, 602:L81–L84, February 2004, arXiv:astro-ph/0312626 ([ADS](#)).
- [123] Wood-Vasey, W. M., Friedman, A. S., Bloom, J. S., et al. Type Ia Supernovae Are Good Standard Candles in the Near Infrared: Evidence from PAIRITEL. *ApJ*, 689:377–390, December 2008, 0711.2068 ([ADS](#)).
- [124] Kattner, S., Leonard, D. C., Burns, C. R., et al. The Standardizability of Type Ia Supernovae in the Near-Infrared: Evidence for a Peak-Luminosity Versus Decline-Rate Relation in the Near-Infrared. *PASP*, 124:114–127, February 2012, 1201.2913 ([ADS](#)).
- [125] Kawabata, K. S., Maeda, K., Nomoto, K., et al. A massive star origin for an unusual helium-rich supernova in an elliptical galaxy. *Nature*, 465:326–328, May 2010, 0906.2811 ([ADS](#)).
- [126] Mannucci, F., Della Valle, M., Panagia, N., et al. The supernova rate per unit mass. *A&A*, 433:807–814, April 2005, arXiv:astro-ph/0411450 ([ADS](#)).
- [127] Sullivan, M., Le Borgne, D., Pritchett, C. J., et al. Rates and Properties of Type Ia Supernovae as a Function of Mass and Star Formation in Their Host Galaxies. *ApJ*, 648:868–883, September 2006, arXiv:astro-ph/0605455 ([ADS](#)).
- [128] Lampeitl, H., Smith, M., Nichol, R. C., et al. The Effect of Host Galaxies on Type Ia Supernovae in the SDSS-II Supernova Survey. *ApJ*, 722:566–576, October 2010, 1005.4687 ([ADS](#)).
- [129] Brandt, T. D., Tojeiro, R., Aubourg, É., et al. The Ages of Type Ia Supernova Progenitors. *AJ*, 140:804–816, September 2010, 1002.0848 ([ADS](#)).
- [130] Pskovskii, Y. P. The Photometric Properties of Supernovae. *Soviet Astronomy*, 11:63–+, August 1967 ([ADS](#)).
- [131] Howell, D. A., Sullivan, M., Conley, A., & Carlberg, R. Predicted and Observed Evolution in the Mean Properties of Type Ia Supernovae with Redshift. *ApJ Lett.*, 667:L37–L40, September 2007, arXiv:astro-ph/0701912 ([ADS](#)).

- [132] Sullivan, M., Conley, A., Howell, D. A., et al. The dependence of Type Ia Supernovae luminosities on their host galaxies. *MNRAS*, **406**:782–802, August 2010, 1003.5119 ([ADS](#)).
- [133] Tran, H. D., Tsvetanov, Z., Ford, H. C., et al. Dusty Nuclear Disks and Filaments in Early-Type Galaxies. *AJ*, **121**:2928–2942, June 2001, arXiv:astro-ph/0102292 ([ADS](#)).
- [134] Temi, P., Brightenti, F., & Mathews, W. G. Mid-Infrared Emission from Elliptical Galaxies: Sensitivity to Stellar Age. *ApJ Lett.*, **635**:L25–L28, December 2005, arXiv:astro-ph/0511328 ([ADS](#)).
- [135] Smith, M., Nichol, R. C., Dilday, B., et al. The SDSS-II Supernova Survey: Parameterizing the Type Ia Supernova Rate as a Function of Host Galaxy Properties. *ApJ*, **755**:61, August 2012, 1108.4923 ([ADS](#)).
- [136] Hicken, M., Wood-Vasey, W. M., Blondin, S., et al. Improved Dark Energy Constraints from ~100 New CfA Supernova Type Ia Light Curves. *ApJ*, **700**:1097–1140, August 2009, 0901.4804 ([ADS](#)).
- [137] Chandrasekhar, S. The Maximum Mass of Ideal White Dwarfs. *ApJ*, **74**:81–+, July 1931 ([ADS](#)).
- [138] Hoyle, F. & Fowler, W. A. Nucleosynthesis in Supernovae. *ApJ*, **132**:565–+, November 1960 ([ADS](#)).
- [139] Livio, M. The Progenitors of Type Ia Supernovae. In J. C. Niemeyer & J. W. Truran, editor, *Type Ia Supernovae, Theory and Cosmology* (Cambridge Univ. Press), pages 33–+. Cambridge Univ. Press, 2000, arXiv:astro-ph/9903264 ([ADS](#)).
- [140] Kuchner, M. J., Kirshner, R. P., Pinto, P. A., & Leibundgut, B. Evidence for Ni-56 yields Co-56 yields Fe-56 decay in type IA supernovae. *ApJ Lett.*, **426**:L89–+, May 1994 ([ADS](#)).
- [141] Nomoto, K., Thielemann, F.-K., & Yokoi, K. Accreting white dwarf models of Type I supernovae. III - Carbon deflagration supernovae. *ApJ*, **286**:644–658, November 1984 ([ADS](#)).
- [142] Holberg, J. B., Sion, E. M., Oswalt, T., et al. A New Look at the Local White Dwarf Population. *AJ*, **135**:1225–1238, April 2008 ([ADS](#)).
- [143] Kilic, M., Brown, W. R., Allende Prieto, C., et al. The ELM Survey. II. Twelve Binary White Dwarf Merger Systems. *ApJ*, **727**:3–+, January 2011, 1011.4073 ([ADS](#)).
- [144] Whelan, J. & Iben, Jr., I. Binaries and Supernovae of Type I. *ApJ*, **186**:1007–1014, December 1973 ([ADS](#)).
- [145] Gilfanov, M. & Bogdán, Á. An upper limit on the contribution of accreting white dwarfs to the typeIa supernova rate. *Nature*, **463**:924–925, February 2010, 1002.3359 ([ADS](#)).
- [146] Hachisu, I., Kato, M., & Nomoto, K. Supersoft X-ray Phase of Single Degenerate Type Ia Supernova Progenitors in Early-type Galaxies. *ApJ Lett.*, **724**:L212–L216, December 2010, 1010.5860 ([ADS](#)).
- [147] Cassisi, S., Iben, Jr., I., & Tornambe, A. Hydrogen-accreting Carbon-Oxygen White Dwarfs. *ApJ*, **496**:376–+, March 1998 ([ADS](#)).
- [148] Kato, M. & Hachisu, I. A New Estimation of Mass Accumulation Efficiency in Helium Shell Flashes toward Type IA Supernova Explosions. *ApJ Lett.*, **513**:L41–L44, March 1999, arXiv:astro-ph/9901080 ([ADS](#)).
- [149] Maoz, D. & Mannucci, F. A search for the progenitors of two TypeIa Supernovae in NGC 1316. *MNRAS*, **388**:421–428, July 2008, 0801.2898 ([ADS](#)).
- [150] Li, W., Bloom, J. S., Podsiadlowski, P., et al. Exclusion of a luminous red giant as a companion star to the progenitor of supernova SN 2011fe. *Nature*, **480**:348–350, December 2011, 1109.1593 ([ADS](#)).
- [151] Schaefer, B. E. & Pagnotta, A. An absence of ex-companion stars in the type Ia supernova remnant SNR 0509-67.5. *Nature*, **481**:164–166, January 2012 ([ADS](#)).
- [152] Brown, P. J., Dawson, K. S., de Pasquale, M., et al. A Swift Look at SN 2011fe: The Earliest Ultraviolet Observations of a Type Ia Supernova. *ArXiv e-prints*, October 2011, 1110.2538 ([ADS](#)).
- [153] Brown, P. J., Dawson, K. S., Harris, D. W., et al. Constraints on Type Ia Supernova Progenitor Companions from Early Ultraviolet Observations with Swift. *ApJ*, **749**:18, April 2012, 1203.5315 ([ADS](#)).
- [154] Iben, Jr., I. & Tutukov, A. V. Supernovae of type I as end products of the evolution of binaries with components of moderate initial mass (M not greater than about 9 solar masses). *ApJS*, **54**:335–372, February 1984 ([ADS](#)).
- [155] Webbink, R. F. Double white dwarfs as progenitors of R Coronae Borealis stars and Type I supernovae. *ApJ*, **277**:355–360, February 1984 ([ADS](#)).
- [156] Howell, D. A., Sullivan, M., Nugent, P. E., et al. The type Ia supernova SNLS-03D3bb from a super-Chandrasekhar-mass white dwarf star. *Nature*, **443**:308–311, September 2006, arXiv:astro-ph/0609616 ([ADS](#)).
- [157] Hachisu, I., Kato, M., Saio, H., & Nomoto, K. A Single Degenerate Progenitor Model for Type Ia Supernovae Highly Exceeding the Chandrasekhar Mass Limit. *ApJ*, **744**:69, January 2012, 1106.3510 ([ADS](#)).
- [158] Saio, H. & Nomoto, K. Evolution of a merging pair of C + O white dwarfs to form a single neutron star. *A&A*, **150**:L21–L23, September 1985 ([ADS](#)).
- [159] Saio, H. & Nomoto, K. Inward Propagation of Nuclear-burning Shells in Merging C-O and He White Dwarfs. *ApJ*, **500**:388–+, June 1998, arXiv:astro-ph/9801084 ([ADS](#)).
- [160] Pakmor, R., Kromer, M., Röpke, F. K., et al. Sub-luminous type Ia supernovae from the mergers of equal-mass white dwarfs with mass $\sim 0.9M_{\odot}$. *Nature*, **463**:61–64, January 2010, 0911.0926 ([ADS](#)).
- [161] Arnett, W. D. On the theory of Type I supernovae. *ApJ Lett.*, **230**:L37–L40, May 1979 ([ADS](#)).
- [162] Nomoto, K., Thielemann, F.-K., & Yokoi, K. Accreting white dwarf models of Type I supernovae. III - Carbon deflagration supernovae. *ApJ*, **286**:644–658, November 1984 ([ADS](#)).
- [163] Khokhlov, A. M. Delayed detonation model for type IA supernovae. *A&A*, **245**:114–128, May 1991 ([ADS](#)).
- [164] Nomoto, K., Sugimoto, D., & Neo, S. Carbon deflagration supernova, an alternative to carbon detonation. *Ap&SS*, **39**:L37–L42, February 1976 ([ADS](#)).
- [165] Smirnov, N. N. & Tyurnikov, M. V. Experimental investigation of deflagration to detonation transition in hydrocarbon-air gaseous mixtures. *Combustion and Flame*, **100**(4):661 – 668, 1995.
- [166] Hoeflich, P. & Khokhlov, A. Explosion Models for Type IA Supernovae: A Comparison with Observed Light Curves, Distances, H 0, and Q 0. *ApJ*, **457**:500–+, February 1996, arXiv:astro-ph/9602025 ([ADS](#)).
- [167] Hoeflich, P., Khokhlov, A., Wheeler, J. C., et al. Maximum Brightness and Postmaximum Decline of Light Curves of Type IA Supernovae: A Comparison of Theory and Observations. *ApJ Lett.*, **472**:L81–+, December 1996, arXiv:astro-ph/9609070 ([ADS](#)).
- [168] Arnett, W. D. Type I supernovae. I - Analytic solutions for the early part of the light curve. *ApJ*, **253**:785–797, February 1982 ([ADS](#)).
- [169] Stritzinger, M., Mazzali, P. A., Sollerman, J., & Benetti, S. Consistent estimates of ^{56}Ni yields for type Ia supernovae. *A&A*, **460**:793–798, December 2006, arXiv:astro-ph/0609232 ([ADS](#)).

- [170] Lucy, L. B. Improved Monte Carlo techniques for the spectral synthesis of supernovae. *A&A*, 345:211–220, May 1999 ([ADS](#)).
- [171] Mazzali, P. A. Applications of an improved Monte Carlo code to the synthesis of early-time Supernova spectra. *A&A*, 363:705–716, November 2000 ([ADS](#)).
- [172] Sauer, D. N., Mazzali, P. A., Blondin, S., et al. Properties of the ultraviolet flux of Type Ia supernovae: an analysis with synthetic spectra of SN 2001ep and SN 2001eh. *MNRAS*, 391:1605–1618, December 2008, 0803.0871 ([ADS](#)).
- [173] Kromer, M. & Sim, S. A. Time-dependent three-dimensional spectrum synthesis for Type Ia supernovae. *MNRAS*, 398:1809–1826, October 2009, 0906.3152 ([ADS](#)).
- [174] Lucy, L. B. Monte Carlo techniques for time-dependent radiative transfer in 3-D supernovae. *A&A*, 429:19–30, January 2005, arXiv:astro-ph/0409249 ([ADS](#)).
- [175] Kasen, D. Secondary Maximum in the Near-Infrared Light Curves of Type Ia Supernovae. *ApJ*, 649:939–953, October 2006, arXiv:astro-ph/0606449 ([ADS](#)).
- [176] Jack, D., Hauschildt, P. H., & Baron, E. Theoretical light curves of type Ia supernovae. *A&A*, 528:A141, April 2011, 1105.3330 ([ADS](#)).
- [177] Kasen, D., Röpke, F. K., & Woosley, S. E. The diversity of type Ia supernovae from broken symmetries. *Nature*, 460:869–872, August 2009, 0907.0708 ([ADS](#)).
- [178] Milne, P. A., The, L.-S., & Leising, M. D. Late Light Curves of Type Ia Supernovae. *ApJ*, 559:1019–1031, October 2001, arXiv:astro-ph/0104185 ([ADS](#)).
- [179] Lair, J. C., Leising, M. D., Milne, P. A., & Williams, G. G. Late Light Curves of Normal Type Ia Supernovae. *AJ*, 132:2024–2033, November 2006, arXiv:astro-ph/0610084 ([ADS](#)).
- [180] Milne, P. A., The, L.-S., & Leising, M. D. Positron Escape from Type IA Supernovae. *ApJS*, 124:503–526, October 1999, arXiv:astro-ph/9901206 ([ADS](#)).
- [181] Knöldlseder, J., Jean, P., Lonjou, V., et al. The all-sky distribution of 511 keV electron-positron annihilation emission. *A&A*, 441:513–532, October 2005, arXiv:astro-ph/0506026 ([ADS](#)).
- [182] Branch, D. The Hubble constant from nickel radioactivity in type IA supernovae. *ApJ*, 392:35–40, June 1992 ([ADS](#)).
- [183] Stritzinger, M. & Leibundgut, B. Lower limits on the Hubble constant from models of type Ia supernovae. *A&A*, 431:423–431, February 2005, arXiv:astro-ph/0410686 ([ADS](#)).
- [184] Mazzali, P. A., Nomoto, K., Cappellaro, E., et al. Can Differences in the Nickel Abundance in Chandrasekhar-Mass Models Explain the Relation between the Brightness and Decline Rate of Normal Type IA Supernovae? *ApJ*, 547:988–994, February 2001, arXiv:astro-ph/0009490 ([ADS](#)).
- [185] Röpke, F. K., Gieseler, M., Reinecke, M., Travaglio, C., & Hillebrandt, W. Type Ia supernova diversity in three-dimensional models. *A&A*, 453:203–217, July 2006, arXiv:astro-ph/0506107 ([ADS](#)).
- [186] Hansen, L., Jorgensen, H. E., & Norgaard-Nielsen, H. U. Search for supernovae in distant clusters of galaxies. *The Messenger*, 47:46–49, March 1987 ([ADS](#)).
- [187] Norgaard-Nielsen, H. U., Hansen, L., Jorgensen, H. E., Aragon Salamanca, A., & Ellis, R. S. The discovery of a type IA supernova at a redshift of 0.31. *Nature*, 339:523–525, June 1989 ([ADS](#)).
- [188] Alard, C. & Lupton, R. H. A Method for Optimal Image Subtraction. *ApJ*, 503:325–+, August 1998 ([ADS](#)).
- [189] Howell, D. A., Sullivan, M., Perrett, K., et al. Gemini Spectroscopy of Supernovae from the Supernova Legacy Survey: Improving High-Redshift Supernova Selection and Classification. *ApJ*, 634:1190–1201, December 2005, arXiv:astro-ph/0509195 ([ADS](#)).
- [190] Blondin, S. & Tonry, J. L. Determining the Type, Redshift, and Age of a Supernova Spectrum. *ApJ*, 666:1024–1047, September 2007, 0709.4488 ([ADS](#)).
- [191] Blondin, S., Walsh, J. R., Leibundgut, B., & Sainton, G. Extracting clean supernova spectra. Towards a quantitative analysis of high-redshift Type Ia supernova spectra. *A&A*, 431:757–771, February 2005, arXiv:astro-ph/0410406 ([ADS](#)).
- [192] Baumont, S., Balland, C., Astier, P., et al. PHotometry Assisted Spectral Extraction (PHASE) and identification of SNLS supernovae. *A&A*, 491:567–585, November 2008, 0809.4407 ([ADS](#)).
- [193] Matheson, T., Blondin, S., Foley, R. J., et al. Spectroscopy of High-Redshift Supernovae from the ESSENCE Project: The First 2 Years. *AJ*, 129:2352–2375, May 2005, arXiv:astro-ph/0411357 ([ADS](#)).
- [194] Foley, R. J., Matheson, T., Blondin, S., et al. Spectroscopy of High-Redshift Supernovae from the Essence Project: The First Four Years. *AJ*, 137:3731–3742, April 2009, 0811.4424 ([ADS](#)).
- [195] Knop, R. A., Aldering, G., Amanullah, R., et al. New Constraints on Ω_M , Ω_Λ , and w from an Independent Set of 11 High-Redshift Supernovae Observed with the Hubble Space Telescope. *ApJ*, 598:102–137, November 2003, arXiv:astro-ph/0309368 ([ADS](#)).
- [196] Astier, P., Guy, J., Regnault, N., et al. The Supernova Legacy Survey: measurement of Ω_M , Ω_Λ and w from the first year data set. *A&A*, 447:31–48, February 2006, astro-ph/0510447 ([ADS](#)).
- [197] Holtzman, J. A., Marriner, J., Kessler, R., et al. The Sloan Digital Sky Survey-II Photometry and Supernova IA Light Curves from the 2005 Data. *AJ*, 136:2306–2320, December 2008 ([ADS](#)).
- [198] Irwin, M. J. Automatic analysis of crowded fields. *MNRAS*, 214:575–604, June 1985 ([ADS](#)).
- [199] Schmidt, B. P., Suntzeff, N. B., Phillips, M. M., et al. The High-Z Supernova Search: Measuring Cosmic Deceleration and Global Curvature of the Universe Using Type IA Supernovae. *ApJ*, 507:46–63, November 1998 ([ADS](#)).
- [200] Kessler, R., Becker, A. C., Cinabro, D., et al. First-Year Sloan Digital Sky Survey-II Supernova Results: Hubble Diagram and Cosmological Parameters. *ApJS*, 185:32–84, November 2009, 0908.4274 ([ADS](#)).
- [201] Humason, M. L., Mayall, N. U., & Sandage, A. R. Redshifts and magnitudes of extragalactic nebulae. *AJ*, 61:97–162, 1956 ([ADS](#)).
- [202] Kim, A., Goobar, A., & Perlmutter, S. A Generalized K Correction for Type IA Supernovae: Comparing R-band Photometry beyond $z=0.2$ with B, V, and R-band Nearby Photometry. *PASP*, 108:190, February 1996, arXiv:astro-ph/9505024 ([ADS](#)).
- [203] Nugent, P., Kim, A., & Perlmutter, S. K-Corrections and Extinction Corrections for Type Ia Supernovae. *PASP*, 114:803–819, August 2002, arXiv:astro-ph/0205351 ([ADS](#)).
- [204] Schlegel, D. J., Finkbeiner, D. P., & Davis, M. Maps of Dust Infrared Emission for Use in Estimation of Reddening and Cosmic Microwave Background Radiation Foregrounds. *ApJ*, 500:525–+, June 1998 ([ADS](#)).
- [205] Cardelli, J. A., Clayton, G. C., & Mathis, J. S. The relationship between infrared, optical, and ultraviolet extinction. *ApJ*, 345:245–256, October 1989 ([ADS](#)).

- [206] Leibundgut, B. *Light curves of supernovae type, I*. PhD thesis, PhD thesis. Univ. Basel.137 pp. , (1988), 1988 ([ADS](#)).
- [207] Hamuy, M., Phillips, M. M., Maza, J., et al. A Hubble diagram of distant type IA supernovae. *AJ*, **109**:1–13, January 1995 ([ADS](#)).
- [208] Hamuy, M., Phillips, M. M., Suntzeff, N. B., et al. The Morphology of Type IA Supernovae Light Curves. *AJ*, **112**:2438, December 1996, arXiv:astro-ph/9609063 ([ADS](#)).
- [209] Germany, L. M., Reiss, D. J., Schmidt, B. P., Stubbs, C. W., & Suntzeff, N. B. Results of the Mount Stromlo Abell cluster supernova search. *A&A*, **415**:863–878, March 2004 ([ADS](#)).
- [210] Prieto, J. L., Rest, A., & Suntzeff, N. B. A New Method to Calibrate the Magnitudes of Type Ia Supernovae at Maximum Light. *ApJ*, **647**:501–512, August 2006, arXiv:astro-ph/0603407 ([ADS](#)).
- [211] Burns, C. R., Stritzinger, M., Phillips, M. M., et al. The Carnegie Supernova Project: Light-curve Fitting with SNooPy. *AJ*, **141**:19, January 2011, 1010.4040 ([ADS](#)).
- [212] Tonry, J. L., Schmidt, B. P., Barris, B., et al. Cosmological Results from High-z Supernovae. *ApJ*, **594**:1–24, September 2003, arXiv:astro-ph/0305008 ([ADS](#)).
- [213] Riess, A. G., Press, W. H., & Kirshner, R. P. Using Type IA supernova light curve shapes to measure the Hubble constant. *ApJ Lett.*, **438**:L17–L20, January 1995 ([ADS](#)).
- [214] Jha, S., Riess, A. G., & Kirshner, R. P. Improved Distances to Type Ia Supernovae with Multicolor Light-Curve Shapes: MLCS2k2. *ApJ*, **659**:122–148, April 2007, arXiv:astro-ph/0612666 ([ADS](#)).
- [215] Wood-Vasey, W. M., Miknaitis, G., Stubbs, C. W., et al. Observational Constraints on the Nature of Dark Energy: First Cosmological Results from the ESSENCE Supernova Survey. *ApJ*, **666**:694–715, September 2007, arXiv:astro-ph/0701041 ([ADS](#)).
- [216] Freedman, W. L., Burns, C. R., Phillips, M. M., et al. The Carnegie Supernova Project: First Near-Infrared Hubble Diagram to $z \sim 0.7$. *ApJ*, **704**:1036–1058, October 2009, 0907.4524 ([ADS](#)).
- [217] Hsiao, E. Y., Conley, A., Howell, D. A., et al. K-Corrections and Spectral Templates of Type Ia Supernovae. *ApJ*, **663**:1187–1200, July 2007, arXiv:astro-ph/0703529 ([ADS](#)).
- [218] Conley, A., Guy, J., Sullivan, M., et al. Supernova Constraints and Systematic Uncertainties from the First Three Years of the Supernova Legacy Survey. *ApJS*, **192**:1–+, January 2011, 1104.1443 ([ADS](#)).
- [219] Conley, A., Carlberg, R. G., Guy, J., et al. Is There Evidence for a Hubble Bubble? The Nature of Type Ia Supernova Colors and Dust in External Galaxies. *ApJ Lett.*, **664**:L13–L16, July 2007, 0705.0367 ([ADS](#)).
- [220] Bailey, S., Aldering, G., Antilogus, P., et al. Using spectral flux ratios to standardize SN Ia luminosities. *A&A*, **500**:L17–L20, June 2009, 0905.0340 ([ADS](#)).
- [221] Wang, L., Goldhaber, G., Aldering, G., & Perlmutter, S. Multicolor Light Curves of Type Ia Supernovae on the Color-Magnitude Diagram: A Novel Step toward More Precise Distance and Extinction Estimates. *ApJ*, **590**:944–970, June 2003, arXiv:astro-ph/0302341 ([ADS](#)).
- [222] Conley, A., Goldhaber, G., Wang, L., et al. Measurement of Ω_m , Ω_Λ from a Blind Analysis of Type Ia Supernovae with CMAGIC: Using Color Information to Verify the Acceleration of the Universe. *ApJ*, **644**:1–20, June 2006, arXiv:astro-ph/0602411 ([ADS](#)).
- [223] Hayes, D. S. Stellar absolute fluxes and energy distributions from 0.32 to 4.0 microns. In Hayes, D. S., Pasinetti, L. E., & Philip, A. G. D., editors, *Calibration of Fundamental Stellar Quantities*, volume 111 of *IAU Symposium*, pages 225–249, 1985 ([ADS](#)).
- [224] Regnault, N., Conley, A., Guy, J., et al. Photometric calibration of the Supernova Legacy Survey fields. *A&A*, **506**:999–1042, November 2009, 0908.3808 ([ADS](#)).
- [225] Landolt, A. U. UBVRI photometric standard stars around the celestial equator. *AJ*, **88**:439–460, March 1983 ([ADS](#)).
- [226] Landolt, A. U. UBVRI photometric standard stars in the magnitude range 11.5–16.0 around the celestial equator. *AJ*, **104**:340–371, July 1992 ([ADS](#)).
- [227] Johnson, H. L. & Morgan, W. W. Fundamental stellar photometry for standards of spectral type on the revised system of the Yerkes spectral atlas. *ApJ*, **117**:313–+, May 1953 ([ADS](#)).
- [228] Cousins, A. W. J. VRI standards in the E regions. *MmRAS*, **81**:25–+, 1976 ([ADS](#)).
- [229] Johnson, H. L. & Morgan, W. W. On the Color-Magnitude Diagram of the Pleiades. *ApJ*, **114**:522–+, November 1951 ([ADS](#)).
- [230] Bohlin, R. C. Comparison of White Dwarf Models with STIS Spectrophotometry. *AJ*, **120**:437–446, July 2000 ([ADS](#)).
- [231] Bohlin, R. C. & Gilliland, R. L. Hubble Space Telescope Absolute Spectrophotometry of Vega from the Far-Ultraviolet to the Infrared. *AJ*, **127**:3508–3515, June 2004 ([ADS](#)).
- [232] Landolt, A. U. & Uomoto, A. K. Optical Multicolor Photometry of Spectrophotometric Standard Stars. *AJ*, **133**:768–790, March 2007 ([ADS](#)).
- [233] Bohlin, R. C., Dickinson, M. E., & Calzetti, D. Spectrophotometric Standards from the Far-Ultraviolet to the Near-Infrared: STIS and NICMOS Fluxes. *AJ*, **122**:2118–2128, October 2001 ([ADS](#)).
- [234] Bohlin, R. C. & Gilliland, R. L. Absolute Flux Distribution of the SDSS Standard BD +17 4708. *AJ*, **128**:3053–3060, December 2004 ([ADS](#)).
- [235] Stubbs, C. W. & Tonry, J. L. Toward 1% Photometry: End-to-End Calibration of Astronomical Telescopes and Detectors. *ApJ*, **646**:1436–1444, August 2006, arXiv:astro-ph/0604285 ([ADS](#)).
- [236] Stubbs, C. W., Doherty, P., Cramer, C., et al. Precise Throughput Determination of the PanSTARRS Telescope and the Gigapixel Imager Using a Calibrated Silicon Photodiode and a Tunable Laser: Initial Results. *ApJS*, **191**:376–388, December 2010, 1003.3465 ([ADS](#)).
- [237] Juramy, C., Barrelet, E., Schahmaneche, K., et al. SNDICE: a direct illumination calibration experiment at CFHT. *SPIE*, **7014**, August 2008 ([ADS](#)).
- [238] Barrelet, E. & Juramy, C. Direct illumination LED calibration for telescope photometry. *Nuclear Instruments and Methods in Physics Research A*, **585**:93–101, January 2008 ([ADS](#)).
- [239] Tonry, J. L., Stubbs, C. W., Lykke, K. R., et al. The Pan-STARRS1 Photometric System. *ApJ*, **750**:99, May 2012, 1203.0297 ([ADS](#)).
- [240] Burke, D. L., Axelrod, T., Blondin, S., et al. Precision Determination of Atmospheric Extinction at Optical and Near-infrared Wavelengths. *ApJ*, **720**:811–823, September 2010 ([ADS](#)).
- [241] Massey, R., Stoughton, C., Leauthaud, A., et al. Pixel-based correction for Charge Transfer Inefficiency in the Hubble Space Telescope Advanced Camera for Surveys. *MNRAS*, **401**:371–384, January 2010, 0909.0507 ([ADS](#)).
- [242] Sullivan, M., Guy, J., Conley, A., et al. SNLS3: Constraints on Dark Energy Combining the Supernova Legacy Survey Three-year Data with Other Probes. *ApJ*, **737**:102, August 2011, 1104.1444 ([ADS](#)).
- [243] Stritzinger, M. D., Phillips, M. M., Boldt, L. N., et al. The

- Carnegie Supernova Project: Second Photometry Data Release of Low-redshift Type Ia Supernovae. *AJ*, **142**:156, November 2011, 1108.3108 ([ADS](#)).
- [244] Smith, J. A., Tucker, D. L., Kent, S., et al. The u'g'r'i'z' Standard-Star System. *AJ*, **123**:2121–2144, April 2002 ([ADS](#)).
- [245] Albert, J., Foster, K., Battat, J., et al. Satellite-Mounted Light Sources as Photometric Calibration Standards. *ArXiv e-prints*, August 2009, 0908.3343 ([ADS](#)).
- [246] Aldering, G., Knop, R., & Nugent, P. The Rise Times of High- and Low-Redshift Type IA Supernovae Are Consistent. *AJ*, **119**:2110–2117, May 2000 ([ADS](#)).
- [247] Hook, I. M., Howell, D. A., Aldering, G., et al. Spectra of High-Redshift Type Ia Supernovae and a Comparison with Their Low-Redshift Counterparts. *AJ*, **130**:2788–2803, December 2005, arXiv:astro-ph/0509041 ([ADS](#)).
- [248] Blondin, S., Dessart, L., Leibundgut, B., et al. Using Line Profiles to Test the Fraternity of Type Ia Supernovae at High and Low Redshifts. *AJ*, **131**:1648–1666, March 2006, arXiv:astro-ph/0510089 ([ADS](#)).
- [249] Garavini, G., Folatelli, G., Nobili, S., et al. Quantitative comparison between type Ia supernova spectra at low and high redshifts: a case study. *A&A*, **470**:411–424, August 2007, arXiv:astro-ph/0703629 ([ADS](#)).
- [250] Foley, R. J., Filippenko, A. V., Aguilera, C., et al. Constraining Cosmic Evolution of Type Ia Supernovae. *ApJ*, **684**:68–87, September 2008, 0710.2338 ([ADS](#)).
- [251] Walker, E. S., Hook, I. M., Sullivan, M., et al. Supernova Legacy Survey: using spectral signatures to improve Type Ia supernovae as distance indicators. *MNRAS*, **410**:1262–1282, January 2011, 1008.2308 ([ADS](#)).
- [252] Hoeflich, P., Wheeler, J. C., & Thielemann, F. K. Type Ia Supernovae: Influence of the Initial Composition on the Nucleosynthesis, Light Curves, and Spectra and Consequences for the Determination of Omega M and Lambda. *ApJ*, **495**:617–+, March 1998, arXiv:astro-ph/9709233 ([ADS](#)).
- [253] Lentz, E. J., Baron, E., Branch, D., Hauschildt, P. H., & Nugent, P. E. Metallicity Effects in Non-LTE Model Atmospheres of Type Ia Supernovae. *ApJ*, **530**:966–976, February 2000, arXiv:astro-ph/9906016 ([ADS](#)).
- [254] Cooke, J., Ellis, R. S., Sullivan, M., et al. Hubble Space Telescope Studies of Nearby Type Ia Supernovae: The Mean Maximum Light Ultraviolet Spectrum and its Dispersion. *ApJ Lett.*, **727**:L35+, February 2011, 1010.2211 ([ADS](#)).
- [255] Sullivan, M., Ellis, R. S., Aldering, G., et al. The Hubble diagram of type Ia supernovae as a function of host galaxy morphology. *MNRAS*, **340**:1057–1075, April 2003 ([ADS](#)).
- [256] Howell, D. A., Sullivan, M., Brown, E. F., et al. The Effect of Progenitor Age and Metallicity on Luminosity and ^{56}Ni Yield in Type Ia Supernovae. *ApJ*, **691**:661–671, January 2009, 0810.0031 ([ADS](#)).
- [257] Gallagher, J. S., Garnavich, P. M., Caldwell, N., et al. Supernovae in Early-Type Galaxies: Directly Connecting Age and Metallicity with Type Ia Luminosity. *ApJ*, **685**:752–766, October 2008, 0805.4360 ([ADS](#)).
- [258] Kelly, P. L., Hicken, M., Burke, D. L., Mandel, K. S., & Kirshner, R. P. Hubble Residuals of Nearby Type Ia Supernovae are Correlated with Host Galaxy Masses. *ApJ*, **715**:743–756, June 2010, 0912.0929 ([ADS](#)).
- [259] Schneider, P., Ehlers, J., & Falco, E. E. *Gravitational Lenses*. Springer, 1992.
- [260] Narayan, R. & Bartelmann, M. Lectures on Gravitational Lensing. *ArXiv Astrophysics e-prints*, June 1996, arXiv:astro-ph/9606001 ([ADS](#)).
- [261] Fort, B. & Mellier, Y. Arc(let)s in clusters of galaxies. *The Astron. and Astrop. Rev.*, **5**:239–292, 1994 ([ADS](#)).
- [262] Peacock, J. A. Flux conservation and random gravitational lensing. *MNRAS*, **223**:113–128, November 1986 ([ADS](#)).
- [263] Weinberg, S. Apparent luminosities in a locally inhomogeneous universe. *ApJ Lett.*, **208**:L1–L3, August 1976 ([ADS](#)).
- [264] Holz, D. E. Lensing and High-z Supernova Surveys. *ApJ Lett.*, **506**:L1–L5, October 1998, arXiv:astro-ph/9806124 ([ADS](#)).
- [265] Bergström, L., Goliath, M., Goobar, A., & Mörtsell, E. Lensing effects in an inhomogeneous universe. *A&A*, **358**:13–29, June 2000 ([ADS](#)).
- [266] Goobar, A., Mörtsell, E., Amanullah, R., et al. SNOCl: A Monte-Carlo simulation package for high-z supernova observations. *A&A*, **392**:757–771, September 2002, arXiv:astro-ph/0206409 ([ADS](#)).
- [267] Myers, S. T., Jackson, N. J., Browne, I. W. A., et al. The Cosmic Lens All-Sky Survey - I. Source selection and observations. *MNRAS*, **341**:1–12, May 2003 ([ADS](#)).
- [268] Holz, D. E. & Wald, R. M. New method for determining cumulative gravitational lensing effects in inhomogeneous universes. *Phys. Rev. D*, **58**(6):063501–+, September 1998, arXiv:astro-ph/9708036 ([ADS](#)).
- [269] Amanullah, R., Mörtsell, E., & Goobar, A. Correcting for lensing bias in the Hubble diagram. *A&A*, **397**:819–823, January 2003, arXiv:astro-ph/0204280 ([ADS](#)).
- [270] Holz, D. E. & Linder, E. V. Safety in Numbers: Gravitational Lensing Degradation of the Luminosity Distance-Redshift Relation. *ApJ*, **631**:678–688, October 2005, arXiv:astro-ph/0412173 ([ADS](#)).
- [271] Kronborg, T., Hardin, D., Guy, J., et al. Gravitational lensing in the supernova legacy survey (SNLS). *A&A*, **514**:A44+, May 2010, 1002.1249 ([ADS](#)).
- [272] Jönsson, J., Sullivan, M., Hook, I., et al. Constraining dark matter halo properties using lensed Supernova Legacy Survey supernovae. *MNRAS*, **405**:535–544, June 2010, 1002.1374 ([ADS](#)).
- [273] Goobar, A., Paech, K., Stanishev, V., et al. Near-IR search for lensed supernovae behind galaxy clusters. II. First detection and future prospects. *A&A*, **507**:71–83, November 2009, 0810.4932 ([ADS](#)).
- [274] Goobar, A., Mörtsell, E., Amanullah, R., & Nugent, P. Cosmological parameters from lensed supernovae. *A&A*, **393**:25–32, October 2002, arXiv:astro-ph/0207139 ([ADS](#)).
- [275] Oguri, M. & Kawano, Y. Gravitational lens time delays for distant supernovae: breaking the degeneracy between radial mass profiles and the Hubble constant. *MNRAS*, **338**:L25–L29, February 2003, arXiv:astro-ph/0211499 ([ADS](#)).
- [276] Oguri, M. & Marshall, P. J. Gravitationally lensed quasars and supernovae in future wide-field optical imaging surveys. *MNRAS*, **405**:2579–2593, July 2010, 1001.2037 ([ADS](#)).
- [277] Garnavich, P. M., Jha, S., Challis, P., et al. Supernova Limits on the Cosmic Equation of State. *ApJ*, **509**:74–79, December 1998, arXiv:astro-ph/9806396 ([ADS](#)).
- [278] Riess, A. G., Strolger, L.-G., Casertano, S., et al. New Hubble Space Telescope Discoveries of Type Ia Supernovae at $z \geq 1$: Narrowing Constraints on the Early Behavior of Dark Energy. *ApJ*, **659**:98–121, April 2007, arXiv:astro-ph/0611572 ([ADS](#)).
- [279] Frieman, J. A., Bassett, B., Becker, A., et al. The Sloan Digital Sky Survey-II Supernova Survey: Technical Summary. *AJ*, **135**:338–347, January 2008, 0708.2749 ([ADS](#)).
- [280] Riess, A. G., Kirshner, R. P., Schmidt, B. P., et al. BVRI Light Curves for 22 Type IA Supernovae. *AJ*, **117**:707–724,

- February 1999 ([ADS](#)).
- [281] Jha, S., Kirshner, R. P., Challis, P., et al. UBVRI Light Curves of 44 Type Ia Supernovae. *AJ*, **131**:527–554, January 2006, arXiv:astro-ph/0509234 ([ADS](#)).
- [282] Hicken, M., Challis, P., Jha, S., et al. CfA3: 185 Type Ia Supernova Light Curves from the CfA. *ApJ*, **700**:331–357, July 2009, 0901.4787 ([ADS](#)).
- [283] Li, W. D., Filippenko, A. V., Treffers, R. R., et al. The Lick Observatory Supernova Search. In S. S. Holt & W. W. Zhang, editor, *American Institute of Physics Conference Series*, volume 522 of *American Institute of Physics Conference Series*, pages 103–106, June 2000, arXiv:astro-ph/9912336 ([ADS](#)).
- [284] Blondin, S., Matheson, T., Kirshner, R. P., et al. The Spectroscopic Diversity of Type Ia Supernovae. *AJ*, **143**:126, May 2012, 1203.4832 ([ADS](#)).
- [285] Aldering, G., Adam, G., Antilogus, P., et al. Overview of the Nearby Supernova Factory. In *Survey and Other Telescope Technologies and Discoveries*. Edited by Tyson, J. Anthony; Wolff, Sidney. *Proceedings of the SPIE*, Volume 4836, pp. 61–72 (2002),, pages 61–72, December 2002 ([ADS](#)).
- [286] Garnavich, P. M., Kirshner, R. P., Challis, P., et al. Constraints on Cosmological Models from Hubble Space Telescope Observations of High-z Supernovae. *ApJ Lett.*, **493**:L53+, February 1998, arXiv:astro-ph/9710123 ([ADS](#)).
- [287] Perlmutter, S. & Schmidt, B. P. Measuring Cosmology with Supernovae. In K. Weiler, editor, *Supernovae and Gamma-Ray Bursters*, volume 598 of *Lecture Notes in Physics*, Berlin Springer Verlag, pages 195–217, 2003, arXiv:astro-ph/0303428 ([ADS](#)).
- [288] Blakeslee, J. P., Tsvetanov, Z. I., Riess, A. G., et al. Discovery of Two Distant Type Ia Supernovae in the Hubble Deep Field-North with the Advanced Camera for Surveys. *ApJ*, **589**:693–703, June 2003, arXiv:astro-ph/0302402 ([ADS](#)).
- [289] Amanullah, R., Lidman, C., Rubin, D., et al. Spectra and Hubble Space Telescope Light Curves of Six Type Ia Supernovae at $0.511 < z < 1.12$ and the Union2 Compilation. *ApJ*, **716**:712–738, June 2010, 1004.1711 ([ADS](#)).
- [290] Dawson, K. S., Aldering, G., Amanullah, R., et al. An Intensive Hubble Space Telescope Survey for $z>1$ Type Ia Supernovae by Targeting Galaxy Clusters. *AJ*, **138**:1271–1283, November 2009, 0908.3928 ([ADS](#)).
- [291] Suzuki, N., Rubin, D., Lidman, C., et al. The Hubble Space Telescope Cluster Supernova Survey. V. Improving the Dark-energy Constraints above $z > 1$ and Building an Early-type-hosted Supernova Sample. *ApJ*, **746**:85, February 2012, 1105.3470 ([ADS](#)).
- [292] Rodney, S. A., Riess, A. G., Dahlen, T., et al. A Type Ia Supernova at Redshift 1.55 in Hubble Space Telescope Infrared Observations from CANDELS. *ApJ*, **746**:5, February 2012, 1201.2470 ([ADS](#)).
- [293] Miknaitis, G., Pignata, G., Rest, A., et al. The ESSENCE Supernova Survey: Survey Optimization, Observations, and Supernova Photometry. *ApJ*, **666**:674–693, September 2007, arXiv:astro-ph/0701043 ([ADS](#)).
- [294] Kowalski, M., Rubin, D., Aldering, G., et al. Improved Cosmological Constraints from New, Old, and Combined Supernova Data Sets. *ApJ*, **686**:749–778, October 2008, 0804.4142 ([ADS](#)).
- [295] Kessler, R., Bassett, B., Belov, P., et al. Results from the Supernova Photometric Classification Challenge. *PASP*, **122**:1415–1431, December 2010, 1008.1024 ([ADS](#)).
- [296] Sako, M., Bassett, B., Connolly, B., et al. Photometric Type Ia Supernova Candidates from the Three-year SDSS-II SN Survey Data. *ApJ*, **738**:162+, September 2011, 1107.5106 ([ADS](#)).
- [297] Bazin, G., Ruhlmann-Kleider, V., Palanque-Delabrouille, N., et al. Photometric selection of Type Ia supernovae in the Supernova Legacy Survey. *A&A*, **534**:A43+, October 2011, 1109.0948 ([ADS](#)).
- [298] Palanque-Delabrouille, N., Ruhlmann-Kleider, V., Pascal, S., et al. Photometric redshifts for type Ia supernovae in the supernova legacy survey. *A&A*, **514**:A63+, May 2010, 0911.1629 ([ADS](#)).
- [299] Kessler, R., Cinabro, D., Bassett, B., et al. Photometric Estimates of Redshifts and Distance Moduli for Type Ia Supernovae. *ApJ*, **717**:40–57, July 2010, 1001.0738 ([ADS](#)).
- [300] Albrecht, A., Bernstein, G., Cahn, R., et al. Report of the Dark Energy Task Force. September 2006, astro-ph/0609591 ([ADS](#)).
- [301] Peacock, J. A., Schneider, P., Efstathiou, G., et al. ESA-ESO Working Group on “Fundamental Cosmology”. Technical report, October 2006 ([ADS](#)).
- [302] Holland, S. An Overview of CCD Development at Lawrence Berkeley National Laboratory. *Experimental Astronomy*, **14**:83–89, October 2002 ([ADS](#)).
- [303] Bernstein, J. P., Kessler, R., Kuhlmann, S., et al. Supernova Simulations and Strategies For the Dark Energy Survey. *ArXiv e-prints*, November 2011, 1111.1969 ([ADS](#)).